EUROPEAN ORGANIZATION FOR NUCLEAR RESEARCH
European Laboratory for Particle Physics

Large Hadron Collider Project

LHC Project Report 626

LHC Luminosity and Energy Upgrade: A Feasibility Study

O. Brüning[§], R. Cappi[‡], R. Garoby[‡], O. Gröbner[†], W. Herr[§], T. Linnecar[§], R. Ostojic[†],
K. Potter[*], L. Rossi[†], F. Ruggiero[§] (editor), K. Schindl[‡], G. Stevenson[¶], L. Tavian[†],
T. Taylor[†], E. Tsesmelis[*], E. Weisse[§], and F. Zimmermann[§]

Abstract

We discuss a possible staged upgrade of the LHC and of its injectors, with a view to increasing the luminosity from the nominal $10^{34}\,\mathrm{cm^{-2}\,s^{-1}}$ to $10^{35}\,\mathrm{cm^{-2}\,s^{-1}}$ in each of the two high-luminosity experiments. We also consider possible scenarios for an upgrade to a proton beam energy of about 14 TeV. Starting from beam dynamics considerations and fundamental limitations of the hardware subsystems, we derive realistic requirements for the major components, such as superconducting magnets, cryogenic and RF systems, beam dump and vacuum. We also discuss a novel approach to the optimization of the collider performance, compatible with the beam-beam limit for high intensity proton bunches or long 'super-bunches', and sketch a new design of the interaction regions, including an alternative beam crossing scheme. Finally we identify further studies required for an LHC performance upgrade and propose an R&D programme.

[*]CERN–EST Division
[†]CERN–LHC Division
[‡]CERN–PS Division
[§]CERN–SL Division
[¶]CERN–TIS Division

Contents

1   Introduction and Summary

The first LHC design study [1] considered a machine with a peak luminosity of $1.4 \times 10^{33}\,\mathrm{cm^{-2}\,s^{-1}}$ at 8 TeV proton beam energy. Possible ways to attain luminosities significantly higher than at the SSC were first discussed in Ref. [2] and later included in a subsequent design study [3]. The final LHC conceptual design [4] describes a challenging machine, optimised for a nominal luminosity of $10^{34}\,\mathrm{cm^{-2}\,s^{-1}}$ at 7 TeV proton beam energy. In order to exploit fully the potential of the machine, of the injectors, and of the detectors, possible routes to increase the LHC luminosity by an order of magnitude and to double its energy have been explored in Refs. [5, 6]. As explained in Section 2 and in Ref. [7], there is a strong physics interest for such a performance upgrade, that would significantly extend the reach of the LHC and enable precision measurements of rare processes.

The present feasibility study is the result of discussions and investigations by a task force set up in July 2001. Since the effective working time of the task force has been less than three months, we only sketch some baseline options and discuss a few alternative solutions, identifying further studies required for an LHC machine upgrade and proposing an R&D programme. We discuss scenarios for a staged upgrade of the LHC and of its injectors, compatible with established accelerator design criteria and fundamental limitations of the hardware subsystems, aiming at a target luminosity in proton operation of $10^{35}\,\mathrm{cm^{-2}\,s^{-1}}$ in each of the two high-luminosity experiments and consider an upgrade to a proton beam energy of about 14 TeV. An interesting outcome of these discussions has been a novel approach to the optimization of the collider performance, compatible with the beam-beam limit for high intensity proton bunches or long 'super-bunches'.

Any upgrade beyond the nominal LHC performance, including the so called 'ultimate luminosity' of $2.3 \times 10^{34}\,\mathrm{cm^{-2}\,s^{-1}}$ (see Table 1), will be considered as an LHC upgrade and shall be addressed in this feasibility study. We therefore consider the following three phases:
- LHC Phase 0: maximum performance without hardware changes,
- LHC Phase 1: maximum performance keeping the LHC arcs unchanged,
- LHC Phase 2: maximum performance with 'major' hardware changes.

1.1   LHC performance limitations and approximate scaling laws

The LHC performance will be limited by several fundamental effects:
- Magnetic field quality and lattice corrector schemes define the so-called dynamic aperture, i.e. the maximum stable amplitude of single particle betatron oscillations. This sets an upper bound for the beam transverse emittance ε at injection (dynamic aperture dominated by the field quality of the main dipoles) and for the full crossing angle θ_c in collision (dynamic aperture dominated by field quality and beam offsets in the triplet quadrupoles). The maximum crossing angle is also limited by the aperture of the triplet quadrupoles.
- The dynamic aperture is reduced by long range beam-beam encounters. This sets a lower bound for the beam separation at injection and for the crossing angle in collision.
- The single beam intensity is limited by collective effects, both in the LHC and in the injectors, by beam loading and cryogenic heat load, as well as by vacuum, machine protection, and beam dump considerations. Collective effects in the LHC are discussed in Section 6. In particular, depending on the bunch spacing and the secondary electron yield of the beam screen surface, electron cloud effects may be the main limit to the single beam intensity. According to observations at the CERN

parameter	symbol	units	nominal	ultimate	Piwinski
number of bunches	n_b		2808	2808	2808
bunch spacing	Δt_sep	ns	25	25	25
protons per bunch	N_b	10^{11}	1.1	1.7	2.6
average beam current	I_av	A	0.56	0.86	1.32
normalised transv. emittance	ε_n	μm	3.75	3.75	3.75
longitudinal emittance	ε_L	eV s	2.5	2.5	4.0
peak RF voltage	V_RF	MV	16	16	3/1
RF frequency	f_RF	MHz	400.8	400.8	200.4/400.8
r.m.s. bunch length[†]	σ_z	cm	7.55	7.55	15.2
r.m.s. energy spread	σ_E	10^{-4}	1.13	1.13	0.9
IBS long. emitt. growth time[†]	$\tau_{z,\mathrm{IBS}}$	h	65	42	33
IBS hor. emitt. growth time[†]	$\tau_{x,\mathrm{IBS}}$	h	111	72	87
beta at IP1-IP5	β^*	m	0.5	0.5	0.5
full crossing angle[†]	θ_c	μrad	300	315	345
diffusive aperture	d_da	σ	6.3	6.0	6.0
Piwinski parameter	$\theta_\mathrm{c}\sigma_z/\sigma^*$		1.43	1.50	3.29
luminosity reduction factor	F		0.81	0.80	0.52
peak luminosity at IP1-IP5	L	$10^{34}\,\mathrm{cm}^{-2}\,\mathrm{s}^{-1}$	1.0	2.3	3.6

Table 1: List of nominal and ultimate LHC parameters at 7 TeV. The last column refers to operation with large 'Piwinski parameter'. The corresponding beam-beam tune footprints, discussed in Section 3, are compared in Fig. 1. [†] The r.m.s. bunch length corresponds to a Gaussian bunch distribution and the IBS growth times are computed by the Bjorken-Mtingwa formalism implemented in MAD [8] for the LHC collision optics version 6.4, with momentum compaction factor $\alpha_\mathrm{p} = 3.225 \times 10^{-4}$. Note that earlier optics versions are still assumed in some of the following sections together with a nominal crossing angle of $300\,\mu$rad for ultimate beam intensity at nominal $\beta^* = 0.5$ m (respectively $\theta_\mathrm{c} = 414\,\mu$rad at $\beta^* = 0.25$ m), although the corresponding diffusive aperture drops below $6\,\sigma$ and may turn out to be insufficient.

SPS, the threshold bunch intensity for electron cloud build-up scales linearly with the bunch spacing.

− The beam emittance depends on the LHC injector complex. Specifically, space charge effects limit the beam brilliance $N_\mathrm{b}/\varepsilon_\mathrm{n}$, i.e. the ratio between number of particles per bunch and normalised transverse emittance $\varepsilon_\mathrm{n} = \beta\gamma\varepsilon$, where $\gamma = (1 - \beta^2)^{-1/2}$ denotes the relativistic Lorentz factor.

− The peak luminosity is limited by the nonlinear beam-beam interaction. In particular the total beam-beam tune spread, i.e. the amplitude dependent detuning caused by head-on and parasitic collisions in *all* the IPs, should not exceed 0.01 so that the corresponding betatron 'tune footprint', discussed in Section 3, can be accommodated in between resonances of order lower than or equal to 12. Note that so-called 'Pacman bunches', near the edge of the bunch trains, experience different numbers of long range collisions and may have significantly different beam-beam footprints. Coherent beam-beam effects in the so-called strong-strong regime may also limit the LHC performance [9].

− The linear tune shift due to long range encounters cancels if half of the beam-beam crossings take place in the vertical and the other half in the horizontal plane:
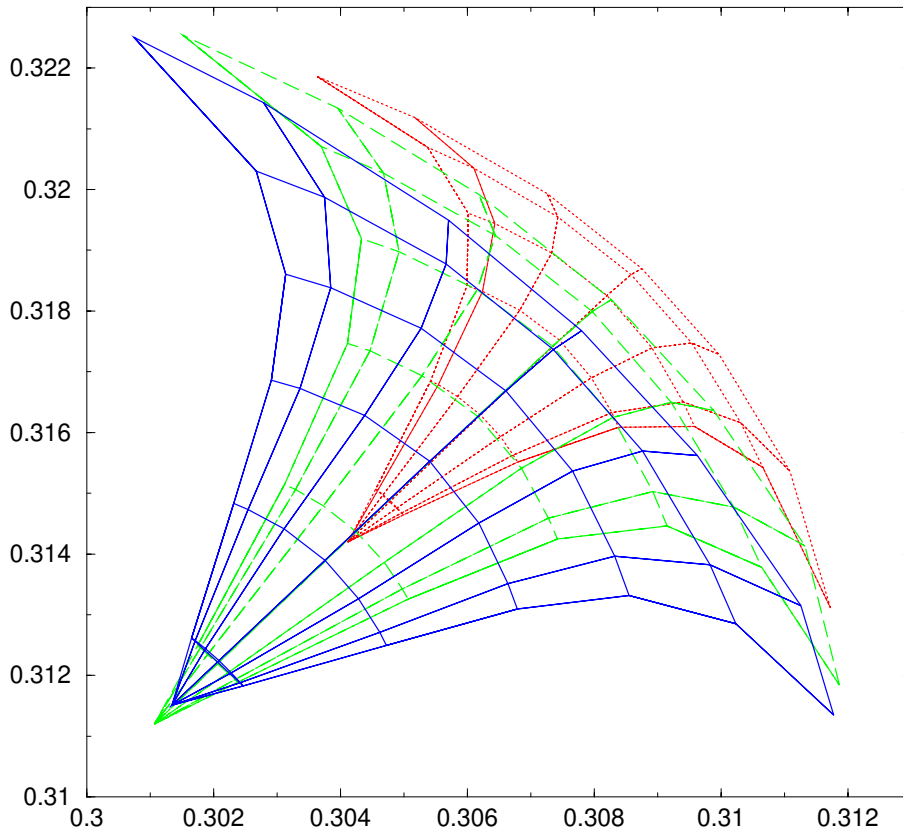
Figure 1: Comparison of beam-beam tune footprints for regular bunches, corresponding to betatron amplitudes extending from 0 to $6\,\sigma$, for LHC nominal (dotted, red line), ultimate (dashed, green line), and large Piwinski parameter configuration (solid, blue line) with two interaction points and alternating horizontal-vertical crossing planes (see Table 1).

this is true also for 'Pacman bunches' (see Section 3 and Ref. [10]). However the tune footprint for particles with large betatron amplitudes is somewhat increased, typically by about 10% (see Fig. 1). As a simplified performance criterion, in the following we therefore assume that the total linear tune shift due to head-on beam-beam collisions does not exceed 0.009. For round[1] proton beams colliding head-on in two IPs, the total linear beam-beam tune shift is $\Delta Q_{\mathrm{bb}} = \xi_{\mathrm{x}} + \xi_{\mathrm{y}} = (N_{\mathrm{b}}/\varepsilon_{\mathrm{n}})\,r_{\mathrm{p}}/2\pi$, with r_{p} the classical proton radius, and depends only on the beam brilliance.

– The luminosity lifetime depends on the rate of nuclear interactions between the two beams and with the rest gas, and on several mechanisms governing the transverse beam size, i.e., blow-up due to intra-beam scattering (IBS), nonlinear beam-beam interaction and possibly electron cloud, and damping due to synchrotron radiation. The horizontal IBS growth rate is approximately proportional to the particle density in the six-dimensional phase space.

– The integrated luminosity depends on the peak luminosity, on the luminosity lifetime and on the average machine turn-around time, as discussed in Section 5.

---

[1] Operation with flat beams is practically excluded in the LHC with the current two-in-one triplet configuration, since a reduction of the ratio β_y^*/β_x^* for one beam corresponds to a reduction of β_x^*/β_y^* for the counter-rotating beam.

For short bunches of length $\sigma_z \ll \beta^*$, the so-called 'hourglass effect' is negligible and the peak luminosity for round beams colliding with full crossing angle θ_c

$$L = \frac{N_b^2 f_{rep}}{4\pi\sigma^{*2}} F$$

is reduced by a factor $F \simeq 1/\sqrt{1 + \left(\frac{\theta_c\sigma_z}{2\sigma^*}\right)^2}$. Here $f_{rep} = n_b f_{rev}$ is the average bunch repetition frequency and $\sigma^* = \sqrt{\varepsilon\beta^*}$ the r.m.s. transverse beam size at the IP. The ratio $\theta_c\sigma_z/\sigma^*$ is known as 'Piwinski parameter'. If the beam intensity is limited by effects other than the beam-beam interaction, the baseline scheme to maximise luminosity consists in operating the machine with short bunches and minimum crossing angle, compatible with adequate beam separation to reduce the effect of long range collisions. As discussed in Section 6.1, however, the total linear tune shift for beams colliding with a crossing angle in alternating horizontal-vertical planes is also reduced by a similar factor

$$\Delta Q_{bb} = \xi_x + \xi_y = \frac{N_b r_p}{2\pi\varepsilon_n} F_{bb}.$$

For short bunches $F_{bb} \simeq F$. Therefore, if the bunch intensity is not limited by the injectors or by other effects in the LHC (*e.g.*, by the electron cloud build-up), it is possible to increase the luminosity without exceeding the beam-beam limit $\Delta Q_{bb} \sim 0.01$ by increasing the crossing angle and/or the bunch length. This alternative approach had not been considered in the original LHC design. Expressing the beam-beam limited bunch intensity N_b in terms of the beam-beam tune shift ΔQ_{bb}, the corresponding peak luminosity is given by the following approximate formula:

$$L = \gamma\Delta Q_{bb}^2 \frac{\pi\varepsilon_n f_{rep}}{r_p^2 \beta^*} \sqrt{1 + \left(\frac{\theta_c\sigma_z}{2\sigma^*}\right)^2}.$$

Another possibility to achieve significant luminosities with large crossing angles consists in colliding very long 'super-bunches', as discussed in Section 6.2 and Ref. [11]. It can be shown [12] that a few super-bunches with flat longitudinal distribution yield a luminosity $\sqrt{2}$ times higher than many short Gaussian bunches with the same total charge and beam-beam tune shift.

An approximate scaling law [13, 14] for the so-called 'diffusive aperture' d_{da} with long range beam-beam encounters is $(d_{sep} - d_{da})/\sigma \propto \sqrt{k_{par} N_b/\varepsilon_n}$, where $d_{sep}/\sigma \simeq \theta_c/\sigma_\theta$ is the relative beam separation (in units of the r.m.s. transverse beam size σ) at the k_{par} parasitic encounters, and $\sigma_\theta = \sqrt{\varepsilon/\beta^*}$ the r.m.s. angular beam divergence at the IP. Note that the ratio $(d_{sep} - d_{da})/\sigma$ is independent of the betatron function and the beam energy; it is again a function of the brilliance N_b/ε_n. For the nominal LHC beam emittance and separation scheme, with $k_{par} = 2 \times 32$ parasitic encounters around the two high luminosity experiments, this scaling law can be written

$$d_{da}/\sigma \simeq \theta_c \sqrt{\beta^*/\varepsilon} - 3\sqrt{N_b/10^{11}}$$

and is in qualitative agreement with particle tracking results [14, 15]. With nominal LHC crossing angle $\theta_c = 300\,\mu rad$ and r.m.s. angular beam divergence $\sigma_\theta = 31.7\,\mu rad$, the beam separation is $d_{sep} \simeq 9.5\,\sigma$ and the diffusive aperture $d_{da} \simeq 6 \div 6.5\,\sigma$ for nominal bunch intensity $N_b = 1.1 \times 10^{11}$ corresponds to a reduction by more than $3\,\sigma$. Preserving a comparable dynamic aperture in collision with higher bunch intensities, shorter bunch spacings (i.e., larger k_{par}), and/or smaller values of β^* requires larger crossing angles.

6

1.2 LHC Phase 0

As discussed in Section 3 and in Ref. [17], the nominal LHC performance at $7\,\mathrm{TeV}$ corresponds to a total beam-beam tune spread of 0.01, with a luminosity of $10^{34}\,\mathrm{cm^{-2}\,s^{-1}}$ in IP1 and IP5 (ATLAS and CMS), halo collisions in IP2 (ALICE) and low-luminosity in IP8 (LHC-b). The steps to reach ultimate performance without hardware changes are shown in Table 2.

---

1. collide beams only in IP1 and IP5 $\rightarrow \beta^* = 0.5\,\mathrm{m}$
2. increase crossing angle to $\theta_\mathrm{c} = 315\,\mu\mathrm{rad}$
3. increase bunch population up to the beam-beam limit $\rightarrow L = 2.3 \times 10^{34}\,\mathrm{cm^{-2}\,s^{-1}}$
4. optionally increase the dipole field to $9\,\mathrm{T}$ (ultimate field) $\rightarrow E_\mathrm{max} = 7.54\,\mathrm{TeV}$

Table 2: Steps for the LHC upgrade to ultimate performance: collisions in ATLAS and CMS only, with alternating horizontal-vertical crossing planes.

Assuming a maximum beam-beam tune spread of 0.01, the beam-beam limit is reached at the ultimate intensity $N_\mathrm{b} = 1.7 \times 10^{11}$ p/bunch and the corresponding ultimate luminosity in ATLAS and CMS is $2.3 \times 10^{34}\,\mathrm{cm^{-2}\,s^{-1}}$. It should be noted that, with nominal crossing angle and ultimate intensity, the diffusive aperture drops below $6\,\sigma$ and may turn out to be insufficient. To recover a diffusive aperture of at least $6\,\sigma$, the crossing angle has to be increased to about $315\,\mu\mathrm{rad}$ and the corresponding reduction of luminosity is negligible. If the LHC can be operated with a beam-beam tune spread larger than 0.01, the ultimate LHC luminosity may be compatible with halo collisions in ALICE. For example, one can choose a working point closer to the coupling resonance ($Q_x - Q_y = 0.005$ instead of 0.01) to reach a total beam-beam tune spread of 0.015, equal to the maximum achieved in the SPS $\mathrm{p\bar{p}}$ collider. Alternatively, it may be possible to reduce the total beam-beam tune spread by the help of compensation schemes, and in particular to reduce the effect of long range beam-beam encounters by means of pulsed electromagnetic lenses [16]. This would open up the possibility of a higher luminosity, provided the injectors can deliver beams with higher brilliance and higher intensity, as discussed in Section 11.1. The ultimate dipole field of $9\,\mathrm{T}$ corresponds to a proton beam energy of $7.54\,\mathrm{TeV}$ and to a beam current limited by cryogenics (see Section 10) and/or by beam dump considerations (see Section 12). The LHC parameters shown in Tables 1 and 5 refer to a beam energy of $7\,\mathrm{TeV}$.

---

1. collide beams only in IP1 and IP5 $\rightarrow \beta^* = 0.5\,\mathrm{m}$
2. increase longitudinal emittance and bunch length, for example to $\sigma_z = 15.2\,\mathrm{cm}$
3. increase crossing angle to $\theta_\mathrm{c} = 345\,\mu\mathrm{rad}$
4. increase bunch population (compatibly with electron cloud and other collective effects) up to the beam-beam limit $N_\mathrm{b} = 2.6 \times 10^{11} \rightarrow L = 3.6 \times 10^{34}\,\mathrm{cm^{-2}\,s^{-1}}$

Table 3: Possible steps for an LHC upgrade beyond ultimate luminosity with large Piwinski parameter: collisions in ATLAS and CMS only, with alternating horizontal-vertical crossing planes.

A possible luminosity upgrade scenario beyond ultimate performance, requiring further studies, is shown in Table 3. If the single bunch population can be increased above the ultimate intensity, keeping the same nominal transverse emittance, operation with large Piwinski parameter becomes interesting. With an increased crossing angle

of $345\,\mu$rad, nominal 25 ns bunch spacing and a bunch population $N_{\rm b} = 2.6 \times 10^{11}$, the diffusive aperture is about $6\,\sigma$, i.e. the same as for ultimate performance (the field quality of the LHC triplet magnets allows a maximum crossing angle of $400\,\mu$rad without significant degradation of the dynamic aperture). In principle, this does not require an upgrade of the injectors if one accepts shorter bunch trains in the PS and thus longer LHC filling times, as discussed in Section 11.1. However a crossing angle of $345\,\mu$rad requires a challenging orbit control during β-squeeze and may not be compatible with the foreseen installation of beam screens in the triplet magnets, resulting in a reduction of the available mechanical aperture. The bunch length has to be doubled in order not to exceed the beam-beam limit and an increased longitudinal emittance is required to reduce IBS growth rates and to avoid longitudinal beam instabilities. The tentative parameters reported in the last column of Table 1 correspond to the combined use of both 200 and 400 MHz RF systems and to a longitudinal emittance of 4 eV s. The use of a wide-band longitudinal feedback system can also be considered if the two RF systems together are insufficient to ensure beam stability. At 7 TeV the corresponding beam-beam limited luminosity is about $3.6 \times 10^{34}\,{\rm cm}^{-2}\,{\rm s}^{-1}$ in IP 1 and IP 5, assuming alternating crossing planes. In case of severe electron cloud problems, with this scheme the LHC could approach its nominal luminosity with a bunch spacing of 75 ns.

1.3   LHC Phase 1

Possible steps to increase the luminosity with hardware changes only in the LHC insertions and/or in the injector complex include the baseline scheme shown in Table 4.

1. modify insertion quadrupoles and/or layout $\rightarrow \beta^* = 0.25\,{\rm m}$
2. increase crossing angle by $\sqrt{2} \rightarrow \theta_{\rm c} = 445\,\mu$rad
3. increase bunch population up to ultimate intensity $\rightarrow L = 3.3 \times 10^{34}\,{\rm cm}^{-2}\,{\rm s}^{-1}$
4. halve bunch length with high harmonic RF system $\rightarrow L = 4.6 \times 10^{34}\,{\rm cm}^{-2}\,{\rm s}^{-1}$
5. increase number of bunches (compatibly with electron cloud effects and long range beam-beam encounters) $\rightarrow L \sim 6 \div 7 \times 10^{34}\,{\rm cm}^{-2}\,{\rm s}^{-1}$

Table 4: Baseline scheme for an LHC luminosity upgrade: collisions in ATLAS and CMS only, with alternating horizontal-vertical crossing planes.

Possible modifications of the insertion layout to reach $\beta^* = 0.25\,{\rm m}$ are discussed in Section 4 and include separation dipoles closer to the IP to reduce the effect of long range beam-beam collisions: the corresponding reduction of the beam-beam tune spread is not included in the present luminosity estimates which require further studies. The reason to increase the (ultimate) crossing angle by $\sqrt{2}$ for half the nominal β^* is to keep the same relative beam separation $\theta_{\rm c}\sqrt{\beta^*/\varepsilon}$ and thus the same (small) contribution of long range collisions to the beam-beam footprint. The corresponding luminosity reduction factor is $F = 0.56$ and the luminosity for ultimate bunch intensity is only $3.3 \times 10^{34}\,{\rm cm}^{-2}\,{\rm s}^{-1}$. Note, however, that the bunch intensity is no longer beam-beam limited. With half the nominal bunch length one can recover the nominal reduction factor $F = 0.8$ and reach a beam-beam limited luminosity of $4.6 \times 10^{34}\,{\rm cm}^{-2}\,{\rm s}^{-1}$ at ultimate bunch intensity. Such a 'modest' luminosity upgrade requires a relatively expensive high harmonic RF system, discussed in Section 11.3, to reduce the bunch length. The longitudinal emittance and the horizontal IBS growth time are reduced by approximately $\sqrt{2}$, as shown in Table 5.

parameter	symbol	units	baseline	Piwinski	super-bunch
number of bunches	n_b		2808	2808	1
bunch spacing	Δt_{sep}	ns	25	25	
protons per bunch	N_b	10^{11}	1.7	2.6	5600
average beam current	I_{av}	A	0.86	1.32	1.0
norm. transv. emittance	ε_n	μm	3.75	3.75	3.75
longitudinal emittance	ε_L	eV s	1.78	2.5	15000
peak RF voltage	V_{RF}	MV	43	16	3.4
RF frequency	f_{RF}	MHz	1202.4	400.8	10
r.m.s. bunch length	σ_z	cm	3.78	7.55	7500
r.m.s. energy spread	σ_E	10^{-4}	1.60	1.13	5.8
IBS long. emitt. growth time	$\tau_{z,IBS}$	h	50	28	856
IBS hor. emitt. growth time	$\tau_{x,IBS}$	h	42	46	63
beta at IP1-IP5	β^*	m	0.25	0.25	0.25
full crossing angle	θ_c	μrad	445	485	1000
diffusive aperture	d_{da}	σ	6.0	6.0	6.0[†]
Piwinski parameter	$\theta_c \sigma_z/\sigma^*$		1.50	3.27	
luminosity reduction factor	F		0.80	0.53	
peak luminosity at IP1-IP5	L	$10^{34}\,\mathrm{cm^{-2}\,s^{-1}}$	4.6	7.2	9.0

Table 5: List of LHC parameters at 7 TeV corresponding to possible luminosity upgrade scenarios with reduced β^*. [†] The last column refers to one or several flat super-bunches, with a total length of about 260 m, confined by barrier buckets. The corresponding estimate of diffusive aperture requires further studies (see Ref. [12]).

With a *reduced bunch spacing* of 15 ns (respectively 12.5 ns) and *ultimate bunch intensity*, one would be able to reach a luminosity of $7.7 \times 10^{34}\,\mathrm{cm^{-2}\,s^{-1}}$ (respectively $9.2 \times 10^{34}\,\mathrm{cm^{-2}\,s^{-1}}$). However, as discussed in Section 6.3, electron cloud effects are expected to severely limit the bunch intensity for a bunch spacing shorter than 25 ns. Moreover, an increased number of long range beam-beam encounters leads to a further reduction of dynamic aperture and to an increased tune footprint, unless beam-beam compensation schemes are successfully implemented or the crossing angle is further increased. Therefore the maximum luminosity with the baseline scheme will presumably never exceed $6 \div 7 \times 10^{34}\,\mathrm{cm^{-2}\,s^{-1}}$. In the baseline scheme, operation with bunched beams and large crossing angles of several mrad, to pass each beam through separate final quadrupoles of reduced aperture, would require crab cavities to avoid a severe luminosity loss (see Appendix A.1).

If the single bunch population can be increased above the ultimate intensity, keeping the same nominal transverse emittance, operation with large Piwinski parameter allows us to reach a luminosity of $7.2 \times 10^{34}\,\mathrm{cm^{-2}\,s^{-1}}$ with nominal bunch length and nominal bunch spacing. The logical steps are summarized in Table 6 and correspond to those of Table 3 with the same bunch population and the same Piwinski parameter, therefore the crossing angle is scaled by $\sqrt{2}$. Other parameters are shown in Table 5.

There is an interesting alternative scheme to increase the LHC luminosity, based on very long 'super-bunches', as shown in Table 7. The crossing angle can be possibly increased to several mrad, to pass each beam through separate final quadrupoles of reduced aperture, as discussed in Section 4. As shown in Section 6.2 and further discussed in

> 1. modify insertion quadrupoles and/or layout $\rightarrow \beta^* = 0.25\,\mathrm{m}$
> 2. increase crossing angle to $\theta_\mathrm{c} = 485\,\mu\mathrm{rad}$
> 3. increase bunch population (compatibly with electron cloud and/or IBS) up to the beam-beam limit $N_\mathrm{b} = 2.6 \times 10^{11} \rightarrow L = 7.2 \times 10^{34}\,\mathrm{cm^{-2}\,s^{-1}}$

Table 6: Possible steps for an alternative LHC luminosity upgrade with large Piwinski parameter: collisions in ATLAS and CMS only, with alternating horizontal-vertical crossing planes.

Ref. [12], a beam current of $1\,\mathrm{A}$ distributed in one or several long super-bunches in each LHC ring, with a total length around $300\,\mathrm{m}$, would be compatible with the beam-beam limit and the corresponding luminosity in ATLAS and CMS (with alternating horizontal-vertical crossing planes) would be about $9 \times 10^{34}\,\mathrm{cm^{-2}\,s^{-1}}$, as shown in the last column of Table 5. The super-bunch option is very interesting for large crossing angles, although it represents a somewhat 'irreversible' choice. It can potentially avoid electron cloud effects and minimize the cryogenic heat load, as discussed in Section 10. However the associated RF manipulations and beam parameters are challenging and require further studies. To keep the pile-up in the experimental detectors down to a reasonable level, the minimum number of super-bunches is estimated to be around 100 [18].

> 1. modify insertion quadrupoles and layout $\rightarrow \beta^* = 0.25\,\mathrm{m}$
> 2. upgrade the detectors $\rightarrow$ effective length of about $20 \div 30\,\mathrm{cm}$
> 3. inject a bunched beam of about $1\,\mathrm{A}$ and accelerate it to $7\,\mathrm{TeV}$
> 4. use barrier buckets to form one or several long super-bunches (see Section 11.4)
> 5. collide super-bunches with a large crossing angle $\rightarrow L \sim 9 \times 10^{34}\,\mathrm{cm^{-2}\,s^{-1}}$.

Table 7: Alternative 'super-bunch scheme' for an LHC luminosity upgrade: collisions in ATLAS and CMS only, with alternating horizontal-vertical crossing planes.

1.4 LHC Phase 2

Possible steps to increase the LHC performance with 'major' hardware changes in the LHC arcs and/or in the injectors include:

— Modify the injectors to significantly increase the brilliance beyond its ultimate value (in conjunction with beam-beam compensation schemes).

— Equip the SPS with superconducting magnets to inject in the LHC at $1\,\mathrm{TeV}$. This implies also a corresponding upgrade of the transfer lines. For given mechanic and dynamic apertures at injection, this option can potentially increase the LHC luminosity by nearly a factor two, in conjunction with higher bunch intensities at constant beam-beam parameter $N_\mathrm{b}/\varepsilon_\mathrm{n}$ and long range beam-beam compensation schemes. Indeed bunch intensity and normalised emittance could be increased by a factor two, keeping the same transverse beam size at injection. The beam size in collision would increase by a factor $\sqrt{2}$ and the relative beam separation would proportionally decrease, leading to a significant reduction of the diffusive aperture unless long range beam-beam effects can be compensated. A Super-SPS would also be the natural first step in view of an LHC energy upgrade, since the corresponding energy swing would be reduced by a factor two.

— Install new superconducting dipoles in the LHC arcs to reach a beam energy around $12.5\,\mathrm{TeV}$. The energy upgrade is much easier to exploit than a luminosity upgrade

as it requires minimal changes to the detectors. Dipole magnets with a nominal field of 15 T and a safety margin of about 2 T can be considered a reasonable target for 2015 and could be operated by 2020. This requires a serious R&D programme on new superconducting materials, as discussed in Section 7.

1.5 Conclusions and recommendations

Reaching the nominal LHC performance is a challenging task. The emittance budget through the injector chain is tight and we have to learn how to overcome electron cloud effects, inject into the LHC ring, accelerate and collide almost 6000 high intensity proton bunches, protect superconducting magnets and experiments, safely dump the beams, etc. Attaining or exceeding the ultimate LHC performance will be even more challenging. Further accelerator physics studies in view of a luminosity upgrade, *e.g.*, by optimizing machine operation near the beam-beam limit, will be directly applicable also to reach nominal machine performance, *e.g.*, with fewer bunches of higher intensity. Similarly, investigating and overcoming intensity limitations in the LHC and its injectors is essential for a fast and effective reduction of electron cloud effects by beam scrubbing. A summary of possible scenarios for the LHC performance upgrade and their implications for the cryogenic system is compiled in Tables 17 and 19.

The present feasibility study has not considered required upgrades of beam instrumentation and possible flat beam schemes at 7 TeV. Also field quality issues for the new magnets have not been addressed. Further studies are needed to compare advantages and disadvantages of long super-bunches versus conventional bunched beams and to finalize the Interaction Region layout. Some experience with barrier buckets may be gained at CERN in connection with the Low Energy Ion Ring (LEIR) project for LHC ion accumulation.

Upgrades in beam intensity and brilliance are a viable option for a staged increase of the LHC luminosity. A possibility being considered also for CNGS beams is to upgrade the proton linac from 50 to 120 MeV, to overcome space charge limitations. Then the ultimate LHC intensity would become very easy to achieve and a further 30% increase would be possible with almost the same emittance. This requires R&D for cryogenics, vacuum, RF, beam dump, radiation issues, and injectors, and operation with large crossing angles. Machine experiments at colliders with large Piwinski parameter and many bunches are important. Beam-beam compensation schemes with pulsed wires can reduce tune footprints and loss of dynamic aperture due to long range collisions. They need experimental validation.

New triplet quadrupoles with high gradient and larger aperture, and/or alternative IR layouts, are needed for the LHC Phase 1 luminosity upgrade with reduced β^*. Increasing the quadrupole aperture has the additional advantage of letting through radiation. A baseline IR design exists based on 200 T/m Nb_3Sn quadrupoles with 90 mm coil aperture. Higher gradients can be reached with new conventional or high temperature superconductors. Some of the related beam dynamics and magnet technology issues have been addressed in a collaboration meeting on the LHC IR upgrade, held at CERN in March 2002 [19] and have been recently reviewed in [20].

An increased injection energy into the LHC, in conjunction with long range beam-beam compensation schemes, would yield a proportional luminosity gain. A pulsed Super-SPS and new superconducting transfer lines could also be the first step for an LHC energy upgrade. An interesting alternative to increase the injection energy into the LHC (or Super-LHC) is to use the present SPS as injector and introduce cheap, compact low field

booster rings in the LHC tunnel. Dipole magnets with a nominal field of 15 T can be considered a reasonable target for 2015. This would allow us to reach a proton beam energy around 12.5 TeV in the LHC tunnel, but requires a vigorous R&D programme on new superconducting materials.

In the following sections we review different aspects of the LHC upgrade, ranging from physics motivation and beam dynamics considerations to technological challenges associated with superconducting magnets, cryogenic and RF systems, beam dump and vacuum.

References

[1] G. Brianti and K. Hübner (eds.), *The Large Hadron Collider in the LEP tunnel*, CERN report 87-05 (1987).

[2] J. Gareyte, *Towards very high luminosities in the LHC*, CERN SPS/88-7 (AMS) and LHC Note 70 (1988).

[3] The LHC Study Group, *Design Study of the Large Hadron Collider (LHC)*, CERN report 91-03 (1991).

[4] P. Lefevre and T. Pettersson (eds.), *The Large Hadron Collider, Conceptual Design*, CERN/AC/95-05 (LHC) (1995).

[5] K. Hübner, *Status of CERN*, CERN SL-2001-008, presented at the 18th International Conference on High Energy Accelerators (HEACC2001), Tsukuba, Japan, 26–30 March 2001.

[6] F. Zimmermann, *Luminosity Limitations at Hadron Colliders*, CERN SL-2001-009-AP (2001), presented at the 18th International Conference on High Energy Accelerators (HEACC2001), Tsukuba, Japan, 26–30 March 2001.

[7] F. Gianotti, M.L. Mangano, and T.S. Virdee, *Physics potential and experimental challenges of the LHC luminosity upgrade*, CERN-TH-2002-078 (2002), see also ICFA Seminar on 'Future Perspectives in High Energy Physics', CERN, 8–11 October 2002, `http://dsu.web.cern.ch/dsu/of/icfasource.html`.

[8] H. Grote and F.C. Iselin, *The MAD Program, User's Reference Manual*, CERN SL/90-13 (AP) (Rev. 4) (1995), see also J. Bjorken and S. Mtingwa, Part. Acc. **13**, 115 (1983).

[9] Y. Alexahin, H. Grote, W. Herr, and M.P. Zorzano, *Coherent Beam-Beam Effects in the LHC*, CERN LHC Project Report 469 (2001), presented at the 18th International Conference on High Energy Accelerators (HEACC2001), Tsukuba, Japan, 26–30 March 2001.

[10] W. Herr, *Features and implications of different LHC crossing schemes*, CERN LHC Project report in preparation (December 2002).

[11] F. Ruggiero and F. Zimmermann, *Luminosity Optimization near the Beam-Beam Limit by Increasing Bunch Length or Crossing Angle*, CERN SL-2002-005-AP (2002) and Phys. Rev. ST Accel. Beams. **5**, 061001 (2002).

[12] F. Ruggiero, G. Rumolo, F. Zimmermann, Y. Papaphilippou, *Beam dynamics studies for uniform (hollow) bunches or super-bunches in the LHC: beam–beam effects, electron cloud, longitudinal dynamics, and intra-beam scattering*, presented at the International Workshop on 'Recent Progress in Induction Accelerators' (RPIA2002), KEK, Japan, 29–31 October 2002, and LHC Project Report 627.

[13] J. Irwin *Diffusive losses from SSC particle bunches due to long-range beam-beam interactions*, SSC-233 (1989).

[14] Y. Papaphilippou and F. Zimmermann, *Weak-strong beam-beam simulations for the LHC*, in Proc. Workshop on Beam-Beam Effects in Large Hadron Colliders (LHC99), CERN, Geneva, Switzerland, 12–17 April 1999, eds. J. Poole and F. Zimmermann (CERN SL-99-039-AP, 1999), pp. 95–107. and F. Zimmermann, *Diffusive aperture due to long range collisions at injection and image charge effects*, CERN LHC Project Note 250 (2001).

[15] H. Grote, F. Schmidt, and L.H.A. Leunissen, *LHC Dynamic Aperture at Collision*, CERN LHC Project Note 197 (1999), see also Y. Luo and F. Schmidt, *Weak-strong beam-beam tracking for LHC v6.1*, in CERN LHC Project Report 502 (2001), presented at the Workshop on Beam-Beam Effects, Fermilab, Batavia, IL, USA, 25–28 June 2001.

[16] J.-P. Koutchouk, *Correction of the Long-Range Beam-Beam Effect in LHC using Electro-Magnetic Lenses*, CERN SL-2001-048-BI (2001) and Proc. IEEE Particle Accelerator Conference (PAC2001), Chicago, IL, USA, 18–22 June 2001, eds. P. Lucas and S. Webber (IEEE, Piscataway, NJ, 2001), pp. 1681–1683.

[17] H. Grote and W. Herr, *Nominal and ultimate luminosity performance of the LHC*, CERN LHC Project Note 275 (2002).

[18] T.S. Virdee, private communication (November 2002).

[19] LHC IR Upgrade Collaboration Meeting, CERN, 11-12 March 2002, see web site at `http://cern.ch/lhc-proj-IR-upgrade`.

[20] T. Taylor, *Superconducting magnets for a super LHC*, CERN LHC Project Report 570 (2002), presented at the 8th European Particle Accelerator Conference (EPAC2002), La Vilette, Paris, France, 3–7 June 2002.

2   Motivation for the Super-LHC

Over the next decade at the LHC and at the Tevatron, precision tests of the Standard Model (SM) will be performed and physics beyond the SM will be explored to an unprecedented reach. The main motivation for a Super-LHC machine to follow the LHC is to explore the physics beyond the SM, while at the same time completing the SM physics started at the LHC. Among the physics issues to be addressed at the Super-LHC are [1, 2]:

− Precision SM physics, for example anomalous gauge boson couplings WWV (where V=γ, Z).
− SM Higgs boson physics.
− Supersymmetry.
− Strong electroweak symmetry breaking.
− New gauge bosons.
− Compositeness (excited quarks and leptons).
− Extra dimensions.

In order to extend the reach of the LHC to high-mass systems in these sectors and to make precision measurements on rare processes, an increase in the luminosity and/or energy is seen as being imperative. The Super-LHC scenarios considered in this report are a luminosity upgrade to $10^{35}\,\mathrm{cm^{-2}\,s^{-1}}$ and/or an energy upgrade to $\sqrt{s} = 28\,\mathrm{TeV}$.

Contrary to what is sometimes assumed, it is not necessary to increase the luminosity proportionally to the square of the increase in energy in order to produce the same number of events. In general, a factor of two increase in the energy corresponds to a factor of about ten increase in the luminosity as the production cross-sections increase by this latter factor. This is because the larger the energy, the smaller the Bjorken-x values of the colliding particles, resulting in a large increase in the cross-section due to the increase of the parton distribution functions at low Bjorken-x values.

In particular, physics processes involving the production of high-mass systems such as exist in the Higgs, Supersymmetry and Extra Dimension sectors have cross-sections which rise rapidly with energy. For example, the production rates of squarks and gluinos can be more than ten times larger at 28 TeV than at 14 TeV for masses greater than 2 TeV. In the case of SUSY Higgs, there are regions of the parameter space where only one Higgs state (h) is likely to be seen at the LHC. In the case of $m_A = 500\,\mathrm{GeV}$ the energy upgrade increases the H/A cross-section by approximately a factor of five thereby increasing the discovery potential for heavy Higgs bosons. Here H and A denote two other SUSY Higgs states.

In general, the energy upgrade is much easier to exploit than a luminosity upgrade as it requires minimal changes to the detectors. It can significantly enhance the physics reach of the LHC by almost a factor of two in terms of mass. If new physics is discovered then the energy upgrade will allow significant further study of the new physics, such as precision measurements of the Higgs couplings to fermions and bosons. In addition, precision tests of the SM can be improved because of the larger statistics expected when running at the higher energy.

The luminosity upgrade also has the potential to significantly enhance the LHC capability. In particular, a significant increase in the reach and precision measurements can be made with an integrated luminosity of 3000 fb^{-1}, assumed to be delivered at an instantaneous luminosity of $10^{35}\,\mathrm{cm^{-2}\,s^{-1}}$ over a reasonable number of years. As is well-known, the guiding figure is the integrated luminosity rather than the instantaneous luminosity.

For an upgrade in the luminosity to be fully exploited, it is important that the performance of the detectors remains at the same level as at the LHC. Major detector upgrades would be needed in order to fully exploit the factor of ten increase in luminosity [3]. In view of this, it is assumed that a detector R&D programme directed towards the Super-LHC, and similar to that launched in the early 1990's for the LHC, would be put in place.

The inner detector would probably need to be changed as a whole. Among the main problems will be the factor of ten increase in occupancy. The high track multiplicity due to the many interactions per bunch crossing is a potential problem as efficient b- and τ-tagging and electron identification become more difficult. In general, in order to preserve the LHC pattern recognition, and momentum resolution, the detector cell sizes must be decreased by a factor of ten. Moreover, due to the high radiation levels, R&D for new pixel detectors to survive the exceedingly high radiation level as exists at a radius $r < 20$ cm would be required. Also, technology used for LHC pixels must be developed for the region 20 cm $< r < 60$ cm for the Super-LHC and that for the LHC Si microstrip detectors must be developed for the region $r > 60$ cm for the upgrade. Finally, R&D on radiation-tolerant electronics would be required. The extent of such upgrades results in the replacement of large parts of the inner detectors.

The calorimeters will have a three times larger pile-up noise. An acceptable measurement for electrons, photons and jets, as required for the high-mass physics, should be possible but a degradation of the forward jet tagging and low-p_T jet veto would result in a worse signal-to-background ratio for some channels. Whereas the technology employed for the LHC is adequate for luminosities up to 10^{34} cm^{-2} s^{-1}, R&D would be required in some cases for the Super-LHC primarily for the end-cap and forward calorimeters, including the active media and electronics.

The ATLAS and CMS muon systems are designed with a minimum safety factor of between three and five with respect to background calculations. The increase in radiation would require a more robust shielding of the Muon Spectrometers at the price of a reduced forward acceptance. An R&D programme would be required to study the limit of the current detectors and to explore different detector technologies. The goal of the programme would be to balance a high-η acceptance with robust detectors versus the requirement for shielding and reduced acceptance.

Concerning the Trigger and DAQ, a bunch spacing reduced by up to about a factor of two, as part of the drive to higher luminosities, would require modifications to the Level-1 trigger and front-end electronics. It would be of benefit to re-build the LVL-1 trigger to operate at higher frequencies matching the bunch spacing. R&D would be required for the data movement at the higher frequencies at LVL-1, for the synchronisation Timing and Trigger Control (TTC), and for processing at the higher frequencies. For the higher-level triggers and DAQ, the issues relate to handling the increased bandwidth.

An increase in instantaneous luminosity may require positioning the low-β quadrupoles closer to the interaction point than that needed at the LHC. If this were to be the scheme chosen, then a re-design of the calorimeters, muon detectors and radiation shielding in the forward region would probably be needed. Integrating the shielding with the calorimeters would be one option to provide a compact lay-out.

Moreover, the option discussed in this report of increasing the machine luminosity by incorporating a single super-bunch of length 300 m and 1 A current would require the effective detector lengths to be extended to between 20 and 30 cm for a β^* of 0.25 m. This would add to the need to re-design the inner tracking detectors and the trigger.

However, it should be noted that a Super-LHC without any major detector upgrades, namely by using only the final states of high p_T jets, photons and muons is expected to provide about a 20-30% improvement in the mass reach for new physics. This increase is significant for signals at the limit of the LHC sensitivity.

The LHC B-physics programme is not expected to benefit from a luminosity or energy upgrade. The programme will be for the most part completed at the luminosities and energy of the LHC.

For the case of heavy-ions, the LHC will be statistically limited for some processes in Pb-Pb collisions and a factor of ten increase in luminosity could have an impact in this field. However, due to the very large nuclear cross-sections, the beam lifetime, and hence the integrated luminosity, would be reduced significantly, perhaps compromising to a large extent any gain in the instantaneous luminosity. An increase in energy seems not to be attainable as the physics processes increase by $\log s$, making a useful energy increase out of reach.

Therefore, the two high-luminosity pp experiments, ATLAS and CMS, and the one heavy-ion experiment ALICE, can potentially add to their physics reach from a Super-LHC, although this report focuses on the machine requirements for the high luminosity pp physics. It is assumed that the detectors would be installed and ready in about 2012 [3].

References

[1] G. Azuelos *et al.*, *Physics in ATLAS at a Possible Upgraded LHC*, ATL-COM-PHYS-2000-030, March 2001.

[2] F. Gianotti, *Presentation to Joint CERN EP-TH Divisions Faculty Meeting*, January 2001.

[3] J. Virdee, *Presentation to the Scientific Policy Committee*, September 2001.

Part I
Beam dynamics

3   Beam-beam effects

One of the limiting factors in high luminosity machines comes from beam-beam effects, i.e. the interaction of the two beams when they meet. The effects are numerous and can be separated into two classes: head-on effects, normally in the centre of experiments and long range interactions at unwanted, parasitic encounters when the beams travel in a common beam pipe. The strengths of both types are usually characterized and measured in terms of the resulting tune shift and non-linear tune spread. Although the problem is much more involved, the comparison of beam-beam effects in a single machine with varying parameters can be done in these units.

3.1   Head-on beam-beam effects

The collision of two beams at a crossing angle falls into the category of head-on collisions since the centres of the bunches normally meet. The beam-beam parameter ξ of a head-on collision can be written as:

$$\xi_{x,y} = \frac{N_{\rm b} r_0 \beta_{x,y}}{2\pi\gamma\sigma_{x,y}(\sigma_x + \sigma_y)} \tag{1}$$

where r_0 is the classical particle radius, $(r_{\rm e}, r_{\rm p})$, $N_{\rm b}$ the number of particles per bunch, and σ_x and σ_y the beam sizes at the interaction point (IP) in the horizontal and vertical planes. For small values ξ corresponds to the tune shift of small amplitude particles. When the operation is beam-beam limited, this determines the bunch intensity and/or the usable emittance. It is worth mentioning that for short round beams, as in the case of the LHC, the head-on tune shift does not depend on the optics at the interaction point, in particular not on $\beta^*_{x,y}$.

The expression for the luminosity of the LHC is given by:

$$L = \frac{N_{\rm b}^2 n_{\rm b} f_{\rm rev}}{4\pi\sigma_x\sigma_y} F \tag{2}$$

where $n_{\rm b}$ the number of bunches per beam and $f_{\rm rev}$ the ring revolution frequency. In the presence of a finite crossing angle in one plane, let us say the vertical in the following calculations, the luminosity is reduced by a factor F. This factor depends on the crossing angle $\theta_{\rm c}$ and the bunch length σ_z. Assuming a negligible dispersion at the collision point, we have:

$$F^{-1} = \frac{\sigma_y^{\rm eff}}{\sigma_y} = \sqrt{1 + \left(\frac{\theta_{\rm c}\sigma_z}{2\sigma_y}\right)^2} \tag{3}$$

where $\theta_{\rm c}$ is the full crossing angle.

The ratio $\frac{\theta_{\rm c}\sigma_z}{\sigma_y}$ is often called normalised crossing angle or also 'Piwinski ratio': it is a measure for the strength of transverse and longitudinal coupling, possibly leading to synchro-betatron resonances and therefore should be kept small, if possible. This is the baseline scheme historically adopted to optimize the operation of existing colliders. The alternative approach based on large Piwinski ratios or long super-bunches, discussed in Section 6, needs further validation by machine experiments.

3.2 Long range beam-beam effects

While an easy expression can be written down for head-on beam-beam effects, the dynamics of long range interactions is much more complicated. It depends on the beam parameters as well as on the geometry of the interaction region and on the optics. Reliable expressions cannot be derived analytically and the most correct computation of tune shifts can only be done by particle tracking. A few approximative scaling 'laws' can be suggested, but should be used carefully since the range of applicability is limited. As for head-on collisions the effects are proportional to the number of particles per bunch and it became a habit to use the linear beam-beam parameter ξ as a scaling parameter, which however serves merely as an expression for the bunch intensity 'normalised' with the beam emittance. It has no further physical relevance except to compare the relative strength of head-on and long range interactions. The long range effects are sensitive to the separation, which has to be computed exactly from the trajectories of the two beams. However for the drift space around a low-β insertion (round beams) the latter can be simplified and expressed as:

$$d_{\mathrm{sep}} = \frac{\theta_{\mathrm{c}} s}{\sigma(s)} \approx \theta_{\mathrm{c}} \sqrt{\frac{\beta^* \gamma}{\varepsilon_{\mathrm{n}}}} \tag{4}$$

where ε_{n} is the normalised emittance of the beam. In first approximation, the induced tune spread scales as $1/d_{\mathrm{sep}}^2$. Varying the emittance and/or the β-functions can largely control the long range induced effects. Obviously the effects have to be summed over the number of parasitic encounters and therefore increase with their number.

One particular feature of long range interactions can be used to minimize their detrimental effects. The tune shift becomes positive in the plane of separation and negative in the orthogonal plane (assuming proton-proton collisions). Using alternating (i.e., vertical and horizontal crossings) a partial compensation can be achieved. The layout of the LHC high luminosity regions relies on this compensation and the nominal luminosity cannot be reached without it.

The increase of the crossing angle is limited by the available aperture in the final focussing elements (triplet magnets) since for large crossing angles the beam samples the very non-linear fields at large amplitudes. An increase of the crossing angle requires a different layout of the interaction region, either a significantly shorter distance of the triplet to the interaction point to keep the offset smaller, or a design with separate triplet magnets for the two beams that can be designed to follow the separate trajectories.

3.3 Beam-beam tune spread (footprints)

The beam-beam induced tune spread must be kept small enough to avoid low order resonances and a standard tool is to calculate so-called tune footprints, i.e. the mapping of the betatron amplitudes into the two-dimensional tune diagram. The size of these footprints must be kept small and various compensation schemes such as alternating crossings are required. Although the size of the footprint alone cannot give a complete picture of the particle's stability behaviour, it is a valuable and easy tool to compare different machines (*e.g.*, SPS collider) or different options of the same machine. We therefore shall try to find a scenario where the footprints for the nominal, the ultimate and higher luminosity options are comparable and assume a similar behaviour. We consider it as a useful upgrade if the usable luminosity is increased by at least a factor 2.

3.4   Possible LHC scenarios

3.4.1   Nominal LHC scheme

The nominal LHC has four interaction points where, for proton operation three
have head-on collisions, and one experiment (IP2) an offset collision ($4\,\sigma$) to reduce the
interaction rate. The contribution of this experiment to the head-on tune shift is therefore
negligible. Crossing angles in the vertical plane are foreseen in IP1 and IP2 and in the
horizontal plane in IP5 and IP8. They ensure a first order compensation of long range
beam-beam effects and the overall size of the tune footprint can be kept around 0.01 for
both planes. This determines the parameters for the nominal scheme, in particular the
full crossing angles of 300 μrad and the bunch intensity of 1.10×10^{11} protons per bunch,
leading to a luminosity of $10^{34}\,\mathrm{cm}^{-2}\,\mathrm{s}^{-1}$.
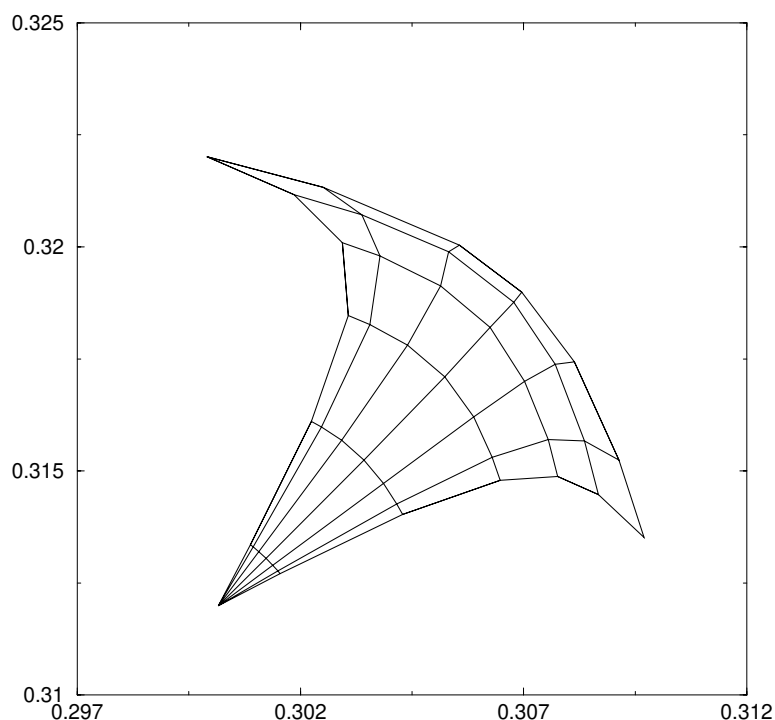
Figure 2: Beam-beam tune footprint, corresponding to betatron amplitudes extending
from 0 to $6\,\sigma$, for nominal LHC configuration with 4 interaction points.

The tune footprint for the nominal configuration is shown in Fig. 2. In both planes
the overall tune spread is about 0.01 by design. A higher luminosity can only be obtained
with a reduced number of experiments. In earlier deliberations [2] a single experiment
was considered for luminosities close to $7 \times 10^{34}\,\mathrm{cm}^{-2}\,\mathrm{s}^{-1}$. We aim at an increase of a
factor two and want to allow for two high luminosity experiments. The footprint with
experiments in IP1 and IP5 only and otherwise unchanged conditions is shown in Fig. 3.
Reducing the number of head-on collisions from four to two and suppressing the minor
contribution of IP2 and IP8 to long range effects shows a significant reduction of the tune
spread (Fig. 3). One is therefore tempted to increase the bunch intensity to a level where
the size of the footprint is approximately restored. For a crossing angle of 300 μrad one
arrives at 1.67×10^{11} protons per bunch. This leads to a significantly higher luminosity
since the latter is proportional to the bunch intensity squared while the beam-beam effects

Figure 3: Beam-beam tune footprint for LHC configuration with two interaction points in IP1 and IP5, alternating vertical-horizontal crossing planes, nominal beam intensity, and nominal crossing angle.
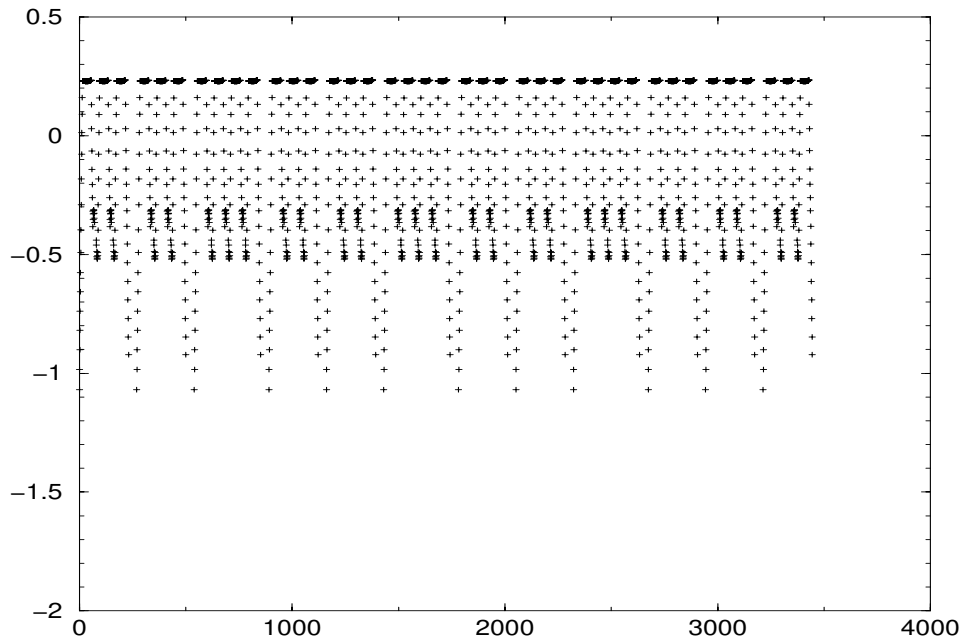
Figure 4: Horizontal orbit offsets for all LHC bunches at interaction point 1 (vertical crossing) in units of μm for LHC configuration with two interaction points and nominal beam intensity.

20

Figure 5: Footprint for LHC configuration with two interaction points in IP1 and IP5, alternating vertical-horizontal crossing planes, nominal crossing angle, and ultimate beam intensity.

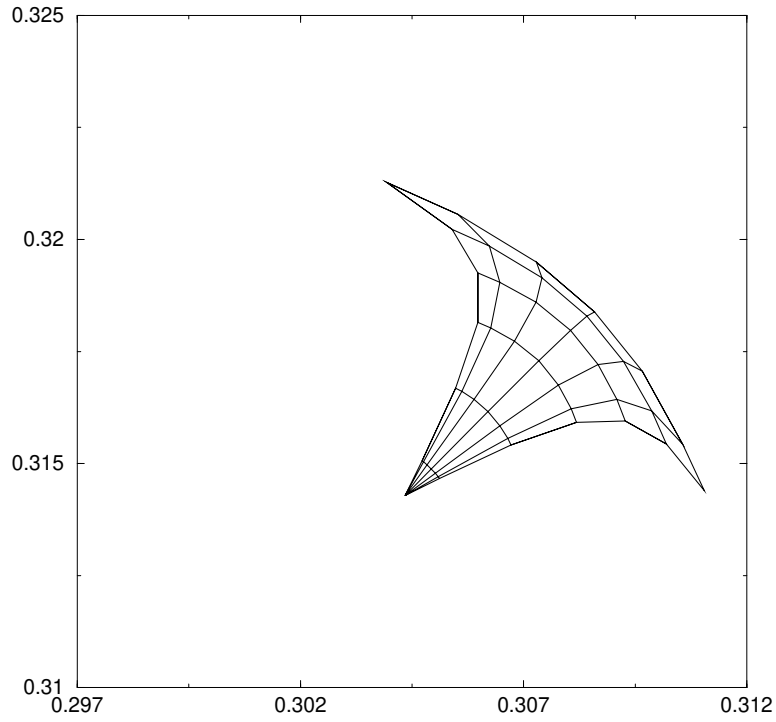Figure 6: Horizontal orbit offsets at interaction point 1 (vertical crossing) for LHC configuration with two interaction points in IP1 and IP5, alternating vertical-horizontal crossing planes, nominal crossing angle, and ultimate beam intensity.
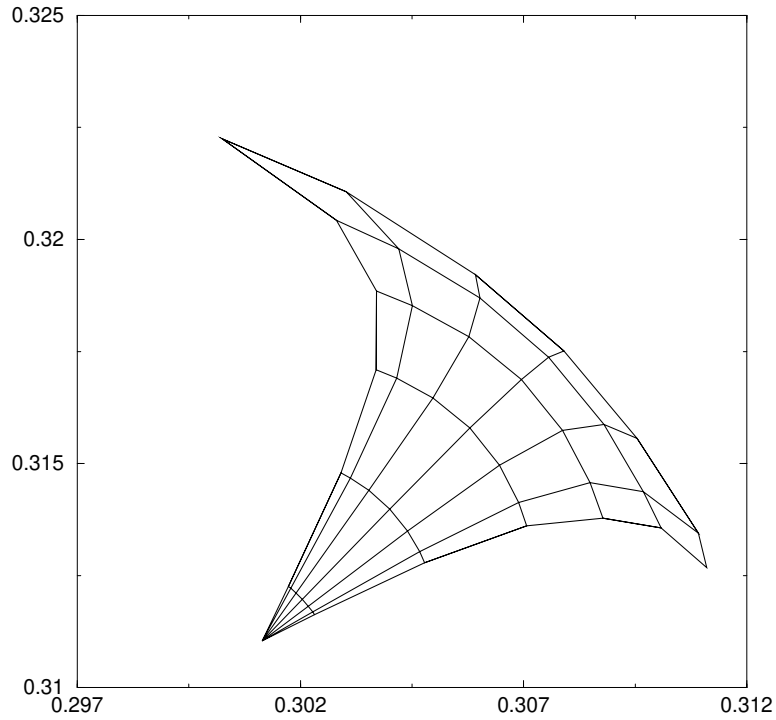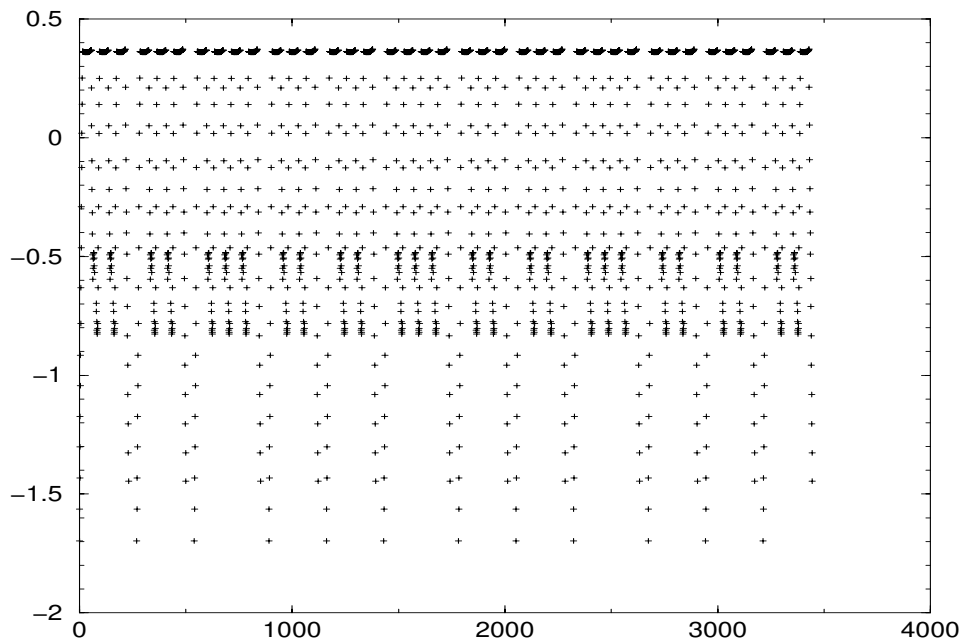
are proportional to the intensity.

The same argument could be used to increase the bunch emittance while increasing the intensity, keeping the ratio $\frac{N_b}{\varepsilon_n}$, i.e. the beam-beam parameter, constant. Provided the single bunch intensity is not limited otherwise, this leads to a higher luminosity and is a valid option if the effect of long range beam-beam encounters can be compensated. The larger aperture required at injection must be evaluated as well. A further very important aspect one has to consider are the orbit distortions coming from long range interactions in the four collision areas. In Fig. 4 we show the orbit offsets assuming the nominal intensity, but using only the interaction points IP1 and IP5. This is justified since the other two interaction points contribute very little to the offsets. As already observed before [3], the total spread of offsets at the head-on collision point are about $1.4\,\mu$m, i.e. about $0.1\,\sigma$.

3.4.2 Ultimate LHC scheme

Operating the LHC with higher luminosities in special configurations was first discussed in Ref. [2]. An important issue is the reduction of the number of experiments. The configuration with two experiments opposite in azimuth and with crossings in orthogonal planes allows a re-optimization of the parameters. The parameters are shown in Table 8 and the resulting footprint is given in Fig. 5. The overall size needed in the tune diagram is only slightly higher for the ultimate option. The effect of the increased intensity on the closed orbits is shown in Fig. 6. Now the spread is larger and increased to about 2.2 μm, i.e. it is approximately scaled with the intensity. This does not come as a surprise since the two omitted experiments did not significantly contribute to the orbit offsets in the nominal configuration and therefore we did not expect a compensation. A comparison of the tune footprints for regular and Pacman bunches with alternating vertical-horizontal crossing planes and horizontal-horizontal crossing planes in IP1 and IP5 is shown in Fig. 7 and further discussed in Ref. [4].

	Nominal parameters	Ultimate parameters
Experiments	2 high-L + 2 low-L	2 (maximum)
β^* in high-L experiments	0.5 m	0.5 m
Full crossing angle θ_c	$300\,\mu$rad	$300\,\mu$rad
Bunch intensity	1.10×10^{11} p/bunch	1.67×10^{11} p/bunch
Bunch spacing	25 ns	25 ns
Normalised emittance $\left(\frac{\sigma^2\gamma}{\beta}\right)$	$3.75\,\mu$m	$3.75\,\mu$m
Beam-beam parameter ξ_0	0.00343	0.00545
Luminosity ($\theta_c = 0\,\mu$rad)	$1.2 \times 10^{34}\,\mathrm{cm}^{-2}\,\mathrm{s}^{-1}$	$2.78 \times 10^{34}\,\mathrm{cm}^{-2}\,\mathrm{s}^{-1}$
Reduction factor F	0.81	0.81
Luminosity ($\theta_c = 300\,\mu$rad)	$1.0 \times 10^{34}\,\mathrm{cm}^{-2}\,\mathrm{s}^{-1}$	$2.27 \times 10^{34}\,\mathrm{cm}^{-2}\,\mathrm{s}^{-1}$
Beam lifetime† τ_b	78 h	49 h
Luminosity lifetime† τ_L	29 h	18 h

Table 8: LHC luminosity parameters for nominal and ultimate running scenarios.
† Beam and luminosity lifetimes include only nuclear proton-proton collisions in the two high-luminosity experiments.

3.4.3 LHC performance beyond ultimate

We believe that what is generally considered as the ultimate performance is a limit for beam-beam effects. A design for luminosities significantly higher should either
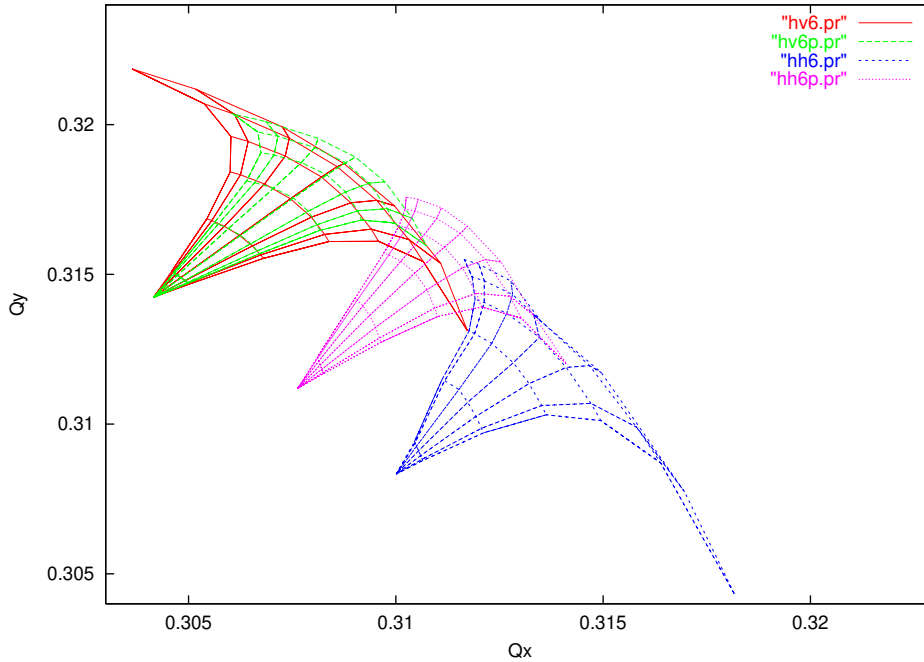
Figure 7: Comparison of beam-beam tune footprints, corresponding to betatron ampli-
tudes extending from 0 to 6σ, for regular and Pacman bunches with alternating and
non-alternating crossing planes. LHC configuration with nominal crossing angle, ultimate
intensity, and two interaction points in IP1 and IP5: horizontal-horizontal crossing planes
(regular bunch: rightmost, dashed blue line, Pacman bunch: intermediate, dotted ma-
genta line) and vertical-horizontal crossing planes (regular bunch: leftmost, solid red line,
Pacman bunch: almost coincident, dashed green line).

have a very different approach (*e.g.*, coasting beams or long super-bunches) or for conven-
tional bunched beams should not exceed the beam-beam effects defined for this ultimate
scheme. The various parameters proposed, such as smaller β^*, shorter bunch spacing,
higher intensity, smaller emittance, etc., must be consistent with a parallel change of geo-
metrical parameters such as an increased crossing angle or rely on yet to be demonstrated
compensation methods such as long range compensation with a pulsed wire.

In no case should the head-on beam-beam parameter significantly exceed a value
of approximately 0.0075 per IP, thus setting limits to parameters such as emittance and
bunch intensity.

References

[1] The LHC Study Group; *The Large Hadron Collider Conceptual Design*,
    CERN/AC/95-05 (LHC), CERN, (1995).

[2] The LHC Study Group; *Design Study of the Large Hadron Collider (LHC)*, CERN
    91-03, CERN, (1991).

[3] H. Grote; *Self-consistent orbit with beam-beam effect in the LHC*, in Proc. EPAC 2000
    (Vienna, 2000), p. 1202.

[4] W. Herr, *Features and implications of different LHC crossing schemes*, CERN
    LHC Project report in preparation (December 2002).

4 Interaction Region Layout

Squeezing the optics to $\beta^* = 0.25\,\mathrm{m}$ creates rather large maximum β-functions inside the triplet magnets. Fig. 8 shows the optics functions in IR5 for the nominal optics with $\beta^* = 0.5\,\mathrm{m}$. The peak β-function is $4750\,\mathrm{m}$. Fig. 9 shows the optics functions in IR5 for $\beta^* = 0.25\,\mathrm{m}$ where the peak β-function has increased to $9500\,\mathrm{m}$.
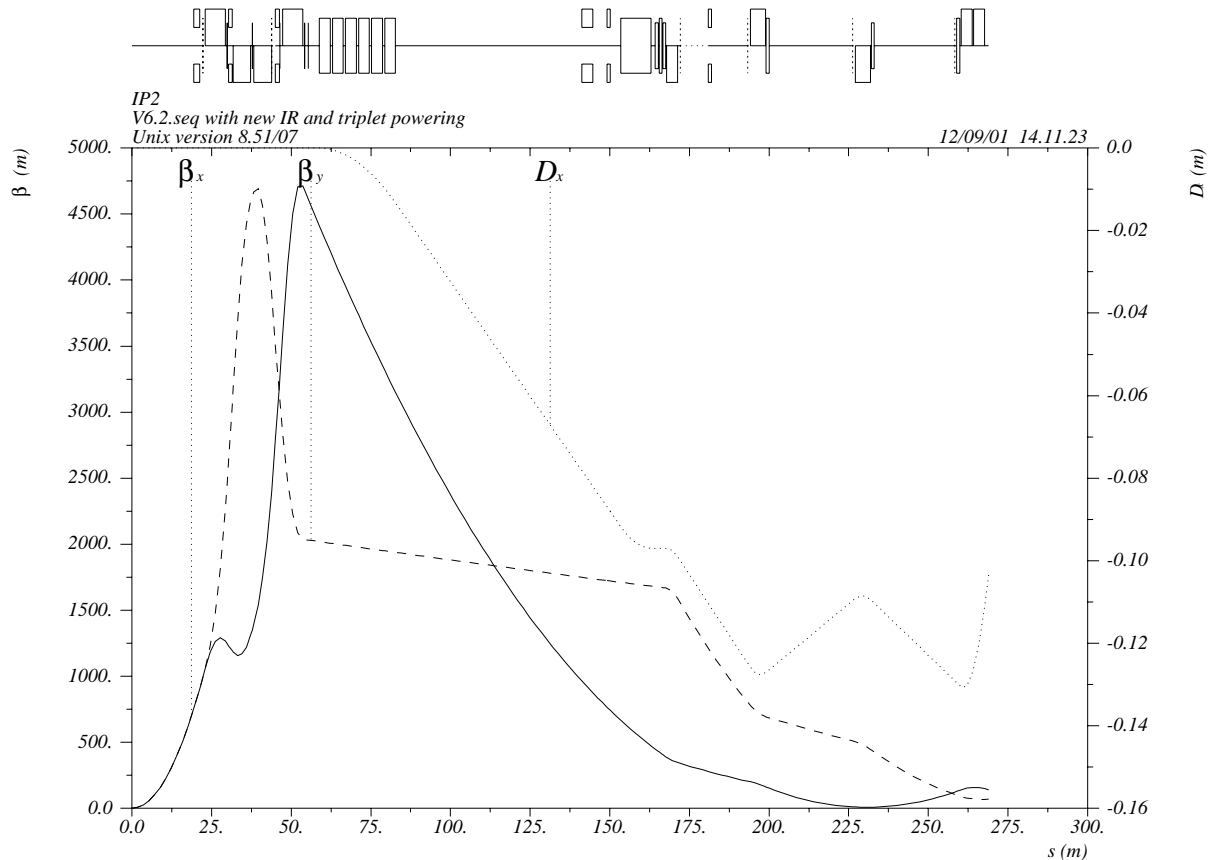
Figure 8: The β-functions right from IP5 for $\beta^* = 0.5\,\mathrm{m}$.

The aperture of the triplet magnets must provide enough space to enclose $9\,\sigma$ of beam envelope per beam, a beam separation of $7.5\,\sigma$, peak orbit excursions of $3\,\mathrm{mm}$, mechanical tolerances of $1.6\,\mathrm{mm}$, a β-beating of 20% and a spurious dispersion orbit of up to $4\,\mathrm{mm}$, yielding an approximate requirement for the triplet diameter D_{trip}

$$D_{\mathrm{trip}} > 1.1 \times (7.5 + 2 \times 9) \cdot \sigma + 2 \times 8.6 \text{ mm.} \tag{5}$$

The nominal normalised beam emittance is $\varepsilon_{\mathrm{n}} = 3.75\,\mu\mathrm{m}$ and the beam size inside the triplet magnets becomes

$$\sigma = \sqrt{\beta \frac{\varepsilon_{\mathrm{n}}}{\gamma}}. \tag{6}$$

For the nominal optics configuration with $\beta^* = 0.5\,\mathrm{m}$ one obtains a maximum beam size of $\sigma = 1.54\,\mathrm{mm}$ and the triplet diameter must satisfy

$$D_{\mathrm{trip}}(\beta^* = 0.5\,\mathrm{m}) > 60.4\,\mathrm{mm} \tag{7}$$

which is compatible with the current triplet aperture of $60\,\mathrm{mm}$. It should be noted here that the above calculation provides only an approximate estimate for the required magnet
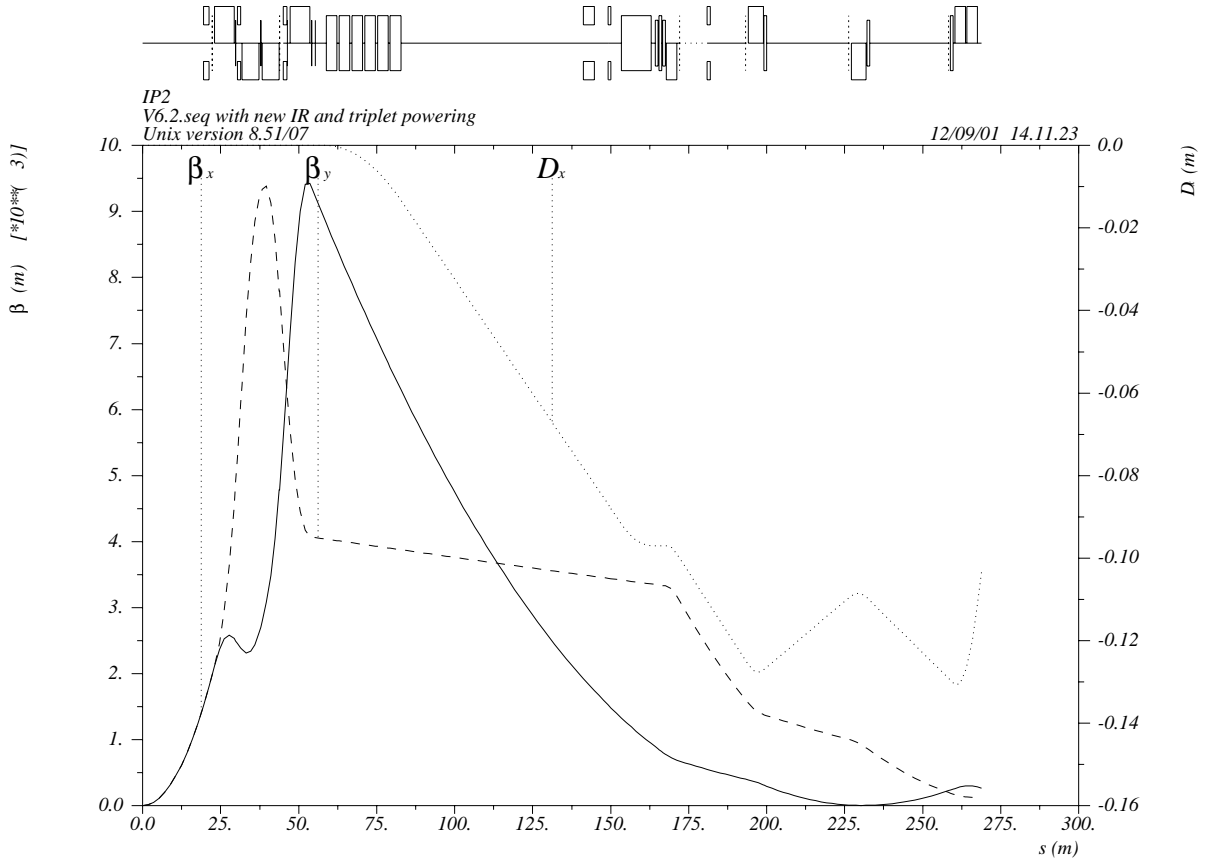
Figure 9: The β-functions right from IP5 for $\beta^* = 0.25\,\mathrm{m}$.

aperture which is sufficient for the comparison of different triplet layouts in this report. A precise calculation of the required magnet aperture requires two-dimensional tracking of the beam halo around the machine [1]. Furthermore it should be underlined that most of the long range beam-beam interactions occur in the drift space between the triplet quadrupole magnets left and right from the IP where the minimum beam separation is much larger than the $7.5\,\sigma$ quoted above (approximately $9.5\,\sigma$).

For an optics configuration with $\beta^* = 0.25\,\mathrm{m}$ one obtains a maximum beam size of $\sigma = 2.185\,\mathrm{mm}$ and the triplet diameter must satisfy

$$D_{\mathrm{trip}}(\beta^* = 0.25\,\mathrm{m}) > 78.5\,\mathrm{mm} \tag{8}$$

which is no longer compatible with the current specification of the triplet aperture of $60\,\mathrm{mm}$. There are three possible solutions to this problem:

- increase the triplet magnet diameter,
- move the triplet magnets closer to the IP,
- separate the two LHC beams before they enter the triplet magnets (i.e., no beam separation required inside the triplet magnets).

The first option has been discussed in Ref. [2, 3]. The second option makes use of the fact that the β-function increases inside the drift space left and right from the IP like

$$\beta(s) = \beta^* + \frac{(s - s_{\mathrm{IP}})^2}{\beta^*}. \tag{9}$$

However, there is not much space to move the triplet magnets closer to the IP. On the contrary, a luminosity upgrade to $L \sim 10^{35}\,\mathrm{cm}^{-2}\,\mathrm{s}^{-1}$ probably requires a longer TAS

25

absorber which would push the magnets even further away from the IP. In the following we will discuss the possibility of separating the two LHC beams before they enter the triplet magnets, as sketched in Fig. 10.

Figure 10: Sketch of a possible IR layout for an LHC luminosity upgrade with separation dipoles close to the IP and separated magnet bores inside the triplet magnets.
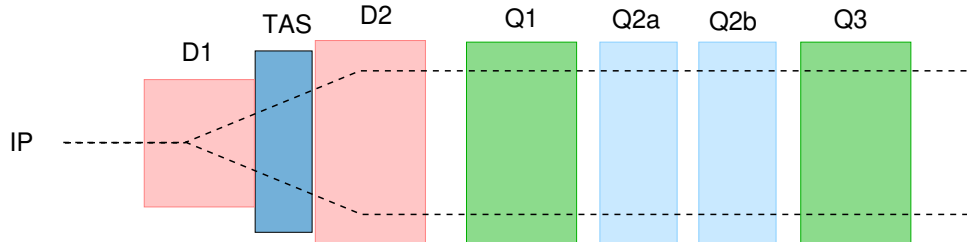
Separating the two beams before the triplet magnets has two additional benefits: 1) it reduces the effective number of long range beam-beam interactions and 2) placing the TAS absorber in between the separation-recombination dipole magnets increases the efficiency of the TAS absorber (provided the D1 dipole magnet located next to the experiments can be operated in the radiation hard environment). It is worthwhile to mention here that the combination of TAS and D2 magnet must also fulfil the functionality of the TAN (neutral) absorber in order to protect the downstream quadrupole magnets. We assume that the beam separation can be done via two 11.4 m long 15 T dipole magnets (possibly with high temperature superconducting coils). The first dipole magnet (D1) is located 25.15 m away from the IP (i.e., the beginning of the magnet is 19.45 m away from the IP which is the same distance as the TAS absorber in the current LHC V6.4 layout). Assuming that the entire D1 magnet is made as one module with one common aperture for both beams, it requires a minimum diameter of 120 mm at the exit of the magnet. Alternatively the magnet could consist of two modules: the first being a single bore magnet and the second a double bore magnet. The second dipole (D2, opposite field direction) is located 38.35 m away from the IP leaving 1.8 m drift space between the two dipole magnets for the TAS installation. The beam separation at the exit of the D2 magnet is equivalent to the standard beam separation of the 2-in-1 arc dipole magnets (194 mm). The first triplet magnet is a 4.5 m long 230 T/m quadrupole magnet. The magnet is placed 48.3 m away from the IP (magnet center), leaving a 2 m drift space between the triplet quadrupole and the second dipole magnet for the installation of additional corrector elements. The second triplet magnet is an assembly of two 4.5 m long 257 T/m quadrupoles which are placed at 54.12 m and 59.94 m from the IP (center position) leaving approximately 1.32 m drift space for installation and additional equipment between the Q1 and Q2a and the Q2a and Q2b quadrupole magnets. The third triplet magnet is a 5.0 m long 280 T/m quadrupole located 65.75 m away from the IP (center position) leaving a 1.06 m drift space for installation between the Q2b and Q3 magnet. The high gradient of the Q3 magnet can be lowered if the magnet length is increased accordingly. The magnet parameters are summarised in Table 9 and Fig. 11 shows the magnet layout and the resulting optic functions (the dispersion function has not been matched, which will require a further optimisation of the whole insertion layout). The maximum β-function inside the triplet magnets is 18.5 km. The maximum β-function inside the matching section quadrupole magnets is approximately 5 km requiring also increased apertures for these magnets.

magnet	type	length	diameter range	beam separation	strength
D1	1 aperture	11.4 m	34 mm ↔ 131 mm	0 ↔ 84 mm	15 T
D2	2-in-1	11.4 m	50 mm ↔ 60 mm	110 mm ↔ 194 mm	15 T
Q1	2-in-1	4.5 m	60 mm ↔ 70 mm	194 mm	230 T/m
Q2	2-in-1	2 × 4.5 m	70 mm ↔ 78 mm	194 mm	257 T/m
Q3	2-in-1	5.0 m	70 mm ↔ 78 mm	194 mm	280 T/m

Table 9: Magnet parameters for a triplet layout with separated beams inside the triplet magnets. The beam separation does not include the additional separation from the crossing angle bump.
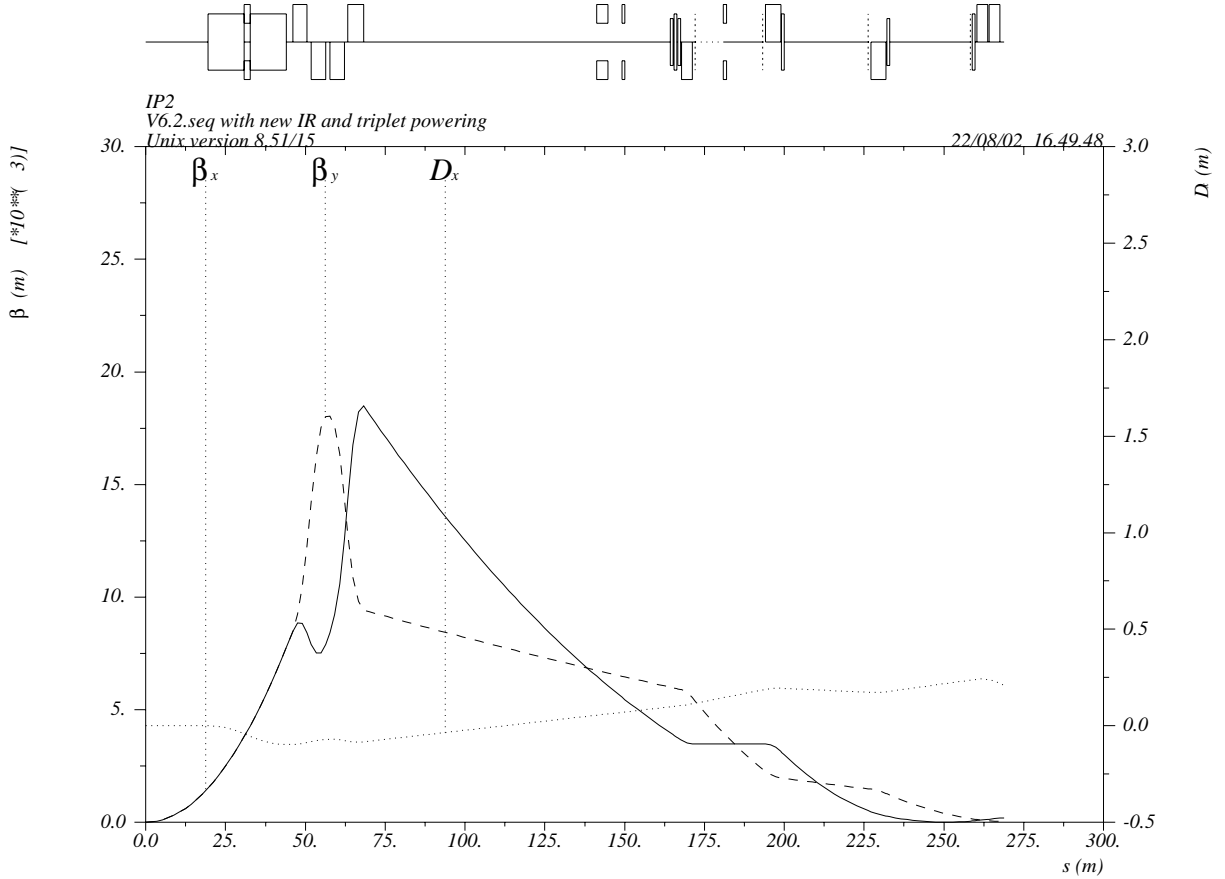
Figure 11: The β-functions right from IP5 for $\beta^* = 0.25\,\mathrm{m}$ and separated magnet bores inside the triplet magnets.

The absence of parasitic beam crossings inside the triplet magnets changes the requirement for the mechanical aperture to

$$D_{\mathrm{trip,sep}} > 1.1 \times 2 \times 9 \cdot \sigma + 2 \times 8.6\,\mathrm{mm}, \tag{10}$$

(assuming the same tolerances on the peak orbit excursions, alignment errors, β-beating and spurious dispersion as for the current IR layout). For a maximum β-function of $\beta_{\max} = 18.5\,\mathrm{km}$ the beam size becomes $\sigma = 3.06\,\mathrm{mm}$ and the minimum required triplet diameter becomes

$$D_{\mathrm{trip,sep}} > 77.8\,\mathrm{mm}. \tag{11}$$

which is still slightly smaller than the required aperture in Eq. (8). The 2-in-1 design has

one more advantage compared to the nominal layout where both beams pass through the same aperture. The 2-in-1 triplet design allows for a local correction of the integrated triplet multipole errors. This is not possible for the single aperture design. Indeed, owing to the antisymmetric optics, the local β functions are different for the two beams. For the ultimate performance with $\beta_{max} > 9\,\mathrm{km}$ the triplet field quality will become an important issue and having the possibility for a local correction of the field errors might significantly simplify the magnet design and construction.
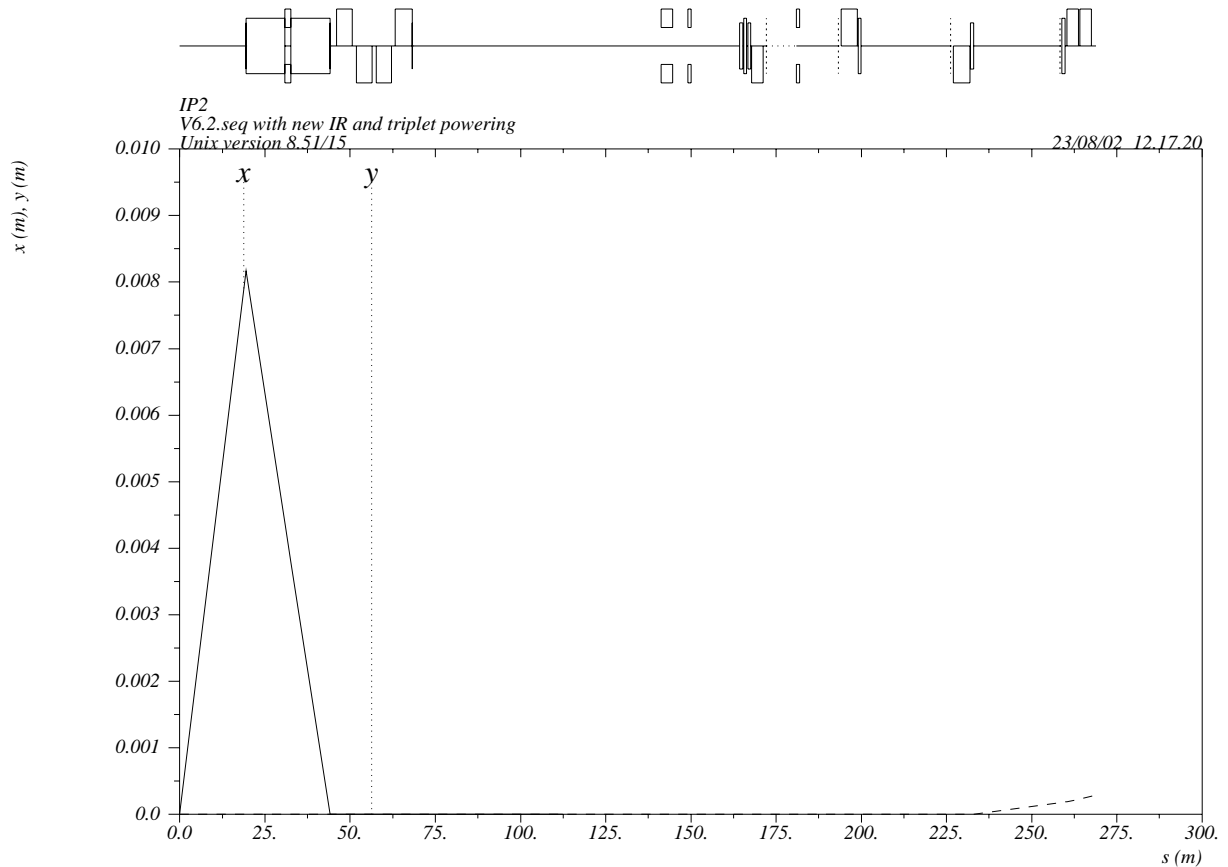
Figure 12: The horizontal crossing angle orbit right from IP5 for $\beta^* = 0.25\,\mathrm{m}$ and separated magnet bores inside the triplet magnets.

In order to avoid parasitic head-on interactions of the two LHC beams in the common region between the two triplet assemblies left and right from the IP, the insertion must provide a crossing angle at the IP. The normalised beam separation in the drift space is approximately given by

$$d_{\mathrm{sep}}(s)/\sigma(s) \approx \theta_{\mathrm{c}} \sqrt{\frac{\beta^*}{\varepsilon}}, \tag{12}$$

where θ_{c} is the total crossing angle, $\varepsilon = \varepsilon_n/\gamma$ the beam emittance and β^* the β-function at the IP. For $\beta^* = 0.5\,\mathrm{m}$ a normalised beam separation of $9\,\sigma$ requires a total crossing angle of approximately $290\,\mu\mathrm{rad}$. For $\beta^* = 0.25\,\mathrm{m}$ a normalised beam separation of $9\,\sigma$ requires a total crossing angle of approximately $400\,\mu\mathrm{rad}$. In order to minimise the required triplet magnet aperture we demand in the following that the crossing angle orbit bump must be closed before the beam enters the triplet magnets. In the following we assume that the crossing-angle orbit bump is generated by the D1 and D2 dipole magnets. Fig. 12 shows a

28

schematic picture of a horizontal crossing angle orbit bump for the new triplet layout. The crossing angle orbit bump in Fig. 12 requires an additional deflection angle of 750 μrad at the D1 magnet and 330 μrad at the D2 magnet. For a crossing-angle orbit bump in the horizontal plane the sign of the crossing angle can be chosen such that the additional deflection reduces the required dipole field strength by 10% and 4.5% at the D1 and D2 magnets, respectively. A crossing-angle orbit bump in the vertical plane can be generated by rotating the D1 and D2 magnets by 5.7° and 2.9°, respectively, which reduces the available horizontal field strength by less than 1%. In summary it can be concluded that the crossing angle orbit bump does not impose additional constraints on the field strength of the D1 and D2 magnets. The main implication of the above separation scheme is that it increases the required aperture of the D1 and D2.

A discussion of crab cavities, that would allow operation with significantly larger crossing angles and early separation of the two bunched beams with a reduced dipole strength (no D1 magnets are required), can be found in Appendix A.1.

References

[1] J.B. Jeanneret and R. Ostojic, LHC Project Note 111.
[2] T. Sen, J. Strait and A.V. Zlobin, PAC 2001.
[3] LHC IR Upgrade Collaboration Meeting, CERN, 11-12 March 2002, see web site at http://cern.ch/lhc-proj-IR-upgrade.

5 Integrated Luminosity

The instantaneous luminosity per bunch is given by

$$L_{\mathrm{b}} = N_{\mathrm{b}}^2 \cdot \frac{f_{\mathrm{rev}} \cdot \gamma}{4\pi \varepsilon_{\mathrm{n}} \beta^*} \cdot F, \tag{13}$$

where N_{b} is the number of particles per bunch, f_{rev} the revolution frequency, γ the relativistic Lorentz factor, ε_{n} the normalised transverse beam emittance, β^* the beta-function at the IP and F a geometrical reduction factor due to the crossing angle.

Assuming that each beam has n_{b} bunches the total instantaneous luminosity becomes

$$L = n_{\mathrm{b}} \cdot L_{\mathrm{b}}. \tag{14}$$

The following section discusses the potential gain in the integrated luminosity once the maximum instantaneous luminosity has been increased to $L = 10^{35}\,\mathrm{cm}^{-2}\,\mathrm{s}^{-1}$. Estimating the integrated luminosity of a storage ring requires assumptions on the average turnaround time and the average number of luminosity fills per year. Having no data available for an operating LHC machine we use data from the HERA proton ring operation as a reference. The HERA proton machine has approximately the same dynamic range in energy (HERA: $40\,\mathrm{GeV} \to 920\,\mathrm{GeV}$; LHC: $450\,\mathrm{GeV} \to 7000\,\mathrm{GeV}$), requires the same time for the total ramp (approximately 20 minutes for both machines), has similar values for the dynamic aperture (DA) and the mechanical aperture (MA), and has approximately the same store length as foreseen for the LHC. The relevant data of both machine is summarised in Table 10 (see Ref. [1]).

	HERA	LHC
run time	10 h	10 h
ramp time	20 min	20 min
energy range	23	15.55
DA_{tracking}	$11\,\sigma$	$12\,\sigma$
$DA_{\mathrm{operation}}$	$6 - 8\,\sigma$	$6\,\sigma^\dagger$
MA	$6\,\sigma$	$7\,\sigma$

Table 10: Comparison of some HERA and LHC parameters. The MA of the LHC is given by the aperture of the collimation system. † The expected DA for the LHC operation is based on the experience that the DA at machine operation is approximately half of the minimum DA obtained in numerical tracking studies. The LHC tracking studies yield a minimum DA of about $12\,\sigma$.

Each proton injection in HERA requires at least 3 'pilot' shots for the machine setup [2]. We will use the same number for the machine setup for each of the two LHC beams. In addition, the final machine setup in the LHC will be verified with one shot of nominal beam intensity before the final injection procedure will be started. Thus, in total, we assume 4 'pilot' shots for the machine set up of each LHC beam.

5.1 Minimum Theoretical Turnaround Time

After 10 years of machine operation, on average, only every third proton injection in HERA leads to a successful proton fill at top energy [2]. The average time between the end of a luminosity run and a new beam at top energy in HERA is approximately 6 h, compared to a theoretical minimum turnaround time of approximately 1 h. In the following analysis we consider two cases for evaluating the integrated machine luminosity:

- Case 1) the minimum theoretical turnaround time of the LHC,
- Case 2) a turnaround time which is 6 times longer then the minimum theoretical turnaround time.

Considering the higher complexity of the LHC machine compared to the HERA machine and the fact that the LHC has to be operated with two proton beams, compared to only one beam in the HERA machine, the second case is still an optimistic assumption.

Filling the LHC requires 12 cycles of the SPS synchrotron and each SPS fill requires 3 cycles of the PS synchrotron. The SPS and PS cycling times are 20 and 3.6 s, respectively, yielding a total LHC filling time of approximately 4 min per beam. Assuming that each LHC aperture requires additional 4 SPS cycles for the injection set up (3 pilot bunches and one nominal intensity) and that the LHC operators require at least 2 min to evaluate the measurements of each pilot bunch shots and to readjust the machine settings, the total (minimum) LHC injection time becomes

$$T_{\mathrm{inj}}(\mathrm{LHC}) \approx 16 \min. \tag{15}$$

The minimum time required for ramping the beam energy in the LHC from 450 GeV to 7000 GeV is approximately 20 min [3]. After a beam abort at top energy it takes also approximately 20 min to ramp the magnets down to 450 GeV. Assuming a programmed check of all main systems of 10 min [4], one obtains a total turnaround time for the LHC of

$$T_{\mathrm{turnaround}}(\mathrm{LHC}) \approx 70 \min^{2)}. \tag{16}$$

5.2 Luminosity Lifetime

The luminosity lifetime of the LHC is determined by five different processes:
- beam lifetime limit due to nuclear reactions,
- beam size blowup due to intra-beam scattering (IBS),
- beam size blowup due to rest gas scattering,
- beam size reduction due to synchrotron radiation damping,
- beam size blowup due to the non-linear beam-beam interactions.

The beam lifetime limit due to nuclear reactions is given by

$$\tau_{\mathrm{nuclear}} = \frac{N_{0\mathrm{b}}}{k_x \sigma_{\mathrm{n}} L_{\mathrm{b}}}, \tag{17}$$

where $N_{0\mathrm{b}}$ is the initial number of particles per bunch, $L_{0\mathrm{b}}$ the initial luminosity per bunch, σ_n the total cross section for proton-proton collisions ($\sigma_{\mathrm{n}} \simeq 100 \,\mathrm{mb} = 10^{-25} \,\mathrm{cm}^2$), and k_x the number of interaction points. In the following we assume two main experimental insertions for the high luminosity operation of the LHC. The bunch intensity decays like

$$\frac{\mathrm{d}N_{\mathrm{b}}}{\mathrm{d}t} = -k_x \sigma_{\mathrm{n}} L_{\mathrm{b}} = -k_x \sigma_{\mathrm{n}} L_{0\mathrm{b}} \frac{N_{\mathrm{b}}^2}{N_{0\mathrm{b}}^2} = -\frac{N_{\mathrm{b}}^2}{N_{0\mathrm{b}} \tau_{\mathrm{nuclear}}}. \tag{18}$$

Solving the above equation for $N_{\mathrm{b}}(t)$ and inserting the result into the equation for the luminosity one obtains

$$N_{\mathrm{b}}(t) = \frac{N_{0\mathrm{b}}}{1 + t/\tau_{\mathrm{nuclear}}} \quad \text{and} \quad L(t) = \frac{L_0}{(1 + t/\tau_{\mathrm{nuclear}})^2}. \tag{19}$$

---

2) The LHC 'pink book' quotes a minimum turnaround time of 2 h [4].

Note that our definition Eq. (17) of τ_{nuclear} corresponds to the beam intensity halving time. The luminosity lifetime, corresponding to a reduction of the initial luminosity by a factor $1/e$, is given by $(\sqrt{e}-1)\cdot\tau_{\text{nuclear}}$. In order to facilitate the summation of the lifetime contributions from other effects we approximate the luminosity decay due to nuclear interactions by an exponential decay[3]

$$L(t) \approx L_0 \cdot e^{-t/(\sqrt{e}-1)\cdot\tau_{\text{nuclear}}}. \tag{20}$$

Fig. 13 shows a comparison between the exact and the exponential decay.
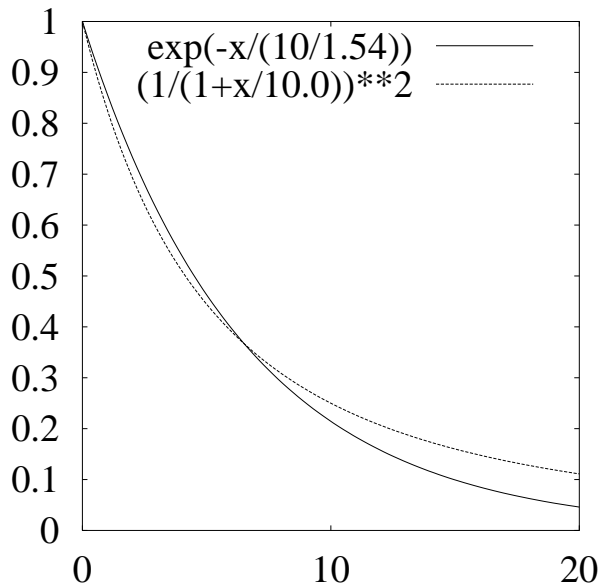
Figure 13: Difference between the exponential approximation and the exact decay of the luminosity due to nuclear disintegrations, given by Eq. (19), for a luminosity lifetime of 10 h. The horizontal axis shows the run time and the vertical axis the luminosity.

The intra-beam scattering horizontal emittance growth time for a bunch intensity of 1.05×10^{11} protons at $7\,\text{TeV}$ is about $100\,\text{h}$ [5]. Observing that the intra-beam scattering growth time is proportional to the bunch intensity one obtains finally:

$$\tau_{x,\text{IBS}} = 100\,\text{h} \cdot \frac{1.05\times10^{11}}{N_{\text{b}}}. \tag{21}$$

The rest gas scattering growth time for a bunch intensity of 1.05×10^{11} protons at $7\,\text{TeV}$ is 85 h [5]. Observing that the rest gas scattering growth time is proportional to the bunch intensity and the number of bunches one obtains:

$$\tau_{\text{rest gas}} = 85\,\text{h} \cdot \frac{1.05\times10^{11}\cdot2835}{N_{\text{b}}\cdot n_{\text{b}}}. \tag{22}$$

Following the argumentation of the LHC 'pink book' [4] we assume that the radiation damping process just cancels the beam blow up due to the beam-beam interactions

---

[3] It is possible to derive analytically the non-exponential luminosity decay caused by nuclear interactions and scattering on the rest gas, either with constant density or with density proportional to the beam intensity. However no simple analytic expression is available for the combined effect of nuclear interactions, rest gas scattering, and IBS.

and get for the final luminosity lifetime

$$\frac{1}{\tau_{\text{lumi}}} = \frac{1}{\tau_{x,\text{IBS}}} + \frac{2}{\tau_{\text{rest gas}}} + \frac{1.54}{\tau_{\text{nuclear}}}. \tag{23}$$

For the nominal bunch intensity of $N_{0b} = 1.1 \times 10^{11}$ and an initial bunch luminosity of $L_b = 3.53 \times 10^{30}\,\text{cm}^{-2}\,\text{s}^{-1}$ in two IP's ($L_{\text{tot}} = 1 \times 10^{34}\,\text{cm}^{-2}\,\text{s}^{-1}$ for $\beta^* = 0.5\,\text{m}$) one obtains

$$\tau_{\text{lumi,nom}} = 14.8\,\text{h}. \tag{24}$$

For an ultimate bunch intensity of $N_{0b} = 1.67 \cdot 10^{11}$ and an initial bunch luminosity of $L_b = 1.78 \times 10^{31}\,\text{cm}^{-2}\,\text{s}^{-1}$ ($L_{\text{tot}} = 4.54 \times 10^{34}\,\text{cm}^{-2}\,\text{s}^{-1}$ for $\beta^* = 0.25\,\text{m}$) one obtains

$$\tau_{\text{lumi,ult}} = 6.5\,\text{h}. \tag{25}$$

5.3 Integrated Luminosity

Integrating the luminosity over one luminosity run yields

$$L_{\text{int}} = L_0 \cdot \tau_{\text{lumi}} \cdot [1 - e^{-T_{\text{run}}/\tau_{\text{lumi}}}] \tag{26}$$

where T_{run} is the total length of the luminosity run.

The overall collider efficiency depends on the ratio of the run length and the average turnaround time. Assuming that the machine can be operated during 200 days per year, the total luminosity per year is given by

$$L_{\text{tot}} = \frac{200 \cdot 24}{T_{\text{run}}[\text{h}] + T_{\text{turnaround}}[\text{h}]} \cdot L_{\text{int}}. \tag{27}$$

The total luminosity per year attains a maximum if the run time satisfies the following equation

$$\ln\left(\frac{T_{\text{turnaround}} + T_{\text{run}}}{\tau} + 1\right) = \frac{T_{\text{run}}}{\tau}. \tag{28}$$

Table 11 presents the optimum run-times for different values of the turnaround time and the luminosity lifetime.

	$T_{\text{turnaround}}$ [h]			
τ [h]	1	6	10	20
6.5	3	6	9.5	11.5
10	4	9	11.5	15
15	5	12	15	20
19	5.5	13	16.5	22

Table 11: The optimum luminosity run time for different combinations of luminosity lifetime τ and turnaround time $T_{\text{turnaround}}$.

Inserting the initial LHC luminosities and the run times from Table 11 into Equations (26) and (27) and assuming 2835 bunches one obtains the maximum total luminosity per year. Table 12 summarises the total luminosity per IP for all luminosity lifetimes and turnaround times in Table 11 ($n_b = 2835$) assuming an initial luminosity per bunch of $L_{bunch,0} = 1.78 \times 10^{31}\,\text{cm}^{-2}\,\text{s}^{-1}$ (ultimate luminosity for $\beta^* = 0.5\,\text{m}$).

τ [h]/$L_{\mathrm b}$ [cm^{-2} s^{-1}] per IP	$T_{\mathrm{turnaround}}$ [h]			
	1	6	10	20
6.5	524 fb^{-1}	286 fb^{-1}	223 fb^{-1}	149 fb^{-1}
10	575 fb^{-1}	345 fb^{-1}	278 fb^{-1}	193 fb^{-1}
15	618 fb^{-1}	400 fb^{-1}	330 fb^{-1}	241 fb^{-1}

Table 12: The integrated luminosity per year for different combinations of luminosity lifetime and turnaround times assuming the ultimate initial luminosity.

τ [h]/$L_{\mathrm b}$ [cm^{-2} s^{-1}] per IP	$T_{\mathrm{turnaround}}$ [h]			
	1	6	10	20
15	122 fb^{-1}	78 fb^{-1}	65 fb^{-1}	47 fb^{-1}
20	127 fb^{-1}	86 fb^{-1}	72 fb^{-1}	54 fb^{-1}

Table 13: The integrated luminosity per year for the nominal beam parameters and different turnaround times.

Table 13 summarises the total luminosity per IP assuming the nominal initial luminosity. While the peak luminosity of the ultimate beam parameters and $\beta^* = 0.25\,$m is approximately 5 times larger than the peak luminosity of the nominal LHC machine the gain in the integrated luminosity is slightly smaller. Comparing the results in Tables 13 and 12 (ultimate beam parameters $N_{\mathrm b} = 1.67 \times 10^{11}$) a machine operation with $\beta^* = 0.25\,$m generates an increase in the integrated luminosity per year by a factor between 3 and 4, depending on the machine turnaround time.

References

[1] O. Brüning in the Chamonix 2000 proceedings.
[2] O. Brüning in the Chamonix 2001 proceedings.
[3] A. Faus-Golfe, LHC Project Note 9 (1995).
[4] Design Study of the Large Hadron Collider, CERN/91-03, (1991).
[5] The Large Hadron Collider, Conceptual Design Report, CERN/AC/95-05, (1995).

6   Collective Effects

In this section we review beam-beam, electron cloud, and conventional collective effects, including a novel approach to the optimization of the collider performance compatible with the beam-beam limit for high intensity proton bunches or long 'super-bunches'. We also discuss the interplay between radiation damping and intra-beam scattering (IBS) for LHC-II.

6.1   Luminosity and Beam-Beam Tune Shift for Bunched Beams

The luminosity can be written as

$$L = \frac{N_b^2 f_{\mathrm{rep}} H_D}{4\pi \sigma_x \sigma_y} \ F \tag{29}$$

where f_{rep} denotes the bunch collision rate, H_D is a factor which describes the change in optics due to the beam-beam interaction (dynamic beta function), and F represents the luminosity reduction by hourglass effect and crossing angle. For a horizontal crossing, the luminosity reduction factor F is

$$F = \frac{2}{\sigma_z \sqrt{\pi}} \int_0^\infty \frac{\exp\left(- \left(\frac{z}{\sigma_z}\right)^2 \left\{ 1 + \frac{\theta_c^2}{4\theta_d^2} \left[\frac{1}{1+(z/\beta_x^*)^2} \right]^2 \right\} \right)}{\sqrt{(1+(z/\beta_x^*)^2)\,(1+(z/\beta_y^*)^2)}} \ dz \tag{30}$$

where $\theta_d = \sigma_x/\sigma_z$ is the bunch diagonal angle, and θ_c the full crossing angle. We have assumed that $\theta_c \ll 1$, so that $\cos\theta_c \approx 1$ and $\sin\theta_c \approx \theta_c$. If the rms bunch length σ_z is much shorter than the interaction-point (IP) beta functions $\beta_{x,y}^*$, the formula simplifies to $F \approx 1/\sqrt{1 + (\sigma_z \theta_c/(2\sigma_x))^2}$.

The loss in luminosity with increasing crossing angle is illustrated in Fig. 14 (left). For 400 μrad crossing angle, $N_b = 1.7 \times 10^{11}$, $n_b = 2800$ bunches, and $\beta^* = 0.25$ m, the luminosity is about 3.5×10^{34} cm^{-2}s^{-1}. For 300 μrad crossing angle the luminosity is 4.1×10^{34} cm^{-2}s^{-1}.
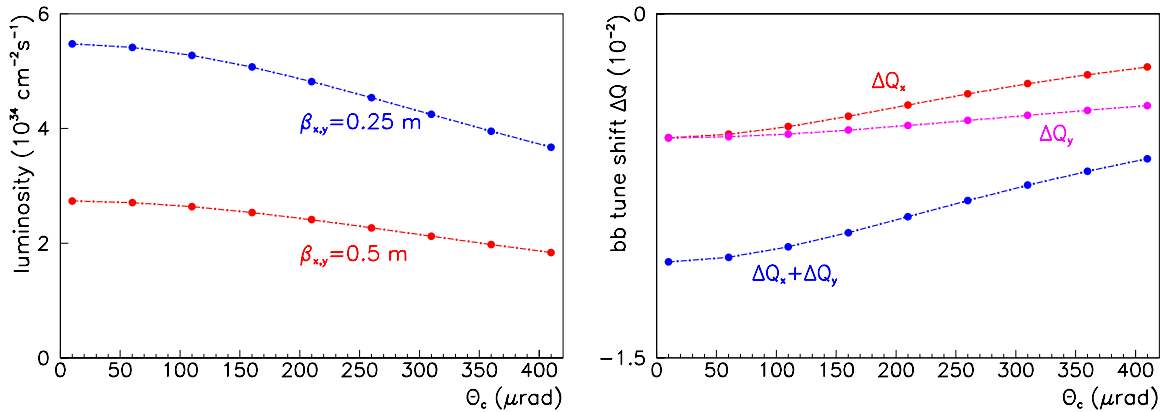

Figure 14: Luminosity (left) and head-on beam-beam tune shifts (right) as a function of crossing angle, for a bunched beam with ultimate LHC parameters, assumed to be equal to $N_b = 1.7 \times 10^{11}$, $\beta^* = 0.25\,\mathrm{m}$, $\sigma_z = 7.7\,\mathrm{cm}$, $n_b = 2800$, $\gamma\epsilon_\perp = 3.75\,\mu$m. The left side also shows the luminosity for $\beta^* = 0.5\,\mathrm{m}$.

Assuming that the crossing angle is sufficiently small so that we can approximate $\cos\theta_c \approx 1$, and that the IP beta functions and emittances are equal in both planes ($\beta_x^* \approx \beta_y^*$ and $\epsilon_x \approx \epsilon_y \approx \epsilon$) the beam-beam tune shifts for a particle at the center of the bunch are

$$\Delta Q_x = -\frac{N_b r_p}{2\pi\gamma}\frac{1}{\sqrt{\pi/2}\sigma_z}\int_{-\infty}^{\infty}\left(\beta^* + \frac{s^2}{\beta^*}\right)\left[\left(\frac{1}{(\beta^* + s^2/\beta^*)\epsilon} + \frac{1}{\theta_c^2 s^2}\right)\right.$$

$$\left.\exp\left(-\frac{\theta_c^2 s^2}{2(\beta^* + s^2/\beta^*)\epsilon}\right) - \frac{1}{\theta_c^2 s^2}\right]\exp\left(-\frac{2s^2}{\sigma_z^2}\right)\,ds \tag{31}$$

$$\Delta Q_y = -\frac{N_b r_p}{2\pi\gamma}\frac{1}{\sqrt{\pi/2}\sigma_z}\int_{-\infty}^{\infty}\left(\beta^* + \frac{s^2}{\beta^*}\right)\left[\frac{1}{\theta_c^2 s^2}\left(1-\right.\right.$$

$$\left.\left.\exp\left(-\frac{\theta_c^2 s^2}{2(\beta^* + s^2/\beta^*)\epsilon}\right)\right)\right]\exp\left(-\frac{2s^2}{\sigma_z^2}\right)\,ds\,, \tag{32}$$

where ϵ denotes the transverse geometric rms emittance and again we have considered a horizontal crossing. The decrease in the beam-beam tune shift with crossing angle is shown in Fig. 14 (right). For 400 μrad crossing angle, $N_b = 1.7 \times 10^{-11}$, $\beta^* = 0.25\,\mathrm{m}$, the beam-beam tune shifts are about $\Delta Q_x \approx -0.0024$, and $\Delta Q_y \approx -0.0040$.

Requiring that the total head-on beam-beam tune shift for two IPs with alternating crossing, $|\Delta Q_{\mathrm{tot}}| = |\Delta Q_x + \Delta Q_y|$, is equal to the maximum conceivable value of 0.01, and considering again $\beta^* = 0.25\,\mathrm{m}$ and $\theta_x = 424\,\mu$rad, the corresponding bunch population amounts to $N_b = 2.7 \times 10^{11}$ and the associated luminosity to $L \approx 8.4 \times 10^{34}\,\mathrm{cm}^{-2}\,\mathrm{s}^{-1}$. However, note that, if uncompensated, the additional tune shift due to the long range collisions may reduce the achievable luminosity.

6.2   Continuous Beams and Super-bunches

Assuming equal emittances and beta functions in both transverse planes, the luminosity for a continuous beam is given by [2]

$$L = \frac{c\lambda_1\lambda_2 l_{\mathrm{det}}}{4\pi\sigma_0^2}\,K\left(\frac{l_{\mathrm{det}}}{2\beta^*}, \frac{\beta^*\theta_c}{\sigma_0}\right) \tag{33}$$

where

$$K(\xi,\eta) = \frac{1}{\xi}\int_{-\xi}^{\xi}\frac{1}{1+u^2}\exp\left[-\frac{\eta^2}{4}\frac{u^2}{1+u^2}\right]\,du \tag{34}$$

and θ_c is the full crossing angle, σ_0 is the minimum spot size at the collision point, $\lambda_{1,2}$ the line charge densities. We have again assumed that $\theta_c \ll 1$.

The effective range of the detector is assumed to be confined to the region between $-l_{\mathrm{det}}/2$ and $l_{\mathrm{det}}/2$. Note that for a finite crossing angle, $\theta_c \geq \sigma_{x,y}'^*$, the effective luminous region does not extend beyond $l_{\mathrm{det}} \leq 10\sigma^*/\theta_c$. The integral $K(\xi,\eta)$ is defined such that $K(\xi,\eta) \to 2$ for $\xi,\eta \to 0$.

For horizontal crossing, the beam-beam tune shifts are [2, 3]

$$\Delta Q_x = \frac{2\lambda r_p l}{4\pi\gamma\epsilon_\perp}\,I_x\left(\frac{l}{2\beta^*}, \frac{\beta^*\theta_c}{\sigma_0}\right) \tag{35}$$

$$\Delta Q_y = \frac{2\lambda r_p l}{4\pi\gamma\epsilon_\perp}\,I_y\left(\frac{l}{2\beta^*}, \frac{\beta^*\theta_c}{\sigma_0}\right) \tag{36}$$

where

$$I_x(\xi, \eta) = \frac{1}{\xi\eta^2} \int_{-\xi}^{+\xi} (1 + u^2) \left[\left(u^{-2} + \frac{\eta^2}{1 + u^2} \right) \exp\left(-\frac{\eta^2}{2} \frac{u^2}{1 + u^2} \right) - u^{-2} \right] du$$

$$I_y(\xi, \eta) = \frac{1}{\xi\eta^2} \int_{-\xi}^{+\xi} (1 + u^{-2}) \left[1 - \exp\left(-\frac{\eta^2}{2} \frac{u^2}{1 + u^2} \right) \right] du \qquad (37)$$

and the interaction between the two beams is assumed to happen between $-l/2$ and $l/2$. Outside of this range the beams are either separated by a bending magnet, or shielded from each other. The distance l could be much larger than the effective detector length l_{det}. The integrals $I_{x,y}(\xi, \eta)$ are defined such that $I_{x,y}(\xi, \eta) \to 1$ for $\eta \to 0$ and all ξ.

The dependence of luminosity and beam-beam tune shifts on the crossing angle is illustrated in Fig. 15, where we have assumed a coasting beam current of 42 A, equal to the bunch peak current for the ultimate LHC-I. This value corresponds to a line density of $\lambda \approx 8.8 \times 10^{11}$ m^{-1}. For 400 μrad crossing angle and $\beta^* = 0.25$ m, the luminosity is about 3.0×10^{36} cm^{-2} s^{-1}, and the beam-beam tune shifts are $\Delta Q_x \approx 0.056$, and $\Delta Q_y \approx -0.064$. The sum of the two beam-beam tune shifts of -0.008 is almost acceptable. This may be the relevant parameter for operation with alternating crossing at two IP's. Assuming a total inelastic cross section of 100 mbarn, the initial luminosity decay time $\tau = L/(dL/dt)$ is about 11 hours. The heat load due to synchrotron radiation for the nominal LHC with 0.56 A current is about 0.2 W/m. For 42 A beam current, the heat load would increase to 15 W/m.
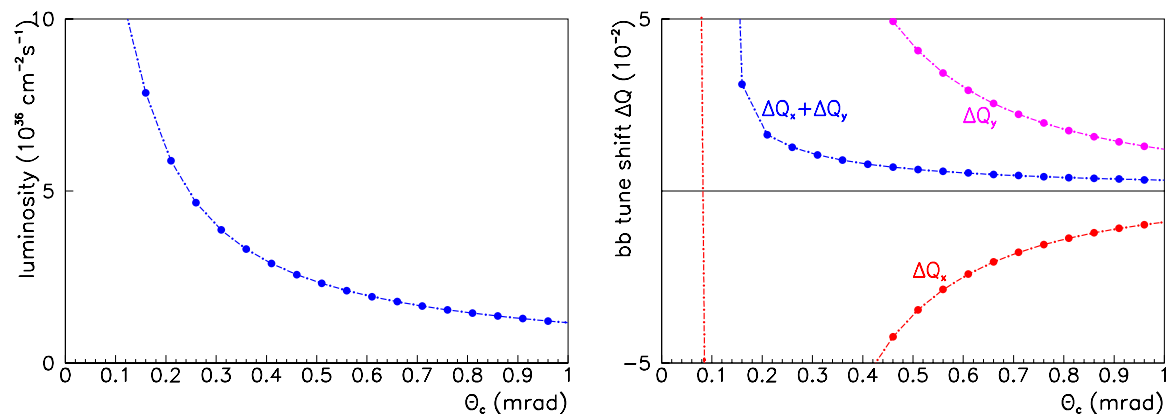
Figure 15: Luminosity (left) and total beam-beam tune shift (right) as a function of crossing angle, for a continuous beam with a line density $\lambda = 8.8 \times 10^{11}$ m^{-1}, $\beta^* = 0.25$ m, $l_{\text{det}} = 1$ m, $l = 40$ m, and $\gamma\epsilon_\perp = 3.75$ μm.

For a larger crossing angle of 1 mrad, the luminosity still is about 1.2×10^{36} cm^{-2} s^{-1}, while the beam-beam tune shifts decrease to $\Delta Q_x \approx 0.0090$, and $\Delta Q_y \approx -0.0122$. Finally, for $\theta_c = 2$ mrad, we find a luminosity $L \approx 6 \times 10^{35}$ cm^{-2} s^{-1}, and beam-beam tune shifts $\Delta Q_x \approx 0.0023$, and $\Delta Q_y \approx -0.0038$. Therefore, if there are no other constraints on the maximum current, the coasting beams would allow for a considerable increase in luminosity.

As for a bunched beam with constant number of bunches, the luminosity curve scales quadratically with the current, and the beam-beam tune shift linearly. For example, at a 10 times lower average beam current of 4 A, the beam-beam tune shifts are about

± 0.006 for a crossing angle of $400\,\mu$rad, and the luminosity then drops to $3 \times 10^{34}\,\mathrm{cm}^{-2}\,\mathrm{s}^{-1}$. The heat load due to synchrotron radiation is about $1.5\,\mathrm{W/m}$.

Higher luminosity can be gained if instead of a continuous beam we employ one or more long 'super-bunches' which are constrained by barrier rf buckets on either side, and only occupy a total fraction f of the ring circumference. The length of the super-bunches should be much larger than the size of the luminous region l_{det}.

Keeping the total beam current constant, and also limiting the total tune shift from two interaction points $|\Delta Q_{\mathrm{tot}}| = |\Delta Q_x + \Delta Q_y|$ to a value of 0.01, the line density λ and the filling factor f are uniquely defined as a function of crossing angle. These two functions are displayed in Fig. 16 for a total current of 1 A. Figure 17 shows the corresponding luminosity. The luminosity increases linearly with beam current.
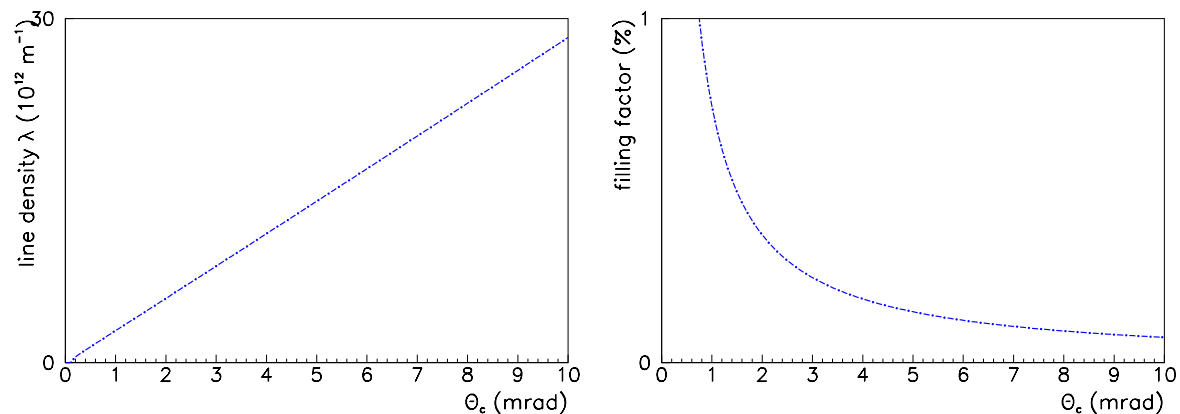
Figure 16: Line density for $|\Delta Q_x + \Delta Q_y| = 0.01$ (left) and resulting filling factor f for $I_{\mathrm{beam}} = 1\,\mathrm{A}$ (right), vs. crossing angle. The filling factor increases linearly with beam current.
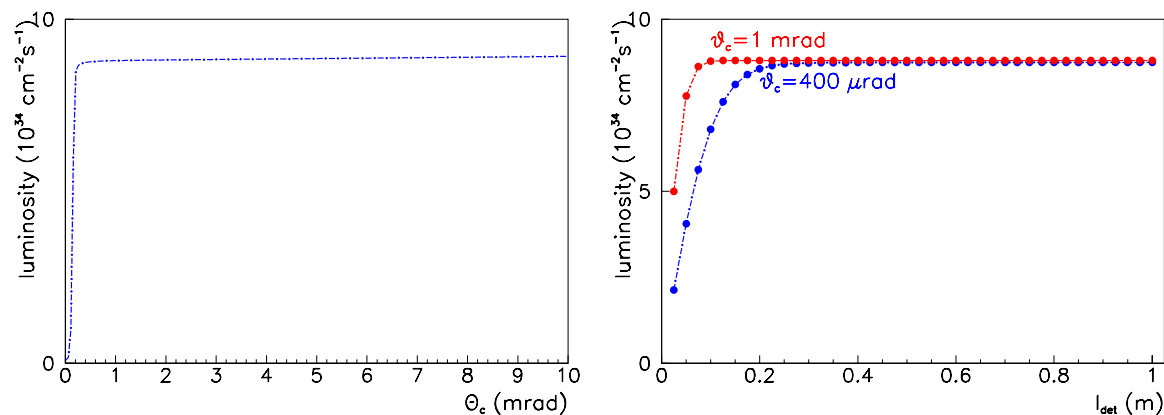
Figure 17: Luminosity for $|\Delta Q_x + \Delta Q_y| = 0.01$ and $I_{\mathrm{beam}} = 1\,\mathrm{A}$ vs. crossing angle (left) and vs. effective detector length l_{det} for two different crossing angles (right). The luminosity increases linearly with beam current.

The beam-beam tune footprint of a super bunch can be obtained from the formula

$$\Delta Q_{x,y} = \left\langle \frac{\partial U}{\partial J_{x,y}} \right\rangle_{\phi_{x,y}} \tag{38}$$

where $J_{x,y}$ denotes the transverse action variable, the angular brackets an average over the two angle variables ϕ_x and ϕ_y, and the potential U for a 'Pacman' particle encountering the opposing beam between s_0 and $l/2$ is

$$
\begin{aligned}
U(J_x, J_y, \phi_x, \phi_y, s_0, \ \theta_c) &= \frac{2r_p\lambda}{\pi\gamma} \int_{-l/2}^{s} ds \int_{-\infty}^{R(s)} dw \frac{1}{w} \left(1 - e^{-w^2/2}\right) \\
&= \frac{r_p\lambda}{\pi\gamma} \int_{-l/2}^{s} ds \ \left[\ln\left(R(s)^2/2\right) - Ei\left(-R(s)^2/2\right)\right] \quad (39)
\end{aligned}
$$

where Ei denotes the exponential integral, $Ei(x) = \int_{-\infty}^{x} \frac{e^{x'}}{x'} dx'$, and

$$R(s) \equiv \left[\frac{(x - \theta_c s)^2 + y^2}{\epsilon\beta_{x,y}(s)}\right]^{1/2}, \tag{40}$$

$$x = \sqrt{2J_x\beta_x(s)}\cos\phi_x, \tag{41}$$

$$y = \sqrt{2J_y\beta_y(s)}\cos\phi_y, \tag{42}$$

$$\beta_{x,y}(s) = (\beta_{x,y}^* + s^2/\beta_{x,y}^*). \tag{43}$$

Equation (39) includes the dependence on the betatron amplitude and on the longitudinal position.
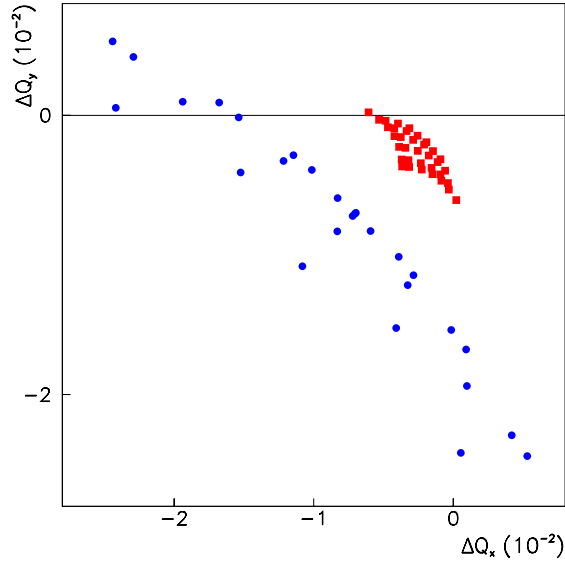
Figure 18: Tune footprints for super-bunches colliding under two different crossing angles: $\theta_c = 400 \ \mu$rad (blue circles) and $\theta_c = 1$ mrad (red squares). The points represent the tune shifts at betatron amplitudes extending from 0 to 6 σ. Other parameters: $\lambda = 8.8 \times 10^{11} \, \mathrm{m}^{-1}$, $\beta_{x,y}^* = 0.25 \, \mathrm{m}$, $l = 40 \, \mathrm{m}$.

Typical tune footprints, obtained by solving Eq. (38) numerically, are displayed in Fig. 18 considering two IPs and two different crossing angles θ_c.

6.3 Electron Cloud

Figure 19 shows the simulated average electron-cloud heat load in the arc [4] as a function of the bunch population, for the nominal bunch spacing of 25 ns. The simulation includes the elastic reflection of low-energy electrons from the chamber wall, parametrized according to Ref. [4]. The various curves refer to different values of the maximum secondary emission yield for perpendicular incidence, as indicated. Also shown is the available cooling capacity of the cryogenics system. It decreases towards higher bunch charges, due to the increasing energy deposition from synchrotron radiation and resistive-wall impedance. The figure suggests that in order to reach the nominal LHC intensity of 1.1×10^{11} per bunch, a secondary emission yield close to 1.1 will be required. In
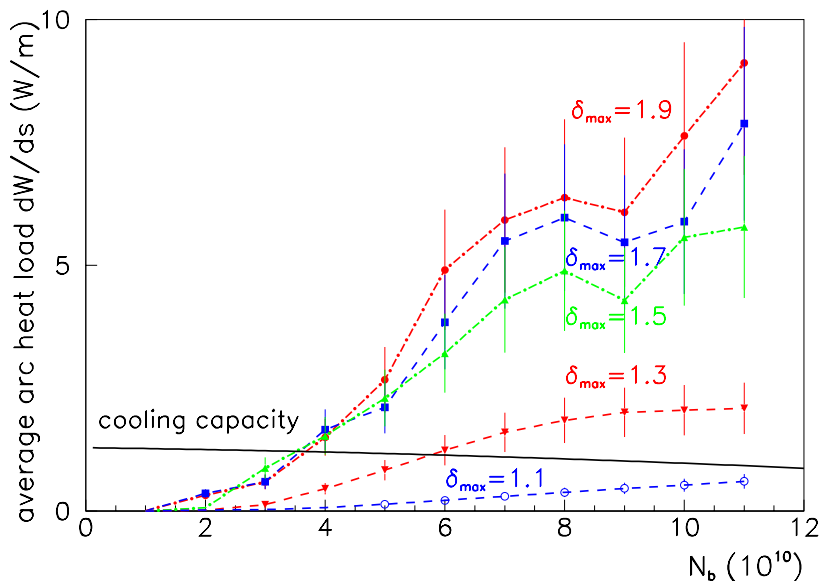
Figure 19: Average arc heat load and cooling capacity as a function of bunch population N_b, for 25 ns bunch spacing and various values of δ_{max}. Other parameters are $\epsilon_{max} = 240$ eV, $R = 5\%$, $Y = 5\%$, and elastic electron reflection is included, parametrized by a Gaussian probability distribution centered at zero primary energies with a peak value of $\delta_{el,E} = 0.56$ and a standard deviation $\sigma_{el} = 52$ eV.

Fig. 20 similar results are shown for three different bunch spacings, assuming a constant maximum secondary emission yield of $\delta_{max} = 1.1$. An increase in the LHC cooling capacity will be required for operation at either ultimate charge per bunch and 25 ns spacing or nominal charge per bunch and reduced spacing. Fig. 21 shows that, even assuming a higher maximum secondary emission yield of $\delta_{max} = 1.3$, operation beyond ultimate bunch intensity is possible with 50 ns spacing. Finally, Fig. 22 displays the simulated arc heat load as a function of the bunch spacing, for the nominal and ultimate bunch populations, and $\delta_{max} = 1.1$. The heat load increases steeply for shorter bunch spacings between 15 and 5 ns.

The heat load for a super-bunch should be much reduced. In the ideal case of a coasting beam with constant line density, an electron emitted from the wall does not gain any energy in the static beam potential, but impinges on the opposing chamber wall exactly with its initial energy. The latter value is of the order of a few eVs, where the true
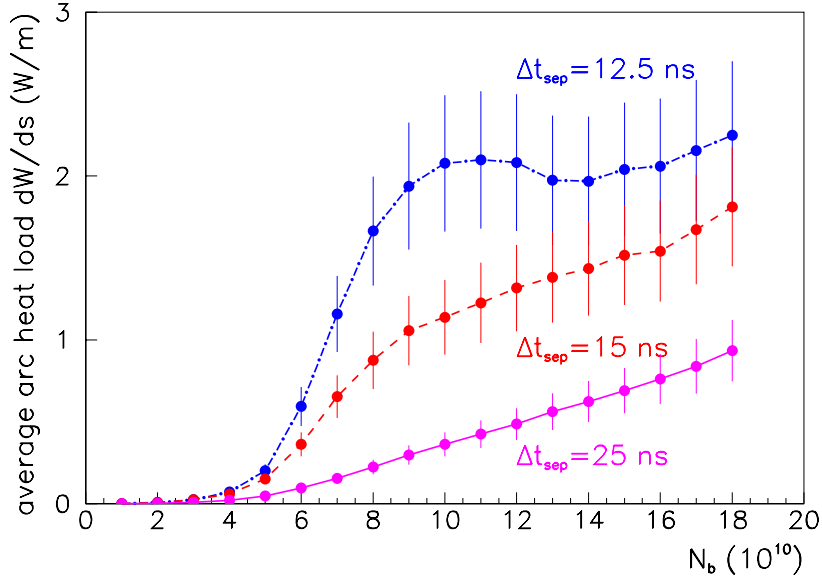
Figure 20: Average arc heat load as a function of bunch population for bunch spacings of 12.5 ns, 15 ns, and 25 ns, and a maximum secondary emission yield $\delta_{max} = 1.1$. Elastically reflected electrons are included.
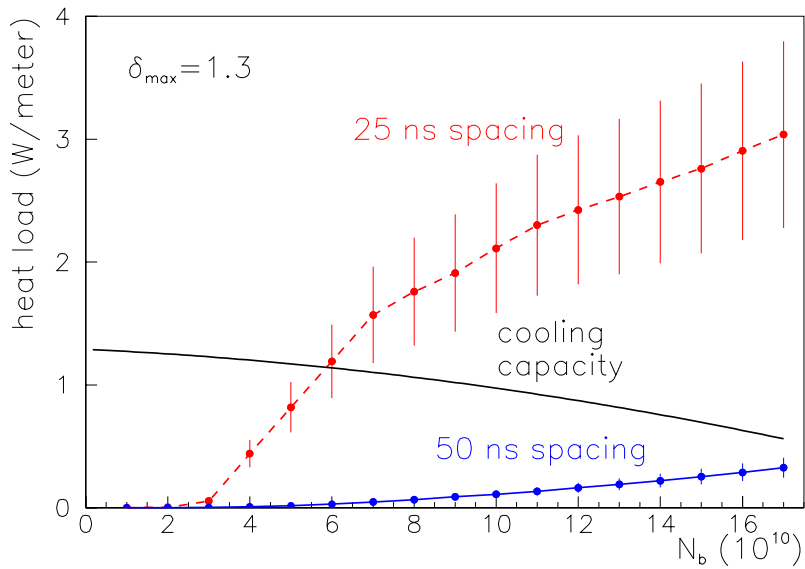
Figure 21: Average arc heat load as a function of bunch population for bunch spacings of 25 and 50 ns, and a maximum secondary emission yield $\delta_{max} = 1.3$. Elastically reflected electrons are included.

secondary emission yield is negligible. Therefore, for a coasting beam the heat load due to the electron cloud is insignificant.

If the beam does not occupy the entire circumference, but instead consists of one or more super-bunches, electrons emitted near the end of the bunch may still acquire
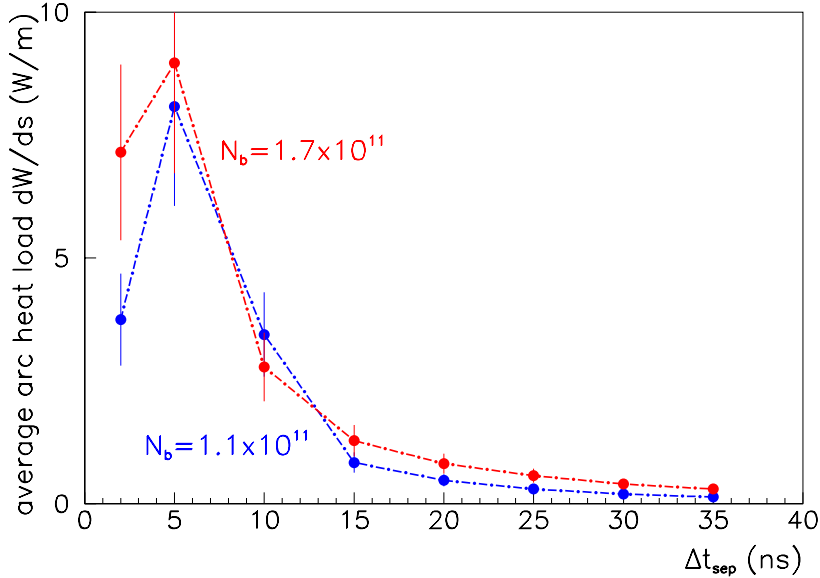
Figure 22: Average arc heat load as a function of bunch spacing, for $\delta_{\max} = 1.1$ and various bunch populations.

energy and multipact. The magnitude of the total heat load in this case is still much smaller than the heat load computed for many separate short bunches with identical total charge. The energy gain of an electron near the end of the bunch is related to the fall-off in line density $d\lambda/dt$ via

$$\frac{dE}{dt} \approx \frac{e^2}{2\pi\epsilon_0} \ln\left(\frac{r(t)}{b}\right) \frac{d\lambda}{dt} \tag{44}$$

where $r(t)$ denotes the radial position of the electron.

Figure 23 displays the simulated average electron energy deposition per passing proton and per meter length of beamline as a function of the full bunch length, where we have considered a flat distribution with a linearly rising and falling edge of 10% each. For longer bunches the heat load per proton decreases clearly. Figure 24 shows the simulated heat load as a function of the super-bunch length at constant luminosity [5]. This confirms the expected effectiveness of super-bunches in suppressing the heat deposition from the electron cloud.

6.4 Intra-Beam Scattering, Radiation Damping, and Equilibrium Emittance

Already at the LHC, radiation damping surpasses the intra-beam scattering growth rate. For post-LHC hadron colliders, synchrotron radiation may decide the choice of machine parameters. The energy loss per turn is $U_0 = C_\gamma E^4/\rho$ where ρ is the bending radius, E the beam energy, and $C_\gamma \approx 4\pi/3 \ r_A/(m_A c^2)^3 \ \approx 0.778 \times 10^{-17} \ Z^2/A^4 \mathrm{m/GeV}^3$. The product of amplitude damping time and partition number is [9]

$$\tau_z J_z = \left(\frac{3(m_A c^2)^3}{e^2 c^3 r_A Z^2}\right) \frac{1}{B^2 E} \left(\frac{C}{2\pi\rho}\right) \tag{45}$$

where z labels either plane, and $C/(2\pi\rho)$ denotes the reciprocal of the dipole filling factor. The damping time decreases inversely with energy and the square of the dipole field.
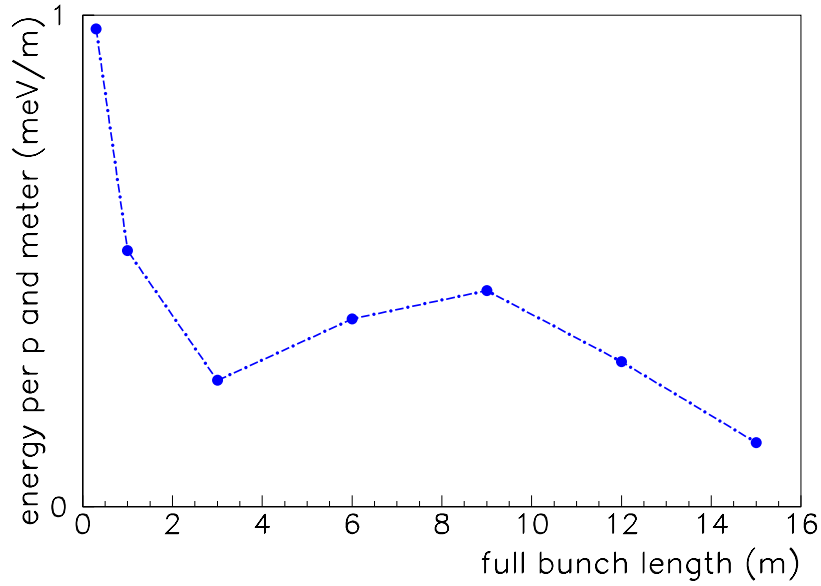
Figure 23: Average energy deposition per passing proton as a function of the full bunch length for an LHC dipole magnet, considering a constant flat top line density $\lambda = 10^{12} \, \mathrm{m}^{-1}$ with 10% linearly rising and falling edge.
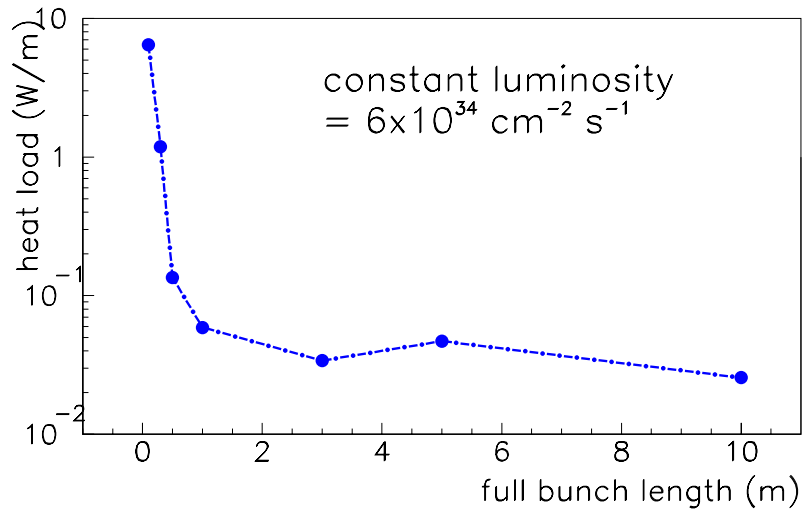
Figure 24: Simulated heat load in an LHC arc dipole due to the electron cloud as a function of super-bunch length for $\delta_{\mathrm{max}} = 1.4$, considering a constant flat top proton line density of $8 \times 10^{11} \, \mathrm{m}^{-1}$ with 10% linearly rising and falling edges. The number of bunches is varied so as to keep the luminosity constant and equal to $6 \times 10^{34} \, \mathrm{cm}^{-2} \, \mathrm{s}^{-1}$.

An important consequence of the synchrotron radiation is the shrinkage of the beam, which allows for higher luminosity. The situation differs from electron storage rings in that the damping times are of the order of hours and not milliseconds. Therefore, the synchrotron radiation leads to a continuous change of the beam emittance during the store. If uncontrolled, this could result in growing beam-beam tune shifts, consequent

blow-up, halo generation and background.

In electron storage rings, an equilibrium emittance is established as a balance of quantum excitation and damping. The corresponding normalised emittance is [9]

$$\epsilon_{x,N}^{\mathrm{SR}} \approx \frac{55}{32\sqrt{3}} \frac{\lambda_e}{J_x} \left(\frac{\gamma^3}{Q_\beta^3} \right) \left(\frac{C}{2\pi\rho} \right)^3 \tag{46}$$

where $\lambda_e = \hbar/(m_A c)$ is the Compton wavelength of the particle ($\lambda_e \approx 2.1 \times 10^{-16}/A$ m). We have employed the smooth approximations $\beta_{x,y} \approx C/(2\pi Q_\beta)$, $\hat{D} \approx \beta^2/\rho$ and $\mathcal{H} \approx \beta^3/\rho^2 \approx \rho/Q_\beta^3 (C/(2\pi\rho))^3$. For LHC parameters, the horizontal equilibrium emittance is several orders of magnitude smaller than the design emittance.

For any reasonable bunch current, the equilibrium emittance will not be determined by quantum fluctuations, but instead it will result from a balance of radiation damping and intra-beam scattering. For $\gamma \gg 1$, the horizontal emittance growth rate, $1/\tau_{x,\mathrm{IBS}} \equiv 1/\sigma_x \, d\sigma_x/dt$, due to intra-beam scattering (IBS) is [8]

$$\frac{1}{\tau_{x,\mathrm{IBS}}} \approx \frac{cr_A^2 N_b A L_c}{16 Q_\beta \epsilon_{x,N}^2 \sqrt{\kappa}\sqrt{\kappa+1}\gamma\sigma_z\sigma_\delta} \tag{47}$$

where L_c ($L_c \approx 20$) denotes a Coulomb logarithm, and $\kappa = \epsilon_y/\epsilon_x$ the emittance coupling ratio.

For $\gamma \gg Q_\beta$, the longitudinal growth rate $1/\tau_{\delta,\mathrm{IBS}} \equiv 1/\sigma_\delta \, d\sigma_\delta/dt$ asymptotically approaches the same value as $1/\tau_{x,\mathrm{IBS}}$, and the rms relative momentum spread becomes [8]

$$\sigma_\delta \approx Q_\beta^{3/2} \sqrt{\epsilon_x/\rho}, \tag{48}$$

where we have assumed equal radiation damping in the horizontal and longitudinal plane. (Otherwise, the momentum spread would be smaller by the additional factor $\sqrt{(1 - J_p + J_x)/(1 + J_p - J_x)}$, where J_x and J_p are the damping partition numbers.)

Combining (48) with Eqs. (45), (47), and $\sigma_s = c\alpha_c/\Omega_s\sigma_\delta$ (Ω_s is the synchrotron frequency), we can solve for the equilibrium emittance [7]:

$$\epsilon_{x,N}^{\mathrm{IBS}} = \frac{\rho^{5/6} N_b^{1/3}}{Q_\beta \gamma^{7/6}} \left(\frac{Z f_{\mathrm{rf}} e V_{\mathrm{rf}}}{c E_A \kappa(\kappa + 1)} \right)^{1/6} \left(\frac{C}{2\pi\rho} \right)^{1/6} \left(\frac{3 r_A L_c A}{16} \right)^{1/3}, \tag{49}$$

where f_{rf} is the rf frequency and V_{rf} the total rf voltage.

In a flat-beam configuration, the horizontal and longitudinal emittances may already halt their decline, while the vertical emittance ϵ_y continues to decrease, until it approaches a value $\kappa\epsilon_x$, where κ is determined by linear coupling and spurious vertical dispersion. If one operates on or near the coupling resonance [9], the horizontal and vertical emittances are approximately equal.

Since the equilibrium emittance depends on the beam current, which, in collision, decays on a time scale comparable to the damping time, no real steady state is established, and the luminosity lifetime is longer than it would be for constant emittances. Figure 25 illustrates the simulated variation of emittances, beam current, beam-beam tune shifts and luminosity during a 10 h store in LHC-II. The simulation includes radiation damping, intra-beam scattering, and particle consumption in collisions at two IPs. The maximum tune shift approaches 0.005. This is only half the peak value reached at the Tevatron. Emittance evolution and tune shift excursions could be further optimized. A constant beam-beam tune shift may be maintained, e.g., by varying the damping partition numbers and the IP beta functions during the store.
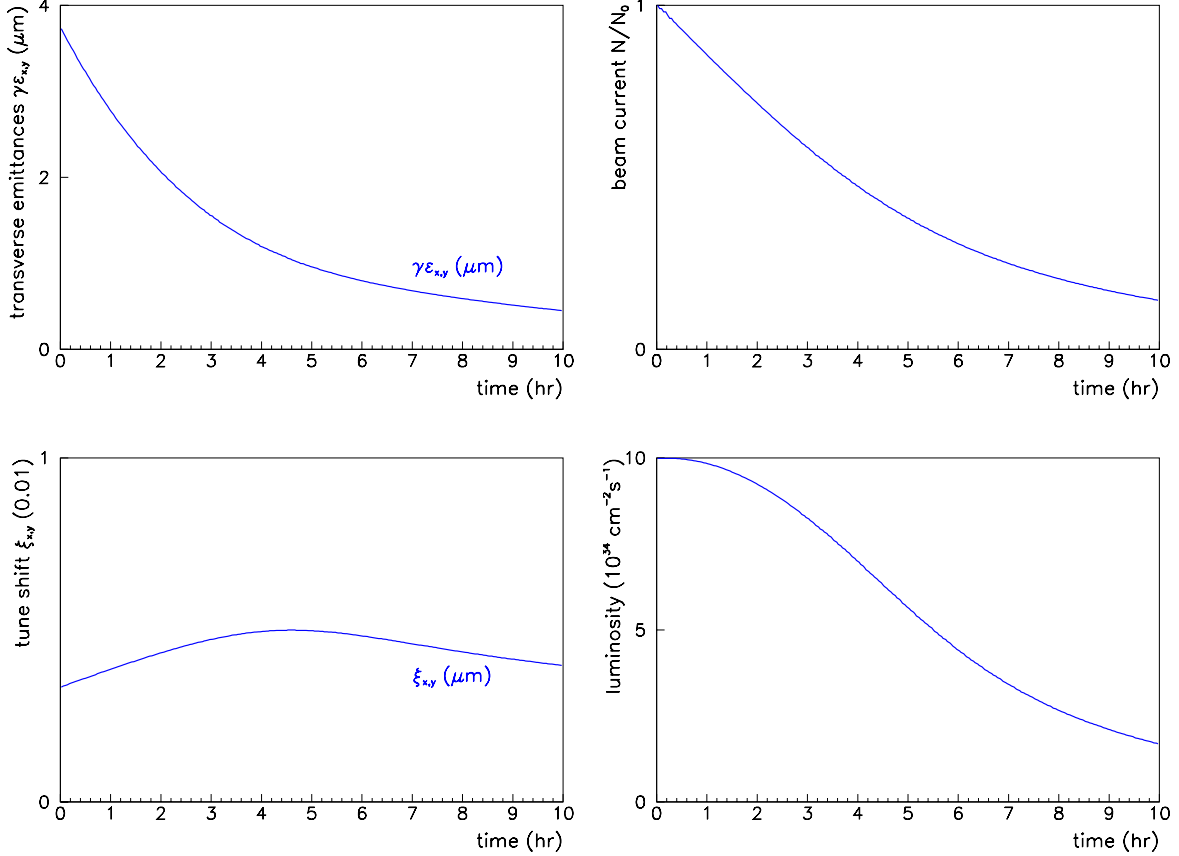
Figure 25: Dynamic changes during a store in a 28-TeV LHC-II for the parameters considered in Ref. [7], and damping partition numbers $J_x = J_y = 1$, $J_s = 2$; emittances (top left), beam current (top right), beam-beam tune shifts (bottom left), and luminosity (bottom right) vs. time [7].

6.5 Conventional Collective Effects

6.5.1 Coherent Synchrotron Tune Shift

If the coherent synchrotron tune shift exceeds the tune spread due to the rf curvature, Landau damping is lost for higher-order longitudinal modes. Introducing the effective impedance $(Z_L/n)_{\mathrm{eff}}$ and harmonic number h_{rf} the condition for stability is [10, 11]

$$\sigma_z \geq \frac{C}{2\pi} \left[\frac{\pi^3}{6} \frac{N_b f_{\mathrm{rev}} e}{h_{\mathrm{rf}}^3 V_{\mathrm{rf}}} \, \mathrm{Im} \left(\frac{Z_L}{n} \right)_{\mathrm{eff}} \right]^{1/5} . \tag{50}$$

If synchrotron radiation damping reduces the rms bunch length, the beam could become unstable during the store. An example for the LHC-II parameters is shown in the left picture of Fig. 26. Assuming an effective impedance of $\mathrm{Im}(Z_L/n)_{\mathrm{eff}} \approx 0.1 \; \Omega$, similar to the present LHC value, Landau damping is lost after about 3 hours. One approach of maintaining a bunch length above the threshold is longitudinal excitation using 'pink noise' [13]. The bunch-length evolution for such scenario is shown on the right.
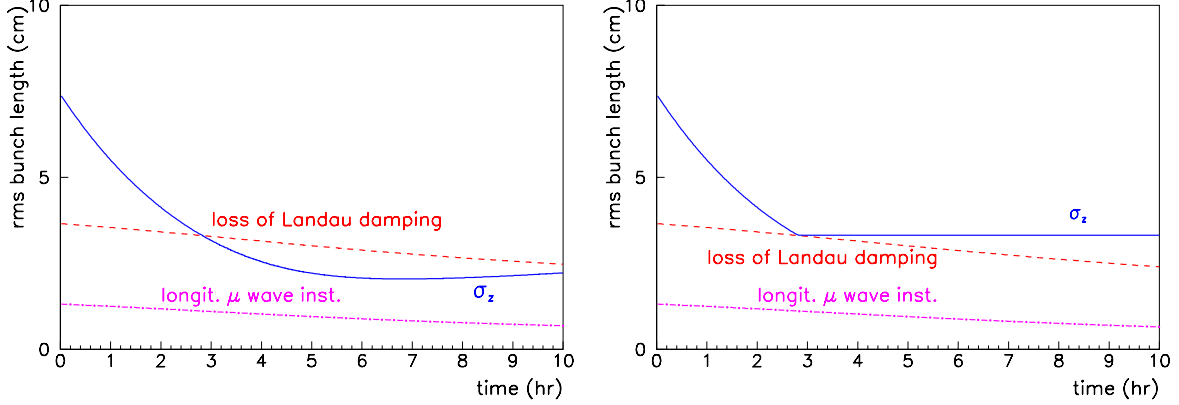
Figure 26: Evolution of the rms bunch length during a store in a 28-TeV LHC-II compared with the threshold values for loss of Landau damping, Eq. (50) and for longitudinal microwave instability [11], for the same parameters as in Fig. 25 (left) and when after 3 hours noise is added to maintain a constant value $\epsilon_L \geq 0.104$ eVs (right) [7].

6.5.2 Longitudinal Microwave Instability

The condition of stability against longitudinal microwave instability is [10, 11, 12]

$$\sigma_z \geq \frac{C}{2\pi} \left[\frac{\pi^3}{12} \frac{N_b f_{\text{rev}} e}{h_{\text{rf}} V_{\text{rf}}} \left| \left(\frac{Z_L}{n} \right)_{\text{eff}} \right| \right]^{1/3}. \tag{51}$$

This is safely fulfilled as illustrated in Fig. 26.

6.5.3 Transverse Mode Coupling

The threshold bunch current for the transverse mode coupling instability is given by [10]

$$I_b^{\text{thr}} \approx \frac{8\pi Q_s E/e}{\bar{\beta} \text{Im}(Z_t)_{\text{eff}}} \frac{\sigma_z}{C} \tag{52}$$

where Q_s is the synchrotron tune, and $\text{Im}(Z_t)_{\text{eff}}$ the sum of the broadband and low-frequency transverse effective impedance. Its value has been estimated as [10]

$$N_b^{\text{thr}} \approx 5.9 \times 10^{11} \tag{53}$$

at injection, and more than twice this value at top energy. In addition, we note that TMCI has rarely been observed for proton beams, presumably due to space-charge effects, which are still large at injection into the LHC, but may be less important in case of injection at higher energy into LHC-II.

6.5.4 Resistive Wall Instability

At injection, coupled-bunch instabilities driven by the resistive wall are also a concern [10, 12]. The resistive wall growth rate is

$$\tau_w^{-1} = \frac{r_p \bar{\beta} N_b n_b c F_\omega}{Z_0 \gamma b^3} \sqrt{\frac{\mu_0 \rho_w c}{\pi C (n - Q)}} \tag{54}$$

where Z_0 is the vacuum impedance, and b the chamber radius. The penetration factor F_ω describes the effect of a beam screen consisting of two layers, an inner thin copper layer

46

of thickness t and an outer thick stainless steal layer of thickness t'. The factor is given by $F_\omega = \mathrm{Re}[(1 + i)\xi]$ with [10, 12]

$$\xi = \frac{f + \rho_{\mathrm{rel}}f'}{1 + \rho_{\mathrm{rel}}ff'} \tag{55}$$

with $\rho_{\mathrm{rel}} = \sqrt{\rho'/\rho}$ and

$$f(\delta, t) = \frac{1 - \exp[-2(1 + i)t/\delta]}{1 + \exp[-2(1 + i)t/\delta]} \tag{56}$$

where $\delta = \sqrt{2\rho/(\mu_0\omega)}$ is the skin depth, ρ the resistivity of the inner layer, and ρ' that of the outer layer. At the LHC, the effective chamber radius is $b \approx 19\,\mathrm{mm}$, and the skin depths in copper at $20\,\mathrm{K}$ and stainless steel are $\delta_{\mathrm{Cu}} \approx 0.1\,\mathrm{mm}$, and $\delta_{\mathrm{ss}} \approx 6.2\,\mathrm{mm}$. The resistivities are $\rho_{\mathrm{Cu}} \approx 5.5 \times 10^{-10}\ \Omega\mathrm{m}$, and $\rho_{\mathrm{ss}} \approx 7.1 \times 10^{-7}\ \Omega\mathrm{m}$.

Some of these numbers have been revised by D. Brandt and L. Vos. Also the LAWAT code [14] can be used.

Assuming $(n - Q) \approx 0.25$ and the above values of resistivities and thicknesses, for nominal LHC parameters, the growth rate (54) at injection evaluates to about 30 ms, or roughly 300 turns. If we double the number of bunches, and increase the bunch population by a factor 1.6 the rise time decreases to about 100 turns. The transverse feedback must then be able to act on this time scale.

6.5.5 Tune Shift Variation for Partially Filled Ring

The magnetic image Laslett tune shift may vary along the bunch train for a partially filled ring, due to a leakage of the ac magnetic field [10]. Also the finite resistive wall will cause a coherent or incoherent tune variation [15, 16, 17]. These effects are estimated to be small.

6.5.6 Incoherent Tune Shift due to Collective Fields

The Laslett tune shifts due to the dc image currents in the magnet poles are [18]

$$\Delta Q_y = -\Delta Q_x = -\frac{r_p N_b n_b C}{48\gamma b^2 Q} \tag{57}$$

where Q is the betatron tune, and b the effective magnetic dipole gap half height. For nominal LHC parameters, and taking $b \approx 19\,\mathrm{mm}$, this incoherent tune shift is about 0.02. If we double the number of bunches, and increase the bunch charge by a factor 1.6 the tune shift becomes 0.06–0.07. This could cause two types of problems [18]: (1) a reduction of the dynamic aperture by the nonlinear image fields, and (2) resonance crossing of the coherent tunes for the multi-bunch modes.

6.5.7 Touschek Scattering at Ultimate Intensity

The coasting beam component generated by Touschek scattering for the nominal LHC parameters was discussed in Ref. [19]. The name Touschek effect [20] refers to a particle-particle collision within a bunch, by which so much energy is transferred from transverse into longitudinal phase space, that the scattered particles leave the stable rf bucket. Since it is caused by a particle-particle collision, the loss rate due to Touschek scattering is quadratic in the bunch population, namely

$$\frac{\mathrm{d}N_b}{\mathrm{d}t} = -\alpha N_b^2. \tag{58}$$

47

The number of particles outside the rf bucket increases as

$$N_{\text{coast}} = \frac{\alpha N_0 t}{1 + \alpha N_0 t} \, N_0 \tag{59}$$

where $N_0 = N_b(0)$ denotes the initial bunch population.

For round beams, a Touschek lifetime formula was derived by Miyahara [21]. After correcting his formula by a factor of two, the Touschek scattering rate is

$$\alpha_{\text{rd}} = \frac{\pi r_0^2 c}{\gamma^4} \frac{\beta_x \beta_y}{\sigma_x \sigma_y V \eta} \, D\left(\frac{\eta}{\delta q}\right) \tag{60}$$

with

$$D(\epsilon) = \sqrt{\epsilon} \int_\epsilon^\infty \frac{e^{-u}}{u^{3/2}} \left(\frac{u}{\epsilon} - 1 - \frac{1}{2} \ln \frac{u}{\epsilon}\right) \, du. \tag{61}$$

For a round beam, Miyahara's expression gives results consistent with a formula derived by Piwinski for arbitrary aspect ratio [22, 23]. Ignoring the contribution from dispersion Piwinski's expression reads

$$\alpha_{\text{piw}} = \left\langle \frac{r_0^2 c}{8\pi\gamma^2 \sigma_z \sigma_x \sigma_y} \tilde{F}(\tau_m, B_1, B_2) \right\rangle \tag{62}$$

where the brackets denote the average over the whole circumference, and

$$\tilde{F}(\tau_m, B_1, B_2) = 2\sqrt{\pi(B_1^2 - B_2^2)} \int_{\kappa_m}^{\pi/2} \left((2\tau + 1)^2 \left(\frac{\tau/\tau_m}{1+\tau} - 1\right) / \tau + \tau - \sqrt{\tau\tau_m(1+\tau)} \right.$$
$$\left. - \left(2 + \frac{1}{2\tau}\right) \ln \frac{\tau/\tau_m}{1+\tau} \right) e^{-B_1\tau} I_0(B_2\tau) \sqrt{1+\tau} \, d\kappa \tag{63}$$

with I_0 the modified Bessel function, $\tau = \tan^2 \kappa$, $\kappa_m = \sqrt{\arctan \tau_m}$, $\tau_m = \beta^2 \eta^2$ (β is the relativistic factor),

$$B_1 = \frac{1}{2\beta^2\gamma^4} \left(\frac{\beta_x^2}{\sigma_x^2} + \frac{\beta_y^2}{\sigma_y^2}\right) \tag{64}$$

and

$$B_2 = \left[B_1^2 - \frac{\beta_x^2 \beta_y^2}{\beta^4 \gamma^4 \sigma_x^2 \sigma_y^2}\right]^{1/2}. \tag{65}$$

For a double rf system with voltages $\hat{V}_1$ and $\hat{V}_2$ operating at harmonic numbers h_1 and h_2, the rf energy acceptance η provided by this double rf system is computed as

$$\eta \equiv \left(\frac{\Delta E}{E}\right)_{\text{max}} = \left(\frac{2e}{\pi\alpha_c E_0} \left[\frac{\hat{V}_{\text{rf},1}}{h_1} + \frac{\hat{V}_{\text{rf},2}}{h_2}\right]\right)^{1/2}, \tag{66}$$

where α_c denotes the momentum compaction factor.

Beam parameters for the nominal LHC at injection and at top energy are listed in Table 14. The rf parameters are taken from Ref. [24].

In case of the LHC, the round beam estimate, Eq. (60), evaluates to $\alpha_{\text{rd}} \approx 5.0 \times 10^{-19}$ s^{-1} at injection, and $\alpha_{\text{rd}} \approx 2.0 \times 10^{-19}$ s^{-1} at 7 TeV. From Piwinski's formula, Eq. (62), we obtain similar numbers: $\alpha_{\text{piw}} \approx 5.3 \times 10^{-19}$ s^{-1} and $\alpha_{\text{piw}} \approx 2.1 \times 10^{-19}$ s^{-1},

48

respectively. Thus, using $N_0 = 1.7 \times 10^{11}$ and Eq. (59), coasting beam is produced at a rate per proton of 3×10^{-4} hr^{-1} during injection and 1.3×10^{-5} hr^{-1} at top energy.

Once the protons are outside of the bucket, they lose energy due to synchrotron radiation. This energy loss amounts to $\mathrm{d}\delta/\mathrm{d}t \approx -2.8 \times 10^{-9}$ s^{-1} at 450 GeV and $\mathrm{d}\delta/\mathrm{d}t \approx -1.0 \times 10^{-5}$ s^{-1} at 7 TeV [25]. If the collimators provide an energy aperture of 3.9×10^{-3} [26], a scattered proton is lost after about $\tau_{\mathrm{loss}} \approx 390$ hours at injection or after $\tau_{\mathrm{loss}} \approx 6.5$ minutes at top energy, respectively. While the energy drift due to synchrotron radiation is unimportant at injection, in collision it gives rise to a steady-state coasting beam fraction of $\alpha_{\mathrm{piw}} N_0 \tau_{\mathrm{loss}} \approx 1.4 \times 10^{-5}$.

variable	symbol	value (inj.)	value (top)	rf upgrade
rms horizontal beam size	σ_x	883 μm	220 μm	220 μm
rms vertical beam size	σ_y	883 μm	220 μm	220 μm
rms bunch length	σ_z	130 mm	77 mm	38.5 mm
average beta function	$\beta_{x,y}$	100 m	100 m	100 m
momentum compaction factor	α_c	0.000325	0.000325	0.000325
beam energy	E	450 GeV	7000 GeV	7000 GeV
number of proton bunches	n_b	2800	2800	2800
number of protons per bunch	N_b	1.7×10^{11}	1.7×10^{11}	1.7×10^{11}
revolution time	T_0	800 μs	800 μs	800 μs
transverse emittance (1σ)	$\epsilon_{x,y}$	7.8 nm	0.5 nm	0.5 nm
relativistic factor	γ	480	7461	7461
bunch volume	V	4515 mm^3	166 mm^3	83 mm^3
rms uncorrel. trans. momentum in units of $m_0 c$	δq	0.00424	0.0171	0.0171
1st rf voltage	$\hat{V}_{\mathrm{rf},1}$	750 kV	16000 kV	43000 kV
2nd rf voltage	$\hat{V}_{\mathrm{rf},2}$	3000 kV	0 kV	16000 kV
1st harmonic number	h	35640	35640	106920
2nd harmonic number	h	17820	17820	35640
energy acceptance	η	0.88×10^{-3}	0.34×10^{-3}	0.49×10^{-3}

Table 14: LHC parameters at injection and top energy for ultimate parameters, and for the moderate upgrade.

References

[1] KEKB B-Factory Design Report, KEK Report 95-7 (1995).

[2] E. Keil, *Luminosity Optimization for Storage Rings with Low-β Sections and Small Crossing Angles*, NIM 113, p. 333 (1973).

[3] E. Keil, C. Pellegrini, A.M. Sessler, CRISP Report 72-34 (BNL, 1972).

[4] F. Zimmermann, *Electron-Cloud Simulations: An Update*, Proceedings of Chamonix XI, CERN-SL-2001-003-DI (2001); see also G. Rumolo, F. Ruggiero, F. Zimmermann, *Simulation of the Electron-Cloud Build Up and Its Consequences on Heat Load, Beam Stability and Diagnostics*, in Proc. ICAP 2000, Darmstadt, PRST-AB 012801 and CERN-SL-2000-073 AP (2000).

[5] F. Zimmermann, *Two-Stream Effects in Present and Future Accelerators*, invited talk, Proc. EPAC 2002, Paris.

[6] K. Takayama, J. Kichiro, M. Sakuda, Y. Shimosaki, M. Wake, *Super-bunch Hadron Colliders*, Phys. Rev. Letters, vol. 88, 144801 (2002).

[7] F. Zimmermann, *Luminosity Limitations at Hadron Colliders*, CERN-SL-2001-009 AP (2001).

[8] J. Wei, *Intrabeam Scattering Scaling for Very Large Hadron Colliders*, unpublished draft (2001); J. Bjorken and S. Mtingwa, Part. Acc. 13, 115 (1983).

[9] E. Keil, *Synchotron Radiation Dominated Hadron Colliders*, in Proc. PAC 97, p. 104, 1996, and Proc. 34th Eloisatron Workshop, Erice 1996.

[10] F. Ruggiero, *Single-Beam Collective Effects in the LHC*, CERN SL/95-09, 1995.

[11] J.T. Rogers, *Collective Effects and Impedances in the RLHC(s)*, CBN 96-14, 1996.

[12] E. Keil, *Synchrotron Radiation Dominated Hadron Colliders*, 34th Eloisatron Workshop, Erice, November 1996, CERN SL/97-13 (1997).

[13] T. Toyama, et al., in Proc. EPAC 2000, Vienna; similar methods were used at the S$p\bar{p}$S by T. Linnecar.

[14] E. Keil and B. Zotter, *Impedance of Layered Vacuum Chambers for Large Colliders*, CERN-SL-98-019-AP (1998).

[15] J. Gareyte, *Azimuthally Dependant Space-Charge Effects in the SPS and LHC*, CERN-SL-Note-2000-056 (2000).

[16] V.I. Balbekov, *The Effect of Chamber Wall Conductivity of an Accelerator on the value of Coulomb Tune Shifts*, EPAC 92, Berlin (1992).

[17] L. Vos, in Proc. EPAC 2000, Vienna (2000).

[18] A. Chao, *Report of VLHC Instability Workshop*, SLAC, March 21–23, SLAC-PUB-8800 (2001); and V. Lebedev, presentation at this workshop (2001).

[19] F. Zimmermann and M.-P. Zorzano, *Touschek Scattering in HERA and LHC*, LHC-Project-Note-244 (2000).

[20] C. Bernadini et al., Phys. Rev. Letters, vol. 10, p. 407 (1963).

[21] Y. Miyahara, Jap. J. Appl. Phys., vol. 24, p. L742 (1985).

[22] A. Piwinski, *The Touschek Effect in Strong Focusing Storage Rings*, DESY 98-179 (1998).

[23] A. Piwinski, *Touschek Effect and Intrabeam Scattering*, in A. Chao and M. Tigner (eds.), "Handbook of Accelerator Physics and Engineering", World Scientific (1999).

[24] E. Shaposhnikova, *Longitudinal beam parameters during acceleration in the LHC*, LHC Project Note 242 (2000).

[25] The LHC Study Group, *The Large Hadron Collider - Conceptual Design*, CERN/AC/95-05 (1995).

[26] D. Kaltchev, private communication (2000).

Part II
Hardware components and injectors

7   Superconducting magnets

7.1   Panorama of High Field Accelerators Magnets

The peak field in the coil is limited by superconductor performance. Niobium titanium (NbTi) is the practical superconductor from which all accelerator magnets are built today. It is a very good engineering material, being strong, easy to draw and maintains its qualities when bent through sharp angles, but cannot be used in fields above about 10 T. At present the only practically developed superconductor capable of considerable transport current in fields beyond 10 T is niobium tin (Nb_3Sn), but being very brittle this is a much more difficult material to use for magnets. For comparison the critical surfaces of NbTi and of Nb_3Sn are shown in Fig. 27.
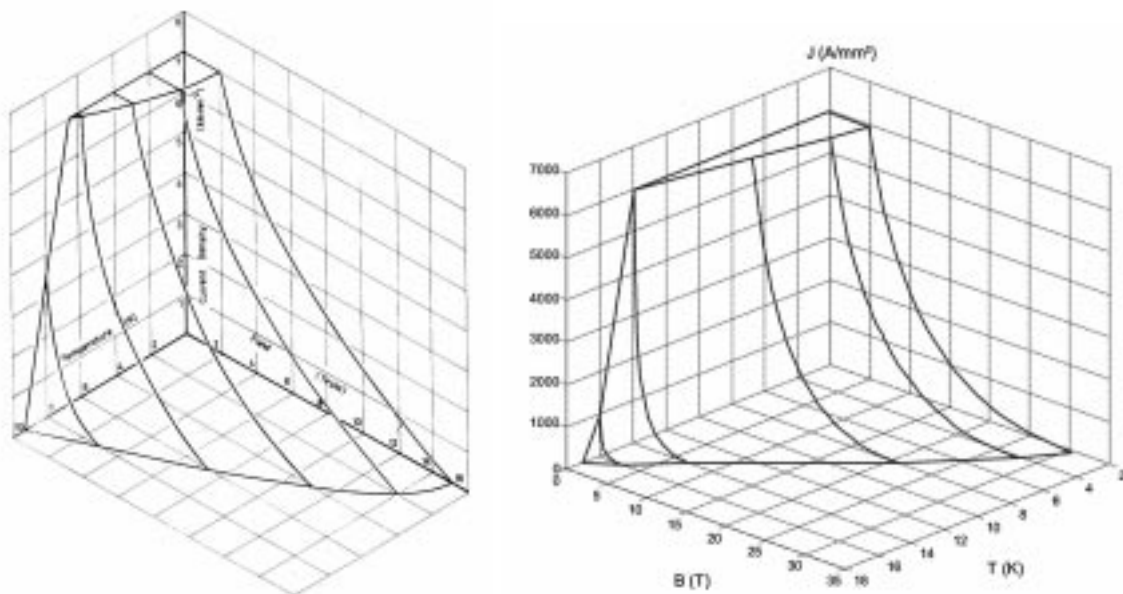
Figure 27: Critical Surface of NbTi (left) and of Nb3Sn (right).

R&D on Nb_3Sn magnets progressed very slowly in the nineties. In practice after the termination at the beginning of the decade of the CERN and BNL Nb_3Sn programmes (dipoles of about 10 T [1] and 8.5 T [2], respectively), only two projects were pursued: one at the University of Twente (UT) [3], in collaboration with CERN, the other at LBNL [4]. Both projects made use of Nb_3Sn strands made into a flat "Rutherford" cable. The UT magnet was the first dipole to break soundly the "10 T" barrier, in 1995, passing 11 T at the first quench and reaching its limit at 11.5 T @ 4.2 K, near its short sample limit. Then in 1997 the LBNL dipole D20 reached 12.8 T @ 4.2 K and 13.5 T @ 1.8 K (with current densities of half those available today!). This is still the record field for an accelerator-type magnet. However, D20 was plagued by very long training and some of the techniques employed (four layers, pre-stressing obtained by winding a rope, etc.) would not be easy to adopt for a large production of long magnets. All such magnets built to date were short models having full size cross section. In the same period studies were carried out at INFN-LASA and CEA, Saclay on a second generation of LHC low-beta quadrupoles. At

LASA the work, which was later on carried out jointly with LBNL, aimed to design and build a model [5], based on Nb_3Sn under development in Italy. The CEA-Saclay project was oriented initially to technological development and subsequently to the design of quadrupoles for LHC or Tesla [6].

At present four laboratories in the U.S., three in Europe and one in Japan are pursuing the study of high field magnets for accelerators, the most vigorous effort being in the U.S.

1. LBNL. It is the centre for the development of practical SC material for application in the field of HEP in the US. In addition it has its own high field magnet programme, pursuing presently the line of the so-called Common Coil (CC) with the Wind and React (W&R) technique. In May 2001 a basic model magnet of this type reached 14.5 T in a 25 mm aperture. A considerable effort is now being put into the testing of design concepts in dedicated small coils for fast turn around.

2. FNAL. The superconducting magnet group has been reconstituted over the last five years. Fermilab is pursuing several different lines:

   (a) An 11-11.5 T classical $\cos\vartheta$ design, as being the most probable candidate for a future VLHC. This choice of a moderately high field is based on a study of the machine problems, in particular the synchrotron radiation, and cost optimization of a new machine, including the tunnel.

   (b) A 10-11 T Common Coil design manufactured with the R&W technique. If this design can be made to work, avoiding damage to the fragile Nb_3Sn, it has potential for bringing down cost with respect to the $\cos\vartheta$ design.

   (c) High gradient and large aperture quadrupoles for LHC low-beta triplet upgrade (up to 240 T/m in a 90 mm bore) [7].

   (d) R&D on conductor and cables.

3. BNL. The laboratory continues to experiment with high field magnets based on both Nb_3Sn and High Temperature Superconducting (HTS) material. Having suffered in the past with the problems of R&W Nb_3Sn $\cos\vartheta$ coils it was at the origin of the CC design and a small design team works to solve the problems of this design with regard to field quality.

4. Texas A&M University. This laboratory has been concentrating on a block coil using so-called stress management to limit the local forces on the Nb_3Sn conductor. This design, proposed earlier and then overshadowed by the CC design, is now attracting renewed interest. Although it appears that the conductor is less sensitive to stress than previously believed, such techniques may be necessary for very high fields, and especially for magnets with small bores.

In comparison the effort elsewhere is at present rather modest:

1. The University of Twente (UT), in collaboration with CERN is building a large bore (88 mm) model 10 T dipole, using W&R Nb_3Sn. If successful it may open the door to possible use of shorter separation dipoles in the LHC. It uses conductor supplied by SMI, a Dutch company developing Nb_3Sn with the promising Powder In Tube (PIT) technique. The most recent achievement is J_c in excess of 2000 A/mm^2 @ 12 T and 4.2 K with a very attractive filament size of 20 μm. The strand is cabled by LBNL.

2. INFN-LASA stopped the low-beta quadrupole project a few years ago in order to concentrate on detector magnets. The Italian company developing the material, Nb_3Sn via the ITD (Internal Tin Diffusion) route, also stopped the activity in this sector after having achieved a record current of 1950 A/mm^2 @ 12 T and 4.2 K, as

measured at LASA in 1998. Some activity is restarting on new HTS materials.

3. CEA-Saclay is still pursuing the quadrupole models on a longer time scale than originally planned and meanwhile is developing special insulating techniques. The project is based on ITD Nb_3Sn being developed by a French company. In its present phase the CEA program is more aimed at assessing technical feasibility and learning the technology and the conductor than at reaching high peak field.

4. KEK together with the National Research Institute for Metals (NRIM) in Japan is investigating the possibility of using Nb_3Al as an alternative to Nb_3Sn, for use in high performance magnets such as could be needed for an LHC insertion upgrade. This material, produced by the technique of rapid quenching, is less sensitive to stress than Nb_3Sn.

CERN is involved to a greater or lesser degree in all of these latter studies. Its large team of experts is however fully occupied with the huge number of magnets for the LHC project, and will only be able to invest significant effort in R&D for high field magnets when this work is sufficiently advanced and when new funds become available.

7.2 Quadrupoles for an LHC luminosity upgrade

The last INFN-LASA design exercise was for a 70 mm bore quadrupole, like the present LHC inner triplet, with a 300 T/m design gradient @ 1.9 K, some 25% increase over the NbTi quadrupoles being provided by Fermilab and KEK. All the main issues were addressed in some detail, including stability against secondary radiation and protection in case of quench. These points are not trivial, because Nb_3Sn requires impregnation, reducing the advantage of superfluid as coolant, and the very high current density puts severe constraints on safety for long magnets. No major obstacles were found and the same design scaled with the present J_c performance should achieve the same goal, namely 300 T/m $\times$ ⌀70 mm, but @ 4.5 K.

The LASA design work led to the postulation of a relatively simple scaling law [5], a revised version of which is shown in Fig. 28. In this figure the $J_{overall}$ (i.e. the "engineering" current density that gives the field), is derived by taking the best J_c (the non-copper current density) of 2800 A/mm^2 recently measured in the US on Nb_3Sn short samples, and by considering strands with 50% copper content, a 89% cable compaction factor, and some 175 μm turn-to-turn insulation (parameters just reachable today).

The scaling law presented indicates that the maximum gain with Nb_3Sn properties is for larger apertures rather than for the very high current density required for small apertures. In fact, for apertures of less than 65 mm NbTi is probably sufficient since very high gradients, almost 280 T/m can be reached with this material (albeit at @ 1.9 K). A possible advantage of Nb_3Sn for a small aperture is that very high gradients of 300-350 T/m, and may be up to 400 T/m $\times$ ⌀50 mm, can be reached at 4.5 K, rather than at superfluid helium temperature, with potential benefits in terms of cryogenic load. However, although a higher luminosity LHC will be cryogenically very demanding, the power density is such that removing the heat from the coil may still have to rely on the large thermal conductance of superfluid helium.

With its large aperture, the option of 200/240 T/m (operation/design) $\times$ ⌀90 mm proposed recently by Fermilab [7] for a possible low-beta triplet quadrupole, is certainly reasonable and still larger apertures may be reachable in the future without compromising the gradient. Besides providing adequate space for the beam envelope with reduced β^*, this might also be useful to avoid too large a heat deposition from radiation in the upgraded inner triplet (by opening the quads to let the radiation through, to be absorbed at room
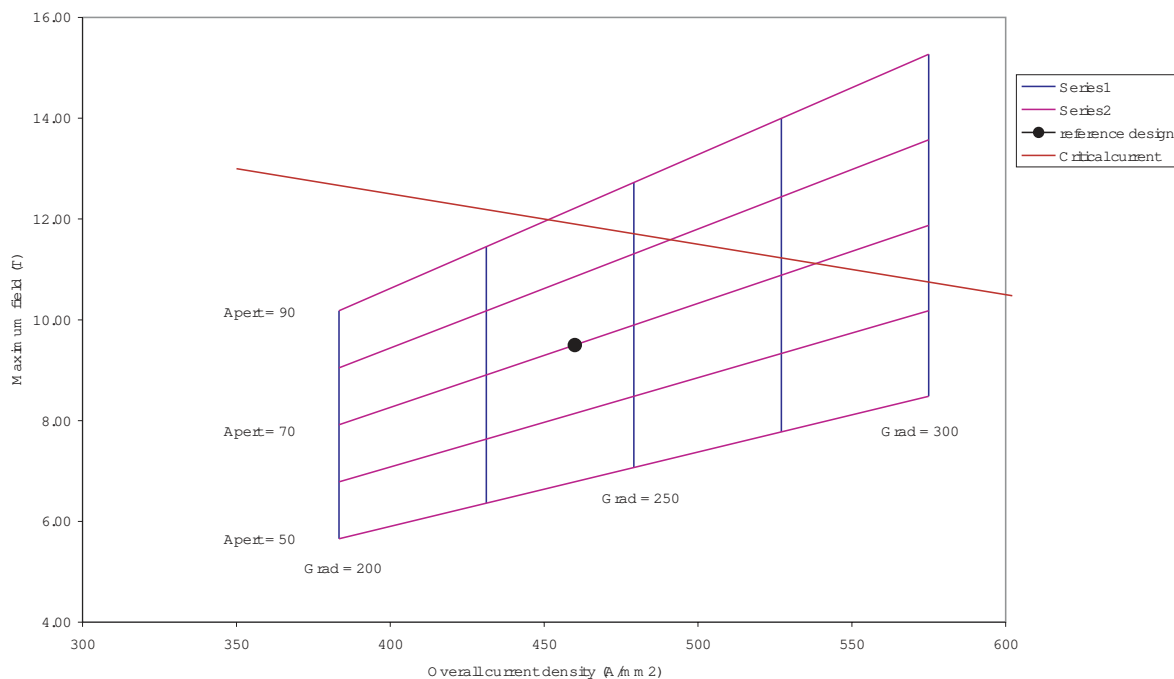
Figure 28: Approximate scaling law to determine possible gradient/aperture options with respect to actual best Nb$_3$Sn critical current density. The limiting current is based on J_c of 2800 A/mm^2 @ 12 T, 4.2 K, 50% copper, and approximately 30% of voids and insulation in the coils.

temperature in less susceptible regions).

7.3 Dipoles and Quadrupoles for an Energy Upgrade (the Super-LHC option)

The most optimistic scenario would foresee dipole magnets with an operating field of 15 T, with about 2 T margin, i.e. having a maximum field of 17 T. This would bring the collision energy up from about 15 TeV, ultimately possible in the present LHC, to nearly 25 TeV. It is not totally unrealistic to think of this if we consider that the Common Coil dipole of LBNL has recently reached 14.5 T, and that the performance of the best Nb$_3$Sn conductor has improved by about 20% in the two years since conductor was supplied for this test.

With superconducting magnets it is important to confine the dynamic range as much as possible. Ideally, a factor 3 between injection and flat top energy would nicely contain the detrimental dynamic effects in cable and magnets, and would limit the need for non-linear correctors. If we suppose that 15 T magnets will be available in due course for the S-LHC ring, we should also study appropriate schemes for the accelerator chain. A non-exhaustive list of possibilities may read as follows:

1. To use the present LHC to boost the energy from 450 GeV to about 6 TeV. This would allow operation at 4.5 K, reducing the absorbed cooling power). The S-LHC ring will ramp from 6 to 15 T. As the two (four, in fact) rings would have to share the same tunnel, the problem of space may rule out this option. Probably the only way would be to change the present cryostat (whose values is less than 10% of the total cost of the cryomagnet system) and put the LHC dipole cold masses together with those of the S-LHC in a common insulating vacuum vessel. Problems would

54

include that of getting the stiff beams from the LHC to the S-LHC.

2. To double the present injection energy from the SPS ring. Filling the SPS tunnel with 4 T superconducting dipoles, re-actualizing the Super-SPS project (see next paragraph), would increase the injection energy from SPS to 1 TeV. The LHC ring would then be replaced by the S-LHC ring. Although large, the energy swing of about 12 should be compared with 14 for the present LHC (16 for ultimate performance). Problems would include a new transfer line and dealing with the dynamic range which would be very hard to cope with, at least for the present high performance Nb_3Sn, which has effective filament diameters of around 60 μm.

3. Use the present SPS as injector, as for the LHC, at 450 GeV, and introduce two low field (2 to 2.5 T) boosters in the LHC tunnel to inject into the S-LHC at about 2 TeV. This would at least partially alleviate the problems cited above. How to house all this equipment in the LHC tunnel is another matter. An idea suggested by Gupta would be to have one single magnet structure which allows accelerating the beam in a low field channel to about 2 TeV, from which the beam is injected into the high field channel for final acceleration up to about 13 TeV. Such a system has already been studied at BNL in the framework of the Common Coil development and the VLHC. Of course this idea would need a critical appraisal for the highly constrained case of the S-LHC. It is not even obvious that the CC approach is the correct one. The simplicity of making the four channels separate, albeit in the same vacuum vessel, is also highly appealing. In this scenario nothing is used of the present LHC, except possibly some of the power and cryogenics infrastructure. But it does have the merit of leaving unchanged the injection chain.

7.4 Super-SPS

The option of an S-SPS calls for a clear expression of interest from the point of view of accelerator physics. It has been suggested that such an option may allow:

1. A direct luminosity increase in the present LHC (e.g., if the beam intensity or quality is limited due to difficulties in the control of fields due to persistent currents).

2. Injection directly into the S-LHC at something approaching a reasonable energy.

It may be possible to install a pulsed SC ring on top of the existing SPS machine (see Fig. 29), although some creative solution would be needed to bypass the existing 200 MHz RF system.

This option would require moderately fast ramping SC magnets. Many problems have to be faced, such as AC losses, heat removal, field quality during ramping, etc. These problems are however already the subject of serious studies [8] and solutions can be envisaged. The R&D could be shared with other laboratories (*e.g.*, GSI ramped superconducting synchrotron for Heavy Ions project, Thermonuclear Fusion projects). A ramp rate of 0.2 T/s, i.e. a ramping time of less than 20 s for the SPS is certainly feasibly. The real challenge is to stay within a small budget (150 MCHF?), in order to become already appealing for the LHC in the medium term. Of course the low field (4-4.5 T) suggests the adoption of very economical techniques to build magnets (plastic collars, minimum yoke size, etc. . .). Some innovative solution could be explored to reduce dramatically the risk and the cost of Rutherford cables, *e.g.*, to use cheap standard NMR superconductor, with several wire powered independently to create the desired field shape during ramp (thus correcting dynamic effects). The moderate size of the magnets also makes construction accessible to a much wider range of companies than the present LHC dipoles, with the
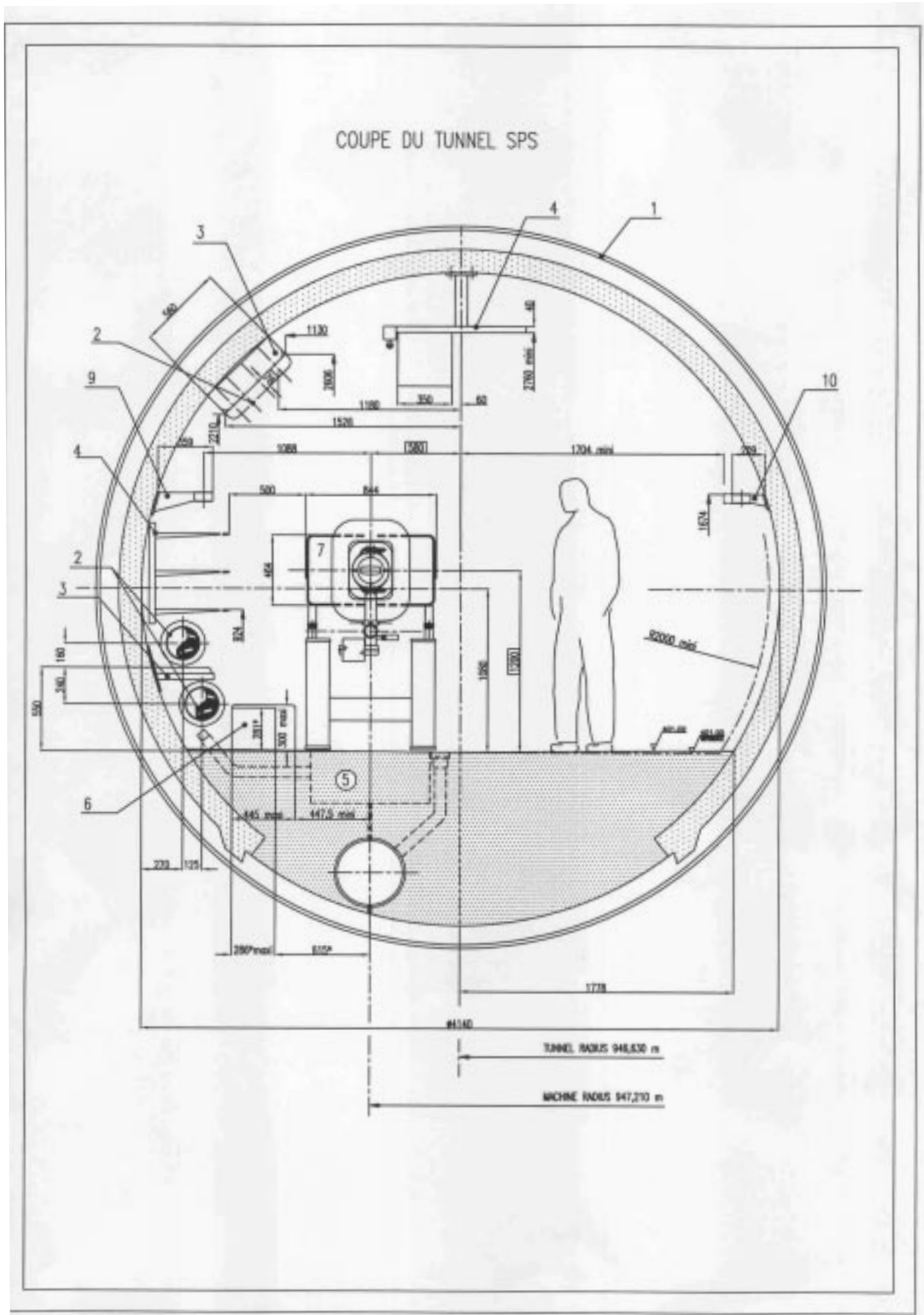
Figure 29: Schematic layout of the SPS tunnel cross section (courtesy G. Arduini).

likely benefit of a normally competitive market situation. The possibility of having the magnets of the Tevatron or HERA, should they become available, could also be explored.

It would also be necessary to install a superconducting transfer line from the S-SPS to the LHC or S-LHC. For this one could possibly make use of the low field economy design (Pipetron) recently developed at Fermilab for the initial phase of the VLHC. These are very interesting superferric magnets, excited by a single superconducting line carrying 80-100 kA. With the advent of HTS (power transmission lines are among the first major applications of HTS) this line might even be cooled using liquid nitrogen, which would simplify the cryogenics.

It should be noted that although the S-SPS may not, technologically speaking, be the most challenging exercise, it is nevertheless outside the mainstream of present development work that is more focused on high field. It would call for innovative techniques to render the magnet system cheap and reliable and would therefore require the setting up of a dedicated team. Before embarking on such a programme it would have to be shown that the benefits for accelerator physics would be worth the investment.

7.5 R&D Program for SC Materials and Magnets

For the LHC upgrade, we need a serious and vigorous R&D program in two steps.

I. For the luminosity upgrades certainly the focus is for quadrupoles which perform 20-40% better than the ones presently under construction, either in terms of aperture or gradient (most likely the former) in order to provide space for the beams in the inner triplet when β^* is reduced to 0.25 m. Dipoles with large bore and high field are also desirable in that they could lead to improvements in the layout of the region. As previously mentioned a few programmes addressing these issues are ongoing (UT, separation dipoles, CEA, quadrupoles) or are about to be started (Fermilab, quadrupoles). Our goal might be reached by endorsing these programs and by collaborating in the development to ensure that the projects satisfy the precise LHC upgrade needs. The best of the present Nb_3Sn, would already satisfy the requirement for current density, but needs further development focused on smaller filament size. Cost should not be a crucial issue for such magnets, given the limited number. An intermediate solution [9] would consist of using weaker but longer, larger aperture NbTi quadrupoles, taking advantage of the space freed by using a shorter, high field, large aperture beam separation dipole D1. The target for such a programme is to complete the R&D by about 2007, to build long magnets in 2008-2011, to be installed in the accelerator after five years of running with the initial magnet system.

II. For the Energy upgrade a much vaster effort is needed, and a longer time scale has to be envisaged. At least 10 years of vigorous development are needed, and an ambitious target would be the production of realistic short models working at 15 T operational field by 2012, the engineering of long prototypes by 2015, and the completion of effective construction by about 2020.

In particular, some of the subjects that need to be addressed are as follows:

1. **Materials.** Nb_3Sn is at present the only viable choice, as it requires only a relatively minor development in term of J_c (mainly optimizing it at high field rather than at 12 T as is done now). The most difficult point is obtaining this current density (3000 A/mm^2 @ 12 T or equivalently 1500 A/mm^2 @ 15 T, 4.2 K) together with acceptable filament size. Dipoles fill 20 km of the 27 km of the tunnel and filament size beyond 20-25 μm may be impossible to correct. For large scale use

the process has to be tuned to reduce the cost substantially; this will require significant development effort. It has also to be verified that the magnetic forces in a 15 T magnet can be handled in such a way as to avoid damaging the conductor. Given the time scale, the use of other superconductors should also continue to be explored:

(a) Nb_3Al. This material, which has only yet been produced on a laboratory scale, is superior to Nb_3Sn as regards strain dependence. The work at LBL has shown that Nb_3Sn is less sensitive to strain than was originally thought, but its use at higher fields may lead to requiring complicated and possibly expensive stress management technology, which could be avoided if Nb_3Al technology were to become available. It would be wise to invest some development effort on this material, at least for special applications.

(b) Bi-2223 or Bi-2212. Of all HTS materials Bi-2223 is by far the most developed. It is not suitable for our application at present, due to too small overall J_c in the interesting range (below 16 T), and because its tape form is not adapted for large current with very high filling factor (although the Common Coil may have an advantage over the other design in this respect). The Bi-2212 material has characteristics that are much better suited for our purpose, and LBL, in collaboration with Showa, has produced lengths of Rutherford cable which are being incorporated into test windings at BNL. This effort is worth intensifying.

(c) YBCO, where the biggest effort of the HTS community is concentrated at present because of its promising properties at 77 K, may be an interesting candidate for a moderate field associated with potentially cheap cryogenics (*e.g.*, S-SPS dipoles). That is if the materials scientists succeed in passing from 10 cm long samples to km long units at economical cost (at the moment the difficulties associated with the deposition technique required to obtain high performance do not inspire confidence).

(d) MgB_2: this recently discovered material has two advantages:

    i. It is intrinsically very cheap.

    ii. It has a potential application for low field (< 5 T) at a temperature of 20 K, as shown in Fig. 30. This could make the material appealing for an application in the small LHC tunnel, where cooling at 20 K would consume less power and may require less space.

2. **Magnet Design and Winding Technology.** Only the W&R technique can be used for the $\cos\vartheta$ design. Here the problems of insulation are severe (the coil has to be heat treated at about 650 C for between one and two weeks). The magnet structure is well known, although probably difficult to push up to the 15-16 T range. Indeed this structure requires in principle a strong azimuthal prestress that goes according to B^2. Considering that Nb_3Sn is sensitive to transverse stress this is a major concern for the $\cos\vartheta$ layout. Experimentally demonstrated strain sensitivity is less important than expected, however, and a 15 T $\cos\vartheta$ dipoles would require 'only' 35% more azimuthal prestress than that required by the LBNL D20. Apart from prestress, the challenge of this design is to devise new winding/collaring/assembly and heat treatment techniques from which to derive economical solutions.

(a) The Common Coil design, see Fig. 31, can be pursued both with the W&R technique and, given the large radius of curvature at the ends, with the R&W
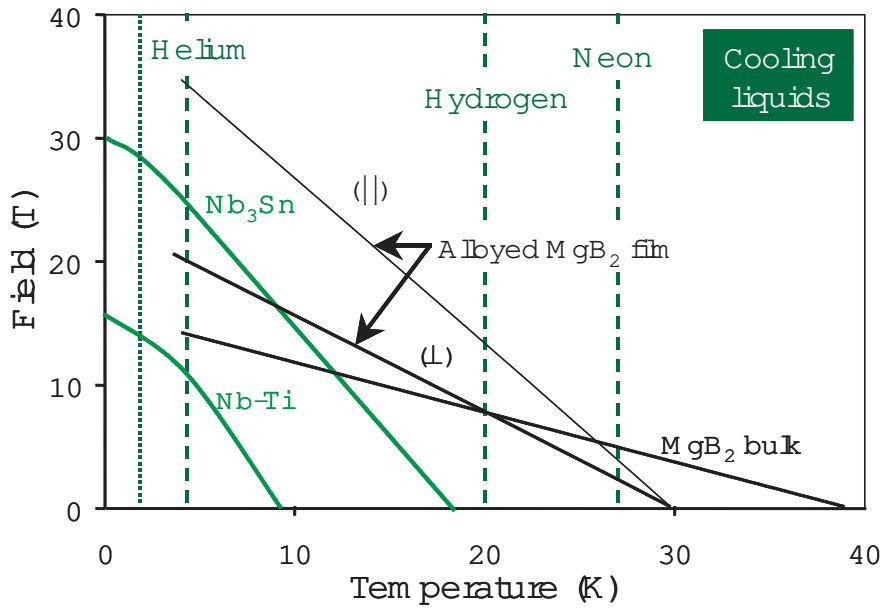
Figure 30: Critical current for Low T_c superconductors and cryogenic temperatures (D. Larbalestiers, CERN Academic Training Lectures).

technique. It will require a thorough understanding of the possible problems of field quality and proposals for solutions. It is also intrinsically less efficient (the same ampere-turns generate less central field than in $\cos\vartheta$ coils), and therefore requires more expensive superconductor (which will be expensive). It is nevertheless very attractive because it is potentially less costly both in winding (flat coils) and assembly, than the $\cos\vartheta$ design, and the problem of prestress is less severe. The additional cost of conductor could be more than compensated if the R&W technique proves to be feasible.
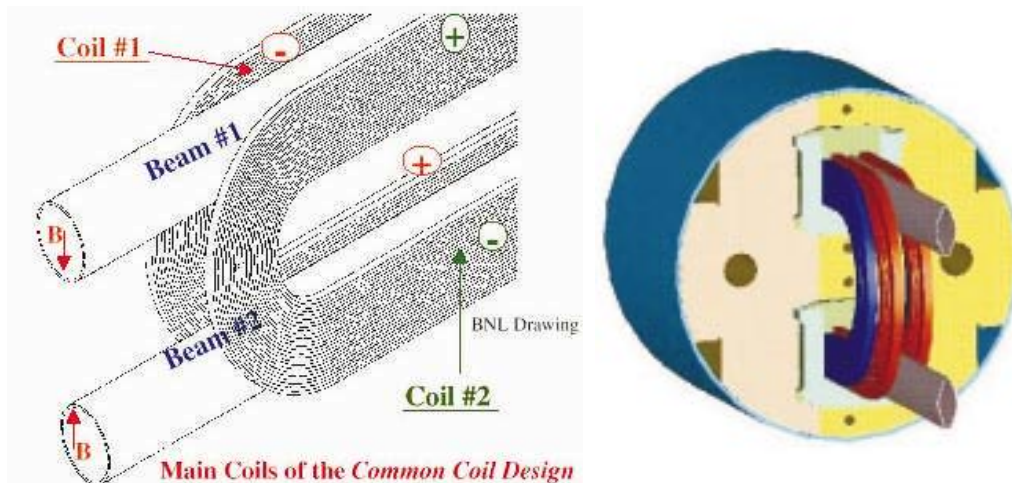
Figure 31: Sketch of the Common Coil design for a double aperture dipole magnet. The coils couple the two apertures and can be flat (no difficult ends). The radius of curvature at the ends is more than 100 mm.

(b)   Other coil block configurations might present some advantage, both for dipoles

and for quadrupoles. For dipoles the lower stresses and simplicity of winding are appealing. For quadrupole it is easy to see how one could reach high gradients with such geometries, albeit at the expense of decreasing greatly the conductor efficiency. It is essential to continue to explore these possibilities.

(c) The problem of multipole correction in magnet systems using conductors with large filament sizes also merits further study.

3. **The Cryomagnet as part of the wider system.** An increase in field implies an inevitable rise of the synchrotron radiation level, that scales as the forth power of the beam energy. The need to remove this power will necessarily impact on the design of the magnets. Some material may require a less onerous cryogenic system. The studies on material and magnet technology must therefore be accompanied by parallel R&D on the full accelerator system including magnets, cryogenics and vacuum, not to mention accelerator physics. Examples of global approach can be found in studies for the Eloisatron [10] and VLHC [11].

7.6 Conclusions

The technology to upgrade the luminosity via an improvement of the low-beta triplet is certainly difficult but is at hand. Given the limited number of magnets the cost should not be too big an issue and there is a general consensus that a $\cos \vartheta$ type design would largely suffice for the scope. With a well-focused program it should be possible to achieve this goal in a few years. For the energy upgrade a goal of an operating field of 15 T is extremely ambitious, being higher that the present record field for accelerator-like dipoles, and will require a large-scale targeted R&D effort. It may just be possible within a ten-year time frame to accumulate sufficient knowledge and experience to make a sound project proposal for a S-LHC. One of the most difficult challenges will be to make it at reasonable cost, less than 5 kEuro/(double)T.m say, including cryogenics, to be compared with about 4.5 kEuro/(double)T.m for the present LHC.

References

[1] A. Asner, R. Perin, S. Wenger, F. Zerobin, "First Nb_3Sn 1 m Long Superconducting Dipole Model Magnet for the LHC break the 10 Tesla Field Threshold", in Proc. of MT-11, Tsukuba, 1988, p. 36.

[2] R. McClusky et al., "A Nb_3Sn High Field Dipole", IEEE Trans. on Mag., Vol. **27**, N.2, March 1991, p. 1993.

[3] A. den Ouden et al., "An Experimental 11.5 T Nb_3Sn LHC Type of Dipole Magnet", in Proc. of MT-13, Victoria, B.C. (Canada), 1993, p. 2320.

[4] R.M. Scanlan et al., "Preliminary test results of a 13 tesla Niobium Tin dipole", in Proc. of Third European Conf. on Applied Superconductivity, The Netherlands, 1997.

[5] G. Ambrosio et al., "Preliminary proposal of a Nb_3Sn Quadrupole Model for the low-beta Insertions of the LHC", INFN-Milan internal report, INFN/TC-9525, and S. Caspi et al., "Design of a Nb_3Sn High Gradient Low-beta Quadrupole Magnet", in Proc. of MT-15, Bejing, 1997, Ed. Science Press, p. 175.

[6] A. Devred et al., "Development of a Nb3Sn quadrupole magnet model", IEEE Trans. Appl. Supercond., Vol. **11**, No. 1, pp. 2184-2187, 2001.

[7] T. Sen, J. Strait, A. Zlobin, "Second Generation High Gradient Quadrupoles for the LHC Interaction Regions", in Proc of PAC2001, IEEE, pp. 3421-3423, 2001.

[8] G. Moritz et al., "Towards Fast-Pulsed Superconducting Synchrotron Magnets", Proc. of PAC2001, IEEE, pp. 211-213, 2001.

[9] R. Ostojic, private communication.

[10] "Hadron Colliders at the Highest Energy and Luminosity", A. G. Ruggiero Editor, World Scientific, 1998.

[11] http://www.vlhc.org/

8 Vacuum effects

The LHC vacuum system is designed to meet the requirements for ultimate machine parameters. Nevertheless, it is assumed that an extended running-in period of a few years with beams may be required to reduce the dynamic outgassing phenomena, mainly the yields for photon, ion and electron stimulated gas desorption compatible with the dynamic pressure requirement. Apart from electron stimulated desorption, which is the primary manifestation of the electron cloud and of beam induced multipacting (BIM), all vacuum related effects depend on the average beam current I rather than on the bunched structure of the beam. From past experience, *e.g.*, the room temperature LEP vacuum system, it is known that initial yields can be reduced by several orders of magnitude within a few months of operation [1]. For cryogenic vacuum systems the corresponding experience from laboratory tests is more limited and based on observation times equivalent to a few days of LHC operation only. Nevertheless, from the existing data one can conclude that while the room temperature photon stimulated desorption yield decreases with photon dose at least as $D^{-0.6}$, the few cryogenic measurements suggest an exponent closer to 0.3 for the LHC. Extrapolations to much larger photon doses are necessary to predict the LHC performance at ultimate conditions. Laboratory measurements of the electron stimulated desorption yield indicate a behaviour similar to the photons. Here again, data at cryogenic temperature and for significant electron doses are few or missing. The ion stimulated desorption yield (at the origin of the ISR-type pressure instability) has been measured in the laboratory at room temperature and at cryogenic temperature for some gas species. Unfortunately these yields and their evolution during the operation of the LHC are very poorly known. For this reason, the LHC vacuum design assumes that the ion stimulated desorption remains constant during operation and the system has been designed so that the vacuum stability criterion $\eta I_{\text{ultimate}} < \eta I_{\text{crit}}$ is met even under pessimistic assumptions for the ion induced desorption yield.

8.1 Synchrotron radiation induced desorption

In the cold arcs of the LHC the instantaneous dynamic pressure rise due to synchrotron radiation induced gas desorption is given by [2]

$$\Delta P = \eta(\varepsilon_c) \frac{1}{S} \frac{\mathrm{d}N_\gamma}{\mathrm{d}s\,\mathrm{d}t},$$

where $\eta(\varepsilon_c)$ is the photon stimulated desorption yield, which is a function of the critical energy of the photon spectrum, and S is the linear pumping speed of the cold walls of the beam pipe and/or of the pumping holes of the beam screen. Denoting by ρ the bending radius, the linear synchrotron radiation photon flux is given by

$$\frac{\mathrm{d}N_\gamma}{\mathrm{d}s\,\mathrm{d}t} = 7 \times 10^{19}\,\mathrm{s}^{-1}\mathrm{m}^{-1}\,\frac{E[\text{TeV}]\,I[\text{A}]}{\rho[\text{m}]}$$

and thus the dynamic pressure rise in the LHC, maintaining the same cryopumping S, should simply scale as $\Delta P = \eta(\varepsilon_c)\,E\,I$.

8.2 Photon stimulated desorption yield

The variation of the photon stimulated desorption yield with critical photon energy has been measured for copper as vacuum chamber material over a critical energy range from about $12\,\text{eV}$ up to about $300\,\text{eV}$ [3, 4]. These data from SSC and LHC work are summarised in Figure 32.
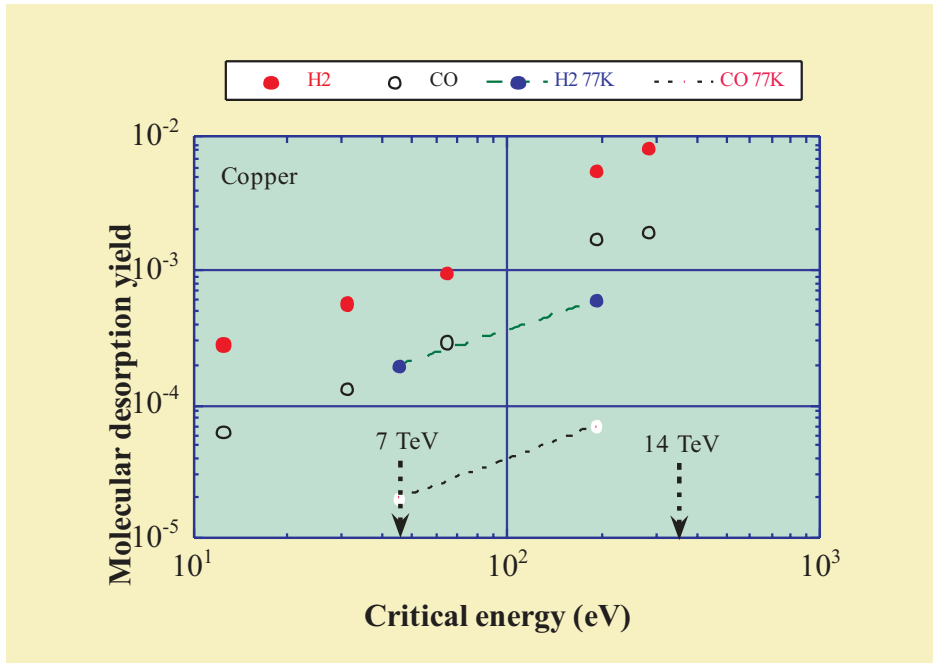
Figure 32: Molecular desorption yield for H_2 and for CO as a function of the critical photon energy. Measurements were done at room temperature and at 77 K.

The room temperature values of the molecular desorption yield are approximately proportional to the critical photon energy and hence would scale as the third power of the beam energy. At 77 K, the dependence on the critical photon energy seems to be weaker, approximately as the power 2/3. The desorption yield in the cold part of the LHC would hence scale rather like the square of the beam energy.

Overall, one can deduce that the dynamic pressure rise would scale as $\Delta P_{\text{cold}} = E^3 I$ in the cold arcs and as $\Delta P_{\text{warm}} = E^4 I$ in the room temperature sections of the LHC.

8.3 Nuclear scattering on the residual gas

Beam losses which can not be collimated and hence cause protons to escape through the cold bore into the cryomagnets can be expressed in terms of the nuclear scattering lifetime τ_{NS}

$$\frac{\mathrm{d}W}{\mathrm{d}s} = 0.93 \, \text{W/m} \, \frac{I[\text{A}] \, E[\text{GeV}]}{\tau_{\text{NS}}[\text{h}]}.$$

For nominal LHC parameters (0.56 A) a beam-gas lifetime of about 100 h has been assumed, which results in a power loss of 36 mW/m per beam. This dissipation has to be taken by the 1.9 K system and represents also a significant radiation dose to machine components (see Section 9).

The lifetime of 100 h requires an average gas density (lifetime limit) of about $10^{15} \, H_2$ molecules/m^3 and correspondingly less for heavier molecules. Laboratory measurements, *e.g.*, with the COLDEX system in EPA at cryogenic temperature, have shown that this lifetime requirement can be satisfied for the nominal beam current without any beam cleaning [5].

Using the scaling of the dynamic pressure with beam energy and with beam current, and since the beam lifetime is inversely proportional to the average gas density, the

nuclear scattering losses would scale as

$$\frac{\mathrm{d}W}{\mathrm{d}s} \propto E^a I^2$$

with $a = 4$ for the cold arcs and $a = 5$ for warm sections.

To meet the requirement for the ultimate beam current, a modest reduction of the desorption yields by a factor of 2.2 will be required. In case of an energy upgrade the average vacuum and hence the photon stimulated desorption yields would have to be improved significantly by an extended beam cleaning period to maintain constant nuclear scattering losses.

8.4 Ion stimulated desorption and vacuum stability

Vacuum stability [6] requires that the effective pumping S_{eff} of the system be significantly larger than the product of the ion stimulated desorption yield η and the average beam current:

$$\eta I < \frac{e}{\sigma_{\mathrm{i}}} S_{\mathrm{eff}}.$$

Here σ_{i} is the ionization cross section of the residual gas molecules by the high energy protons, which has a weak dependence on beam energy.

Typical values of the desorption yield are in the range of 1 to 10 molecules/ion for unbaked systems and of order unity for baked chambers as shown in Figure 33 [7, 8]. For specially pre-treated beam pipes, the desorption yield can be reduced reliably to below unity but, even then, it remains always much larger than the corresponding desorption yields for photons and for electrons.

In the cold arcs of the LHC the pumping is provided by the cryo-pumping on the beam screen and by the pumping holes. Since it is a very effective distributed pumping system, the calculated critical current at which the vacuum would become unstable is a few orders of magnitude larger than the nominal LHC current. The ion induced molecular desorption yield is a function of the incident ion energy and reaches a maximum value at a few keV. In the LHC arcs the ion impact energy is typically 200 to 300 eV depending on machine parameters and hence the desorption yield is low. In the crossing points due to the strong focusing and the overlap of both beams the impact energy may exceed several keV. The baseline design includes baking to about 200 °C and a getter coating of these vacuum chambers to guarantee low and stable pressures.

Scaling of the ion impact energy with the beam parameters depends weakly on the ion species: light H_2 ions are ejected rapidly from the beam and experience only a few bunches. H_2 ions are therefore more strongly affected by the peak field than heavier CO or CO_2 ions, which take about 20 to 40 bunch passages to reach the vacuum chamber wall. In case of a long 'super-bunch', the ions would see a continuous electric field as compared to repetitive kicks and the impact energy increases to several tens of keV for the same average beam current.

In terms of the vacuum stability criterion, the desorption yield corresponding to the peak value of the desorption curves should be assumed. For CO and for H_2 the desorption yield for ions will increase by a factor between 3 to 5 with respect to the nominal LHC conditions which should still be well within the margin of safety of the cold arcs of the present LHC design. In the warm straight sections and in particular in conductance limited vacuum sections the safety margins are likely to be insufficient and local improvements will be required.
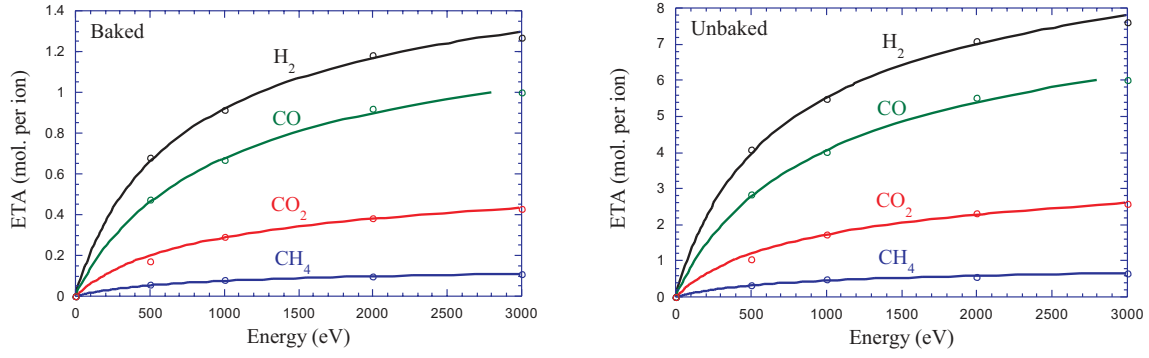
Figure 33: Ion stimulated molecular desorption yields of baked and unbaked stainless steel as a function of the incident ion energy (from A.G. Mathewson).

8.5   Electron stimulated desorption

Electron stimulated desorption which is caused by the bombardment of the vacuum chamber walls by primary photo-electrons and/or beam induced multipacting (BIM) can drastically increase the dynamic pressure in the LHC. The pressure increase can be expressed in terms of the electron stimulated desorption yield, the electron current bombarding the wall and by the effective pumping speed

$$\Delta P = \frac{\eta_{\rm e} I_{\rm e}}{S_{\rm eff}}.$$

Since the electron current can be related to the linear power dissipation of the electron cloud $W_{\rm cloud}$ and to the average energy of the electrons $\langle E_{\rm cloud}\rangle$, the pressure rise can be expressed as

$$\Delta P \propto \eta_{\rm e} \frac{W_{\rm cloud}}{\langle E_{\rm cloud}\rangle S_{\rm eff}}.$$

Since electron stimulated desorption yields are typically two orders of magnitude larger than the photon stimulated desorption yields [9], once BIM has been initiated, this effect is likely to dominate the vacuum behaviour even for low values of electron cloud power and hence limit the machine operation. Fortunately, the electron bombardment wherever it occurs, should also lead to a strong clean-up of the walls and thus to a gradual and very significant reduction of all the desorption effects for electrons, photons and possibly also for ions.

The main concern for an LHC upgrade is the heat load by the electron cloud in the cold sections of the machine. Experience with existing machines and studies in the laboratory have shown that an appropriate choice of machine parameters like bunch intensity, bunch spacing and bunch length can be made to reduce or even to avoid this effect. Since the multipacting phenomenon occurs preferentially within a certain range of parameters, it could be favorable to operate the upgraded LHC with longer or even very long bunches so that electrons can make a very large number of oscillations resulting in a small net energy gain. Alternatively, since the secondary electron yield of the vacuum chamber wall is a vital parameter for the multiplication process and since this yield exceeds unity within a given range of primary electron energies, E_1 to E_2 only, it could be

interesting to operate with very intense bunches so that the mean energy of the electrons becomes much larger than E_2. Following this scheme, Figure 34 shows an example of a model calculation of the average secondary electron yield in an LHC dipole beam screen as a function of the bunch intensity. The contour lines delimit the regions where the average
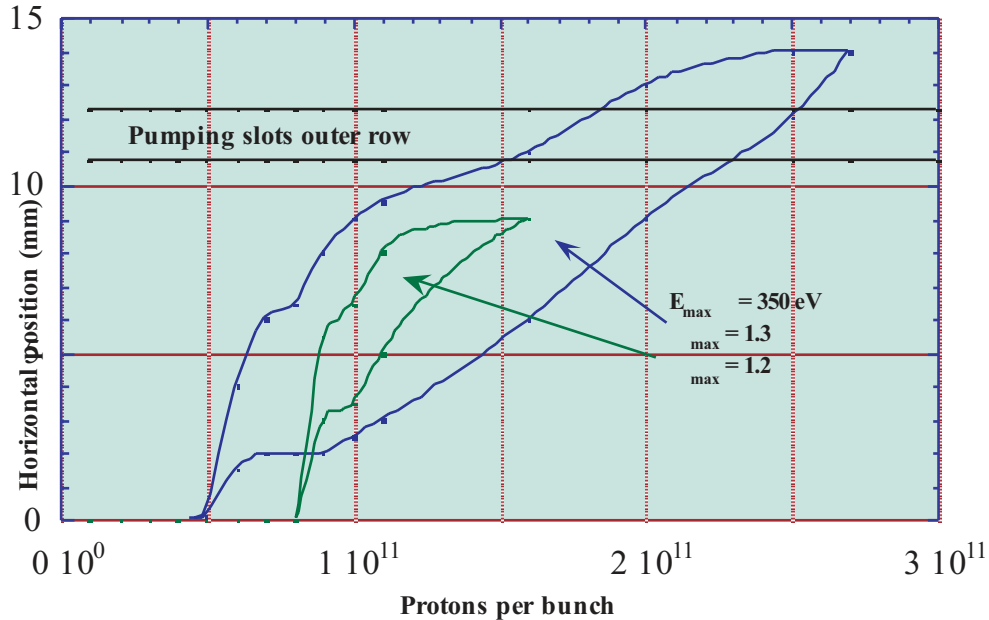
Figure 34: Regions within a dipole beam screen where the average secondary electron yield exceeds unity as a function of the bunch intensity. The characteristic parameters of the secondary electron yield, δ_{max} and E_{max}, are indicated in the figure. Nominal values are assumed for bunch length and for bunch spacing.

secondary electron yield exceeds unity, hence where BIM can occur. It is interesting to note that outside of these regions and for very large bunch currents, conditions for BIM are not fulfilled in this simplified model. In the context of the choice of machine parameters for an LHC upgrade, it could be interesting to explore this possibility in more detail.

8.6 Further studies and essential R&D for vacuum

- Operating COLDEX in the SPS and performing experiments with LHC beams will be important: this program is a must. It will also be important to get measurements in the SPS on heat deposition by e-cloud, scrubbing effects for secondary electron yield as well as electron stimulated desorption.
- So far unknown is the aspect of ion induced desorption at high impact energy (in case of long bunches) and how the desorption yield for ions can be reduced by electron scrubbing. These questions could be studied in the laboratory. Also many questions about surfaces (treatments, memory effects after venting, etc.) could be studied more easily in the lab than in the SPS or later in the LHC.
- The suggestion to use more and more intense bunches needs to be followed up in detail since it will have important implications on the vacuum hardware (bellows and RF-bridges).

- In the scenario of replacing the LHC arcs to double the beam energy, synchrotron radiation power will be quite important. Already now the VLHC, as the SSC in the past, looks into the option of intercepting the synchrotron radiation by localised photon stops. This suggestion could also be studied and its implication on beam pipe apertures, impedance issues, etc. would need to be better understood.
- The ongoing work on surfaces which have low-outgassing properties and in addition provide pumping (NEG's) is an obvious item for a long term development.

8.7   Conclusions

At this very early stage of the study only preliminary conclusions can be made. For the vacuum system it is primarily the average beam current which matters. Bunch currents will have an influence on the electron cloud and on the power dissipation in the copper layer of the beam screen and in the rf-bridges of the bellows.

An upgrade of the cryogenic system would allow to increase the cooling capacity of the beam screen from its present value of 1 W/m by more than an order of magnitude as it has been shown by the study of the cryogenics. Nevertheless, it should not be overlooked that the electron cloud induced pressure rise may put a more stringent limit on the operation than cryogenics alone.

The consequences of an energy upgrade can be assessed with rather good confidence and even a doubling of the beam energy seems to be compatible with the present design. On the contrary increasing the beam intensity has serious implications for the vacuum system in the arc but also for the long straight sections, which would require substantial modifications. An important unknown remains the ion induced desorption yield of cold and warm surfaces and its evolution with beam operation. It will be essential to obtain a better understanding and more reliable data on the various surface conditioning processes and how they mutually interact.

The electron cloud and its consequences for the vacuum system in terms of heat load and electron stimulated gas desorption remains a serious unknown for an upgrade and could be decisive for the choice of some basic machine parameters.

References

[1] O. Gröbner, Vacuum, **43** (1/2), 1992.
[2] R. Calder, O. Gröbner, A.G. Mathewson, V.V. Anashin, A. Dranichnikov, O.B. Malyshev, J. Vac. Sci. Technol. A**14** (4), Jul/Aug 1996.
[3] J. Gómez-Goñi, O. Gröbner, A.G. Mathewson, J. Vac. Sci Technol. A**12** (4), Jul/Aug 1994.
[4] V. Baglin, Doctoral Thesis, Université Denis Diderot Paris 7, May 1997.
[5] V. Baglin, I.R. Collins, O. Gröbner, C. Grünhagel, B. Jenninger, CERN LHC Project Report 518, 1 November 2001.
[6] I.R. Collins, O. Gröbner, O.B. Malyshev, A. Rossi, P. Strubin, R. Veness, CERN LHC Project Report 312, 18 October 1999.
[7] A.G. Mathewson, CERN-ISR-VA/76-5, 1 March 1976.
[8] M-H. Achard, R. Calder, A.G. Mathewson, CERN-ISR-VA/78-2, January 1978.
[9] M. Andritschky, O. Gröbner, A.G. Mathewson, F. Schumann, P. Strubin, Vacuum, **38** (8-10), 1988.

9   Nuclear interactions, radiation dose, and magnet quench limit

For a nominal LHC beam intensity of 3×10^{14} protons the annual dose to the most exposed parts of the arc dipole coils is about 5×10^3 Gy/y, assuming a beam-gas lifetime of 500 hours (see Fig. 35). A residual gas density of 10^{15} H_2 molecules/m^3 and correspondingly less for heavier molecules can be expected from day 1 in the LHC, leading to a beam-gas lifetime of about 100 hours. After some initial surface cleaning, the residual gas density may go down by a factor 1.5.
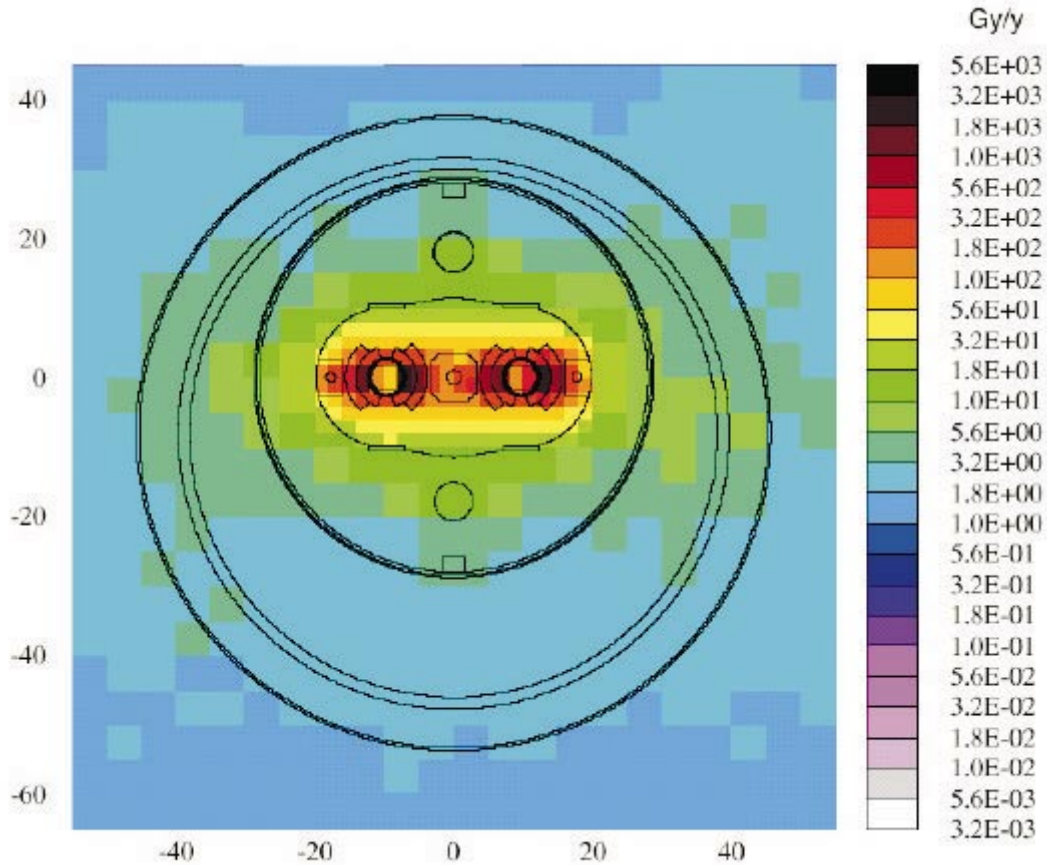
Figure 35: Annual dose [Gy/y] to the inner regions of the arc dipole. The plot shown is the average over 13 m of the dipole coils. Doses are normalised for a proton loss of 1.65×10^{11} m^{-1}y^{-1} for two beams, corresponding to a beam-gas lifetime of 500 h.

For nominal LHC conditions, the average rate of inelastic pp interactions in the high luminosity IP's is 3.5×10^8 s^{-1} and the maximum dose to some dipole coils in the dispersion suppressors (*e.g.*, near Q9, see Fig. 36) approaches 10^6 Gy/y. These results include the effect of the additional collimators discussed in [1]). As shown in Table 15, the estimated magnet lifetime is 10-20 years. Possible radiation damage to the insertion quadrupoles, and especially to the corrector coils, depends on the magnetic lattice: the low-beta quadrupoles are the most critical items and may require additional shielding. Such doses scale linearly with luminosity. Therefore radiation effects are probably not a show stopper for an LHC luminosity upgrade, but require careful consideration. Increasing the dispersion at Q5 would allow a higher collimation efficiency for off-momentum particles and thus a better protection of the dispersion suppressor magnets. Further estimates of

68

energy deposition for an LHC luminosity upgrade can be found in [2].
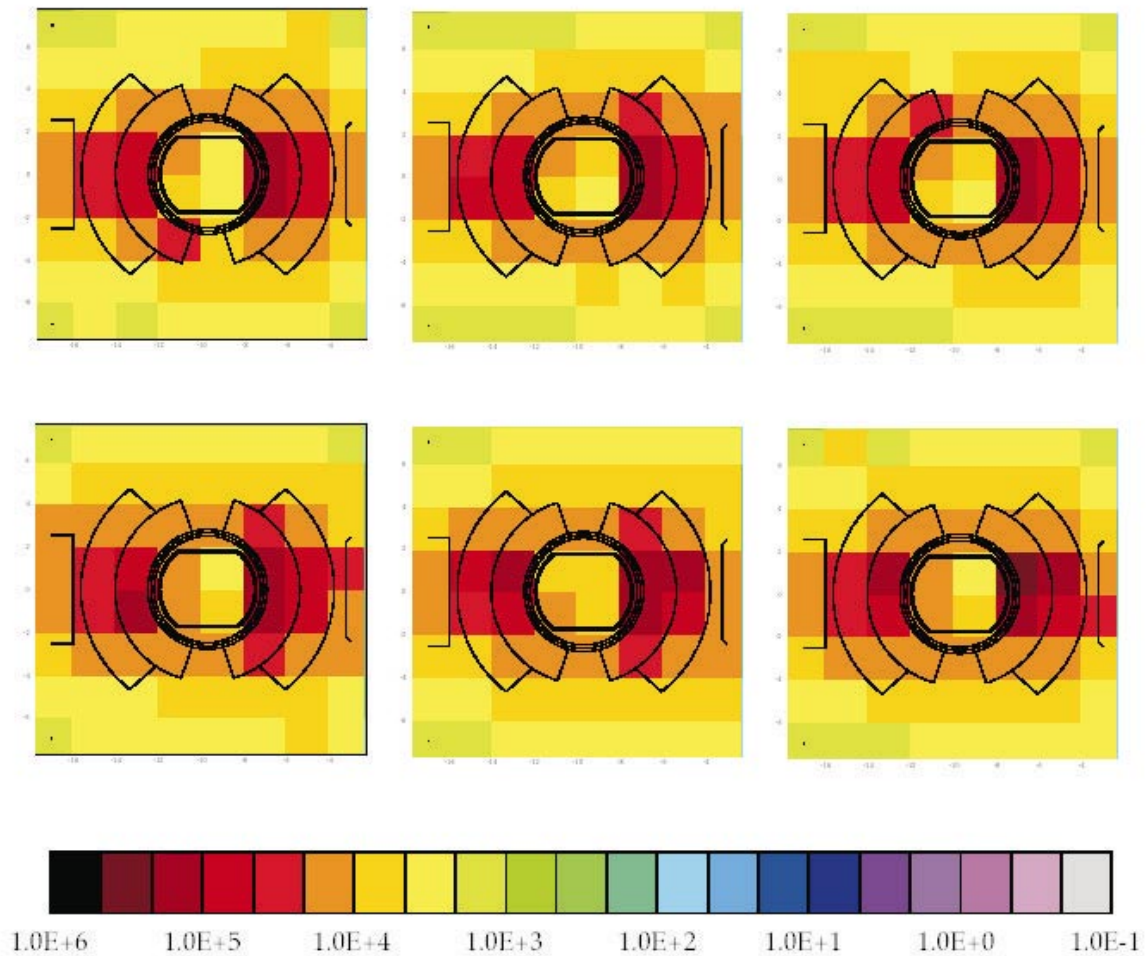
Figure 36: Maximum dose to dipole coils in the dispersion suppressors of IR1 due to point losses arising far downstream of the high luminosity interaction point IP1 for 7 TeV incident protons. The cross-sectional slices show the maximum dose [Gy/y] due to point losses in the coils and beamline of the dipole magnet MB9B. The proton loss distribution used is taken from Ref. [1] for a rate of 3.5×10^8 inelastic interactions per second in the IP. The total proton loss in IR1 is $1.1 \times 10^7 \, \mathrm{s}^{-1}$.

1 Gy = 1 J/kg = 100 rads, 1 Gy/s = 1 (J/kg)/s = 1 mW/g

After an integrated dose of 2×10^9 rads, i.e. about 20 years of exposure at 10^6 Gy/y, the resin used to impregnate magnet coils loses half of its mechanical strength $\longrightarrow$ magnet insulation damage.

Table 15: Radiation units and magnet damage

9.1 Magnet quench limit

The LHC dipole quench limit for direct impact of protons at 7 TeV is 7×10^6 p/m/s. For beam-gas nuclear collisions about 2/3 positively charged products hit the internal side

of the dipoles (and 1/3 the external side, while photons and neutrons go straight), so we can assume a quench limit for beam-gas interactions $\dot{n}_q = 10^7$ p/m/s [3].

The beam lifetime for a gas density corresponding to the quench limit everywhere in the machine would be $\tau_q = N/\dot{N} = N_o/\dot{N}_o$ (since $t = 0$ is the most critical moment of a coast). With $\dot{N}_o = \dot{n}_o C$, where $C = 2.6 \times 10^4$ m is the ring circumference, $N_o = 3 \times 10^{14}$ p the nominal LHC beam intensity, and $\dot{n}_o = \dot{n}_q$, we obtain a beam lifetime

$$\tau_q = \frac{N_o}{\dot{n}_q C} = \frac{3 \times 10^{14}}{10^7 \cdot 2.6 \times 10^4} \, \text{s} = 1.15 \times 10^3 \, \text{s},$$

corresponding to a luminosity lifetime $\tau_L < \tau_q/2 = 10$ min. The gas density corresponding to the quench limit is

$$\rho_{\text{gas}} = \frac{\dot{n}_q}{N_o \cdot f_{\text{rev}} \cdot \sigma_{\text{inel}}} \simeq 10^{17} \, \text{atoms/m}^3,$$

where $f_{\text{rev}} = 1.1 \times 10^4$ Hz is the LHC revolution frequency and $\sigma_{\text{inel}} = 320 \, \text{mb} = 3.2 \times 10^{-25}$ cm^2 is the inelastic cross section for proton collisions on Oxygen, Nitrogen, or Carbon atoms. With $C_{\text{cold}} = 2 \times 10^4$ m the length of the cold mass and $E_{\text{proton}} = 7 \, \text{TeV} = 1.1 \times 10^{-6}$ J, the corresponding overall cryogenic heat load would be

$$P_{\text{tot}} = \dot{n}_q \cdot C_{\text{cold}} \cdot E_{\text{proton}} = 220 \, \text{kW}.$$

In conclusions, operating the LHC close to the quench limit due to high gas pressure would be highly inefficient[4] since the beam and luminosity lifetime would be very short and the cryogenic heat load very high. A reasonable gas density in production should be $\rho_{\text{gas}} = 10^{15} \, \text{atoms/m}^3$.

References

[1] I. Baichev, *Proton losses in the dispersion suppressors of IR1 and IR5 of LHC*, CERN LHC Project Note 240.
[2] N. Mokhov, *LHC IR energy deposition: baseline and upgrade*, presented at the LHC IR Upgrade Collaboration Meeting, CERN, 11-12 March 2002, see web site at http://cern.ch/lhc-proj-IR-upgrade.
[3] B. Jeanneret, private communication, August 2001.

---

[4] It can be interesting to compare the ring beam-gas luminosity with the nominal experimental luminosity $L_{\text{exp}} = 10^{34} \, \text{cm}^{-2} \, \text{s}^{-1}$:

$$L_{\text{ring,gas}} = N_o \cdot \rho_{\text{gas}} \cdot f_{\text{rev}} \cdot C = 8.1 \times 10^{35} \, \text{cm}^{-2} \, \text{s}^{-1}.$$

This is not the best way to use the machine! As a cross-check, one can re-write the beam lifetime for a gas density corresponding to the quench limit as $\tau_q = N_o/\dot{N}_o = N_o/(L_{\text{ring,gas}} \cdot \sigma_{\text{inel}}) = 3 \times 10^{14}/(8.1 \times 10^{35} \cdot 3.2 \times 10^{-25}) \, \text{s} = 1.16 \times 10^3 \, \text{s}$.

10   Cryogenic system

10.1   General considerations

The LHC upgrade in energy and luminosity will increase the cryogenic heat loads especially for the beam screens and cold mass cooling. Some local and distribution restrictions could limit the maximum performance of the upgraded machine. The main restrictions are:

- The beam screen (BS) cooling loop, to be performed using the 3.7 mm inner diameter cooling channel.
- The cold mass (CM) cooling loop and the main pumping line for which the cooling principle does not allow to increase the magnet temperature above the lambda temperature T_λ.

The cryogenic distribution line running in parallel to the machine already corresponds to the maximum size, which can be integrated between the tunnel wall and the machine. Consequently, in the different upgrade scenarios, the present diameters of the distribution line headers will be taken as input data. Table 16 gives the header characteristics with their main functions.

Header	Inner Ø [mm]	Present main functions	Present design conditions	Remarks for upgrade scenarios
B	267	Sub-atmospheric pumping line	Maximum temperature of 1.9 K in the warmest magnet in nominal conditions	The maximum magnet temperature will increase with the heat load deposition
C	100	Cold supercritical helium supply	Cool-down and warm-up flow-rate	The same cool-down and warm-up flow-rate could probably be envisaged
D	150	Cold helium return from beam screen and Cold quench helium buffer	Cold helium buffer during a magnet quench	The same quench buffering could be envisaged if we keep a cold-mass helium content around 20 l/m
E	80	Magnet thermal shield supply	Thermal shield cooling in nominal conditions with a total pressure drop below 1 bar	Beam performance does not affect the thermal shield heat loads, which will not change
F	80	Distribution line thermal shield supply		

Table 16: Header characteristics of the cryogenic distribution line

To increase the performances of the cooling system, several distribution schemes can be envisaged as shown in Fig. 37. The first scheme corresponds to the existing one. In this scheme, the first limitation will be given by the cold mass cooling of the inner triplets of ATLAS (Pt1) and CMS (Pt5), which are far away from the cryoplant. One way to overcome this limitation is to add dedicated cryoplants for the inner triplets at points Pt1 and Pt5 (see scheme 2). By increasing the distributed heat loads, another limitation could be given by the sector-wide distribution. The half-octant distribution scheme 3 halves the distribution length and consequently increases the cooling capability.

| Scheme 1: | Scheme 2: | Scheme 3: |
| Present configuration | Upgrade with dedicated cryoplants for inner triplet cooling | Upgrade for half octant cooling |
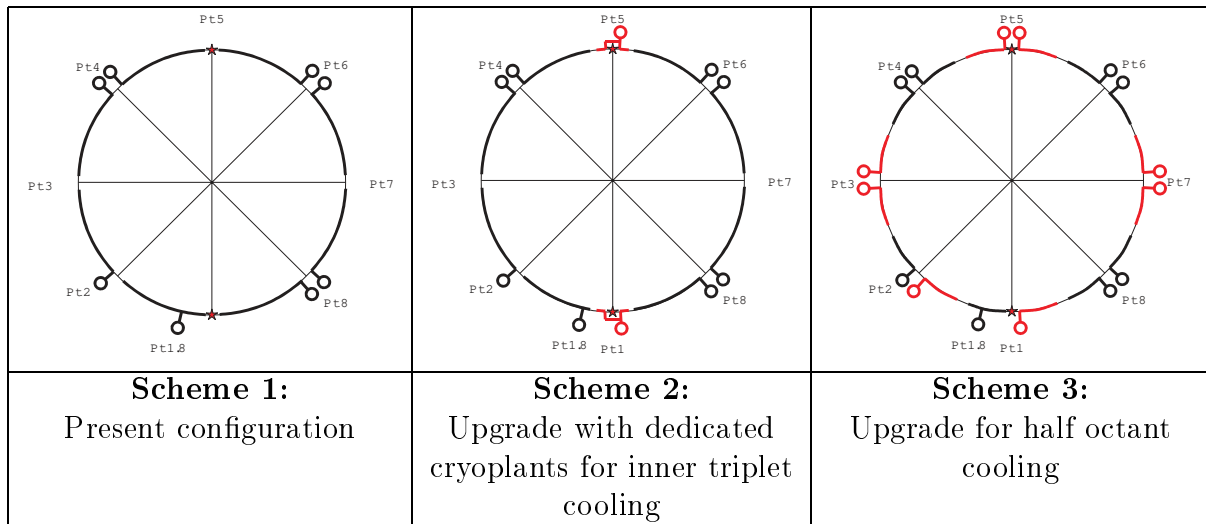
Figure 37: Distribution schemes for the LHC upgrade.

10.2 LHC upgrade scenario

Table 17 gives the beam parameters for different upgrade scenarios of the LHC. The beam parameters which influence the cryogenic heat loads are:

- E the beam energy,
- I_b the bunch intensity,
- n_b the number of bunches per beam,
- σ_z the length of the bunch,
- L the luminosity of the beam collisions.

Scenario		E	I_b	n_b	σ_z	Luminosity
Ref.	Remarks	[TeV]	[mA]	[-]	[mm]	[cm^{-2} s^{-1}]
A	Nominal	7	0.20	2808	77	1.0E+34
A'	Ultimate	7	0.30	2808	77	2.3E+34
A''	Modest upgrade	7	0.30	2808	38.5	4.6E+34
Bbb	With bunched beam	7	0.30	5616	38.5	9.2E+34
Bsb	With super-bunch	7	1000	1	75000	9.0E+34
B'	Strong bunches	7	0.48	2808	77	7.2E+34
Cbb	With bunched beam	14	0.14	2808	54.4	1.0E+34
Csb	With super-bunch	14	75.6	1	8250	1.0E+34
Dbb	With bunched beam	14	0.23	5616	54.4	1.0E+35
Dsb	With super-bunch	14	720	1	75000	1.0E+35

Table 17: Beam parameters for different LHC upgrade scenarios, at 7 TeV (A-B) and at 14 TeV (C-D). As shown in Table 19, scenarios with long super-bunches (sb) are more favourable from the cryogenics point of view, for comparable luminosities.

10.3 Scaling laws and specific cryogenic heat loads

Table 18 gives the scaling laws used to define the heat loads to be extracted in the different upgrade scenarios. Concerning heat loads due to electron clouds, the approximate scaling law corresponds to bunched beam. For super-bunches, the heat loads are reduced and correspond to 5% of the bunched beam scenario. Table 19 gives the specific heat

loads to be extracted for the different upgrade scenarios. As a general rule, scenarios with long super-bunches are less demanding in cooling capacity than bunched or strong-beam scenarios.

Heat loads	Energy	Bunch current	Bunch number	Bunch length	Luminosity
Static heat inleaks	-	-	-	-	-
Resistive heating (splices)	E^2	-	-	-	-
Synchrotron radiation	E^4	I_{b}	n_{b}	-	-
Image currents		I_{b}^2	n_{b}	$\sigma_z^{-3/2}$	-
Beam-gas scattering		I_{b}	n_{b}	-	-
E-cloud		I_{b}^3	n_{b}	-	-
Particle losses	E	-	-	-	L

Table 18: Heat load dependence with respect to beam parameters.

			LHC upgrade scenario									
			A	A'	A"	Bbb	Bsb	B'	Cbb	Csb	Dbb	Dsb
	Synchr. radiation	[W/m]	0.33	0.50	0.50	1.00	0.61	0.79	3.73	0.72	12.49	6.83
	Image currents	[W/m]	0.36	0.83	2.35	4.69	0.11	2.07	0.30	0.02	1.70	0.06
4.6 -	E-cloud	[W/m]	0.89	3.10	3.10	6.20	0.31	12.2	0.31	0.02	2.94	0.15
20 K	Static	[W/m]	0.13	0.13	0.13	0.13	0.13	0.13	0.13	0.13	0.13	0.13
	Total	**[W/m]**	**1.71**	**4.56**	**6.08**	**12.0**	**1.16**	**15.2**	**4.48**	**0.88**	**17.3**	**7.16**
	Synchr. radiation	[W/m]	0.001	0.001	0.001	0.002	0.001	0.002	0.008	0.001	0.025	0.014
	Image currents	[W/m]	0.001	0.002	0.007	0.013	0.000	0.006	0.001	0.000	0.005	0.000
1.9 K	E-clouds	[W/m]	0.009	0.031	0.031	0.062	0.003	0.122	0.003	0.000	0.029	0.001
Arc	Resistive heating	[W/m]	0.10	0.10	0.10	0.10	0.10	0.10	0.40	0.40	0.40	0.40
+ DS	Beam-gas scatter.	[W/m]	0.05	0.07	0.07	0.15	0.09	0.12	0.03	0.01	0.11	0.06
	Static	[W/m]	0.21	0.21	0.21	0.21	0.21	0.21	0.21	0.21	0.21	0.21
	Total	**[W/m]**	**0.37**	**0.41**	**0.42**	**0.53**	**0.40**	**0.55**	**0.65**	**0.62**	**0.78**	**0.69**
IT	**Secondaries**	**[W/m]**	**4.8**	**11.1**	**22.2**	**44.4**	**45.1**	**41.8**	**9.60**	**9.60**	**96.0**	**96.0**

Table 19: Specific heat loads for the different LHC upgrade scenarios of Table 17.

10.4 Cooling loop limitations

10.4.1 Beam screen cooling loop

In our discussion we assume that the beam screen will *not* be replaced and thus that the hydraulic impedance of the cryogenic circuits is unchanged. Fig. 38 shows the basic cooling scheme of the beam screens inside the magnet apertures. The diameters of headers C and D presently designed respectively for cool-down operation and for cold helium buffering during magnet quench are oversized for normal operation. They do not represent a limitation in the helium distribution in the different upgrade scenarios. As a consequence, the following study is valid for the three different distribution schemes.

The main limitation is given by the cooling channels of the beam screen, having an inner diameter of 3.7 mm. The present nominal pressure of header C and D is respectively 3 bar and 1.3 bar. The total pressure difference between these headers has to be shared
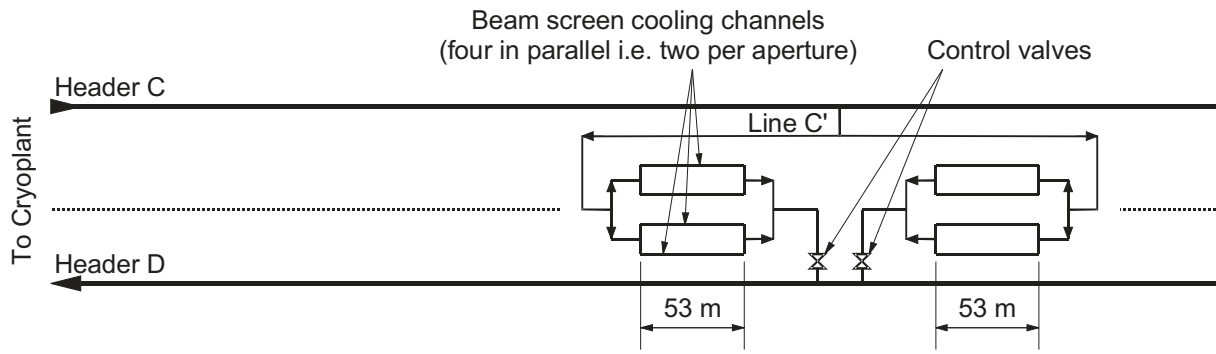
Figure 38: Basic beam screen cooling scheme.

between the channels and the control valves located at the outlet; typically, one third of this pressure difference must be allocated to the control valve. One way to increase the mass-flow in the cooling circuits, and consequently the capacity to be extracted, is to increase the supply pressure of the header C. Fig. 39 shows the required header C supply pressure as a function of the distributed heat load on the beam screens for two outlet temperatures (20 K and 30 K). In this figure the heat load values are given in W/m for the two apertures. One hard limit is given by the maximum pressure produced by the cryoplant (around 19 bar), which gives maximum heat loads to be extracted of 48 W/m and 62 W/m for an outlet temperature of 20 K and 30 K, respectively. Concerning the flow coefficient of the control valves, the flow-rate increase is partially compensated by the pressure increase and a maximum flow coefficient of about twice the present one is required, i.e. the valve body can stay as it is (DN6) and only minor modifications (seat and poppet size) will be needed.

Figure 39: Minimum header C pressure versus beam screen heat loads.

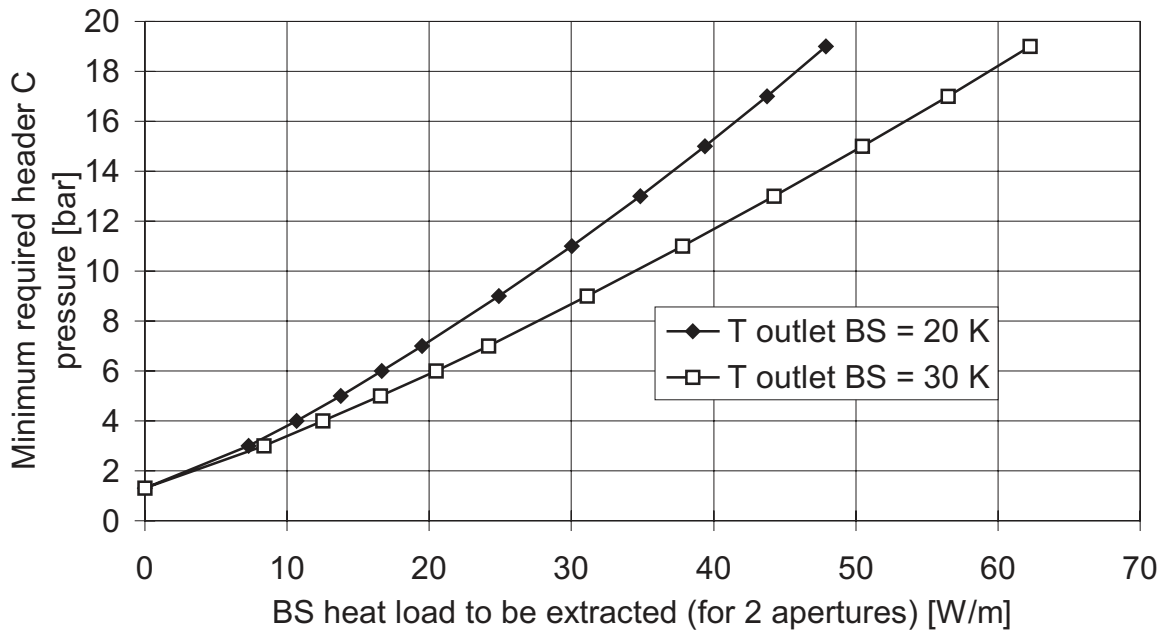Extra cooling capacity must be installed to compensate first the increase of heat load and in addition the loss of capacity of present cryoplants induced by supplying the header C at a higher pressure. Increasing the pressure in header C has a positive consequence of reducing the risk of density wave oscillations in the beam screen channels.

In conclusion, if we envisage to install more refrigeration capacity and to supply the header C at a higher pressure, we can gain a factor 6 to 8 on the beam screen cooling capacity with respect to the present configuration. A remaining issue corresponds to the temperature difference developed radially in the beam screen wall as well as longitudinally in the interconnection regions, that are not directly cooled.

10.4.2 Cold mass cooling loop

Fig. 40 shows the basic cooling scheme of the magnet cold mass. In such a scheme, the cooling of the cold mass is effective as long as its temperature stays below the lambda temperature. The magnet temperature is driven by:

- The pressure evolution in the pumping header B due to frictional pressure drop as well as hydrostatic head due to the tunnel slope.
- The pressure drop in the very-low-pressure stream of the sub-cooling heat exchangers as well as its efficiency.
- The temperature difference across the cold mass heat exchanger.
- The pressure of header C which supply the cold-mass cooling loop and which directly influences the gas title produced in the expansion valve.
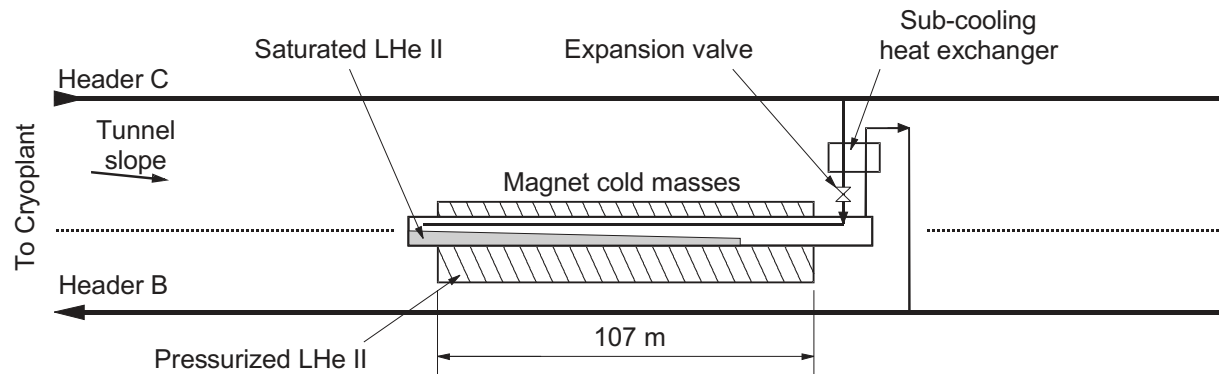
Figure 40: Basic magnet cold-mass cooling scheme.

For Arc and Dispersion Suppressor cooling loops, the specific heat loads (see Table 19) remains compatible with the present design of cold mass heat exchangers, subcooling heat exchangers and expansion valves. The QRL service modules do not need modifications.

Fig. 41 shows the maximum cold-mass temperature as a function of the distributed heat load in the Arc and Dispersion Suppressor cells for different header C supply pressure as well as for the two distribution schemes 2 and 3. Considering a maximum magnet temperature of T_λ, the maximum heat load to be extracted by the cold-mass cooling loops is about $2\,\text{W/m}$ for Scheme 2 and $3.5\,\text{W/m}$ for the Scheme 3.

Concerning Inner Triplet cold mass cooling loops additional R&D is required to study cooling of magnets with specific distributed heat load higher than $10\,\text{W/m}$. It is especially the case of scenarios of types B and D for which the value varies between 50 and $100\,\text{W/m}$. For these cooling loops, the service modules of the QRL must be modified by changing the subcooling heat exchangers, the expansion valves and internal piping.

Figure 41: Maximum cold mass temperature versus 1.9 K specific heat loads.

10.4.3 Application to the different upgrade scenarios

In this application, it is assume that the heat load in the Inner Triplet cold mass can be extracted with temperature differences similar to those obtained in the Arc (To be confirmed by R&D).
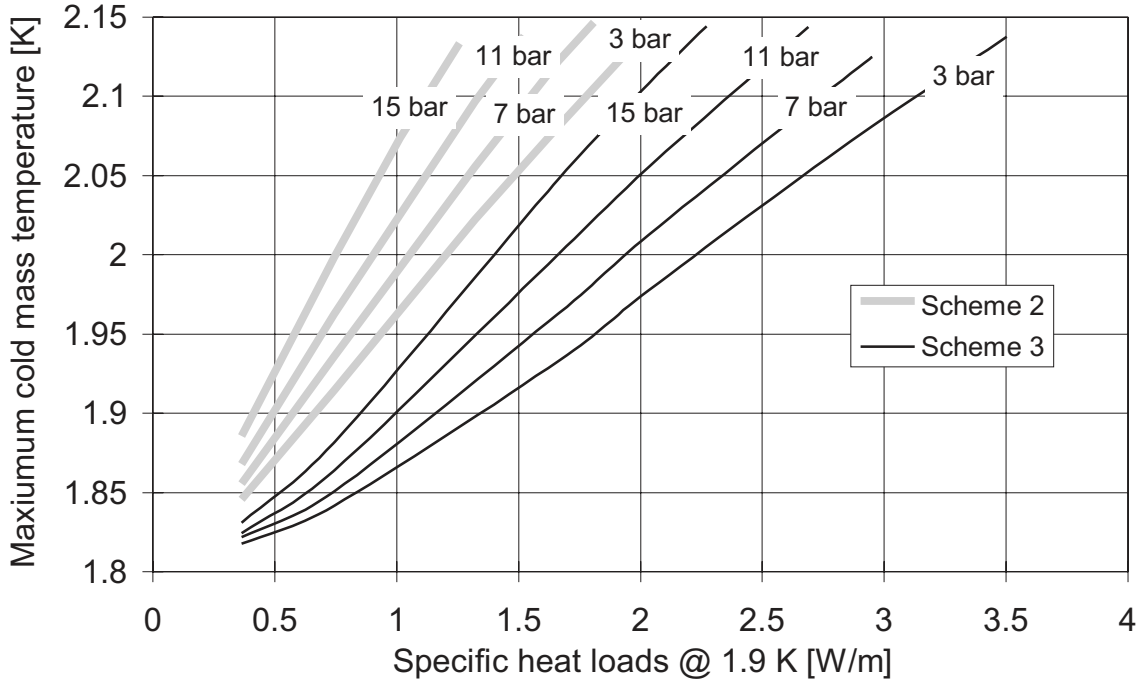
Fig. 42 shows the maximum cold mass temperature as well as the minimum header C pressure requirement for the different upgrade scenarios and distribution schemes. The scheme 1 starts to be limited for scenarios of type B and can not fulfil scenarios of type D. The scheme 2 is compatible with all upgrade scenarios and gives maximum temperature above 1.9 K only for the upgrade scenario Dbb. The scheme 3 gives maximum temperature below 1.85 K for all upgrade scenarios. The minimum Header C supply pressure required for beam screen cooling varies from 3 to 6.2 bar.

10.5 Cryoplant upgrade

The adaptation of the cryoplant to the demand in refrigeration capacity is defined hereafter for the different upgrade scenarios. In the following, only the distribution schemes 1 and 2, which are able to fulfil all scenario requirements, will be considered. Nevertheless, for a given distribution scheme the cryoplant upgrade may reach several levels of adaptation by modifying the existing hardware and by adding new 4.5 K refrigerators and/or 1.8 K refrigeration units and/or interconnection boxes. Fig. 43 shows the different cryogenic architectures that are considered for the different upgrade scenarios. Table 20 gives the required refrigeration capacity of the different cryoplants.

Scenarios A and A', which correspond to the nominal and ultimate operation used for the basic design of the LHC machine, do not (fortunately) require any special cryoplant upgrades.

For the distribution scheme 2, two 1.8 K refrigeration units as well as one or two
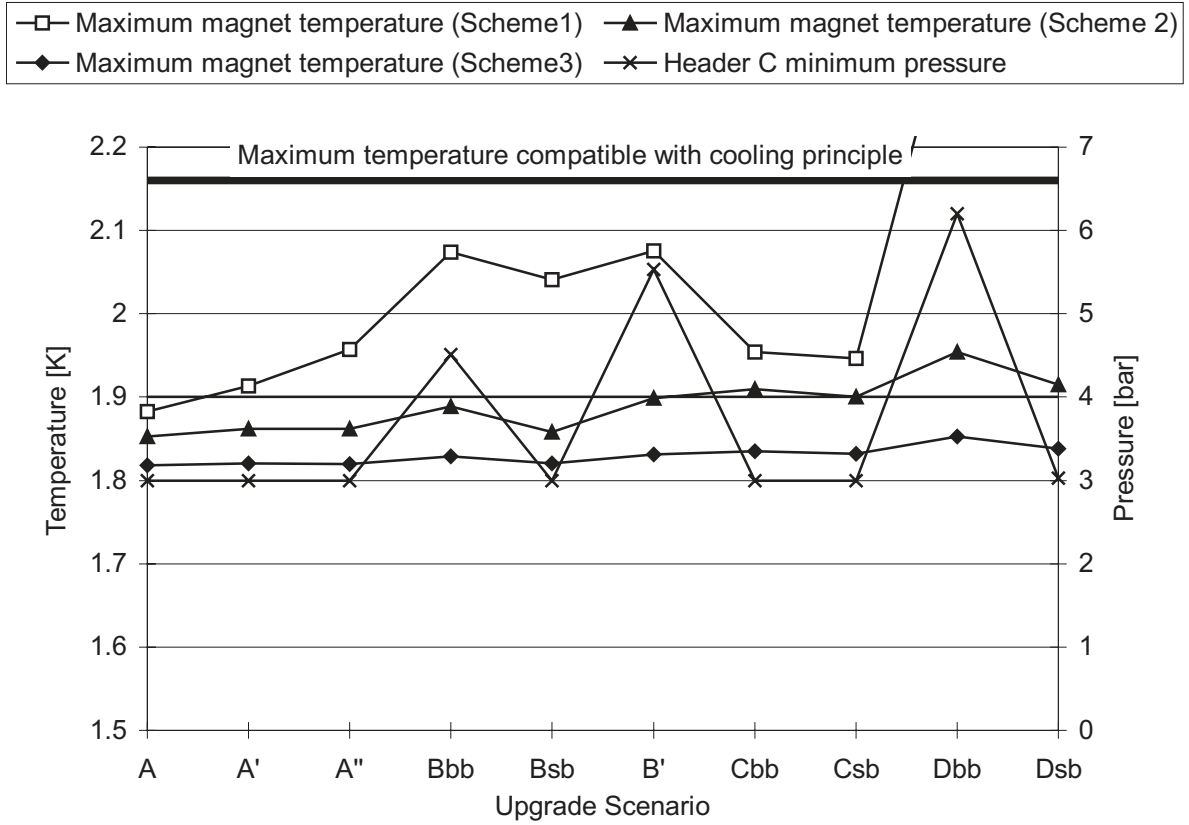
Figure 42: Cooling performance of distribution schemes for different upgrade scenarios.

additional 4.5 K refrigerators have to be added at point 1 and 5 (High luminosity Inner Triplet location). Moreover, for the architecture schemes 2b and 2c, additional 4.5 K refrigerators must be added in parallel to the existing 4.5 K refrigerators. A main issue related to these additional equipments is to find sufficient space to install them at underground and surface level.

Needs in R&D or studies on cryoplants are listed hereafter:

- Existing 4.5 K cryoplant adaptation study is required for scenarios A", Cbb. For ex-LEP cryoplants it will be the third capacity upgrade; consequently, hard limits could be reached for these equipments.
- Existing 1.8 K refrigeration unit adaptation study is required for scenarios Cbb and Dbb.
- Feasibility study of 4.5 K cryoplants with an equivalent capacity of 26 kW @ 4.5 K is required for scenario Dbb.
- Feasibility study of 1.8 K refrigeration units with an equivalent capacity of 3.9 kW @ 1.8 K is required for scenario Dbb and Dsb.
- Feasibility study on parallel operation of two 4.5 K cryoplants coupled to a same sectors for scenarios Bbb, B', Dbb and Dsb.

At equivalent beam energy and luminosity, beams consisting of long super-bunches give reduced losses on the cryogenic system. Consequently, from the cryogenic point of view, the most interesting upgrade scenarios are the scenario Bsb, Csb, and Dsb.

Scenario	Scheme #	Sector cryoplant					IT cryoplant	
		Rb [kW] @ 4.5 K	Ra [kW] @ 4.5 K	R [kW] @ 4.5 K	b [kW] @ 1.8 K	a [kW] @ 1.8 K	Ri [kW] @ 4.5 K	i [kW] @ 1.8 K
A	1	11	10	\	1.4	1.1	\	\
A'	1	18	15	\	1.8	1.3	\	\
A"	1	**22**	18	\	2.2	1.3	\	\
Bbb	2b	18	18	12	1.7	1.7	16	1.8
Bsb	2a	9	9	\	1.2	1.2	15	1.8
B'	2b	18	18	18	1.9	1.9	15	1.7
Cbb	1	**21**	**19**	\	**2.5**	2.0	\	\
Csb	1	14	12	\	2.4	1.9	\	\
Dbb	2c	18	18	**26**	**2.7**	**2.7**	16	**3.9**
Dsb	2c	18	18	6	2.1	2.1	15	**3.9**

Bold : Require some upgrade on existing LHC cryoplant hardware
XX : Non standard equipment with R&D requirement

Table 20: Cryoplant capacity requirements for the different LHC scenarios.

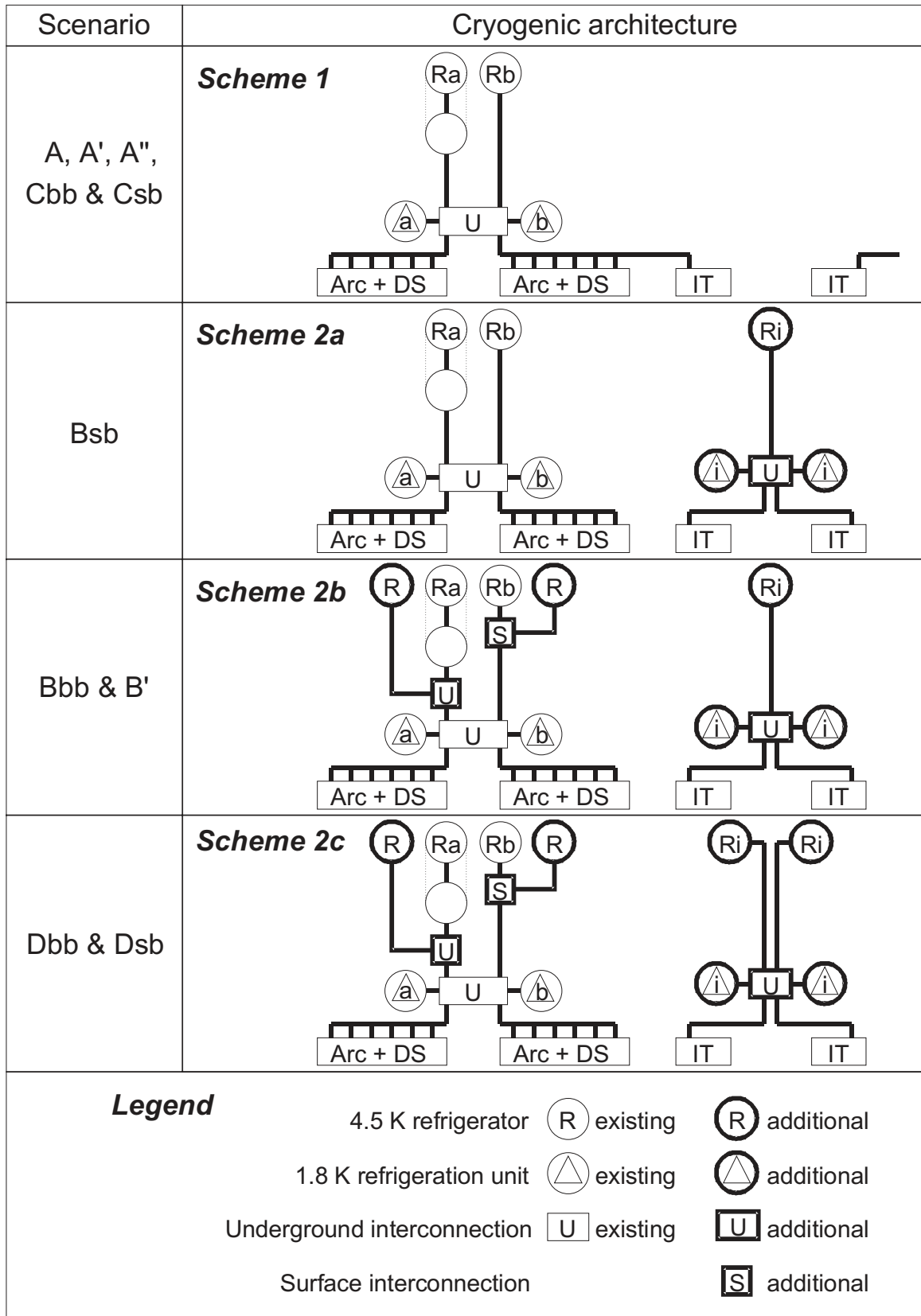| Scenario	Cryogenic architecture
A, A', A", Cbb & Csb	**Scheme 1**
Bsb	**Scheme 2a**
Bbb & B'	**Scheme 2b**
Dbb & Dsb	**Scheme 2c**
Legend	4.5 K refrigerator (R) existing (R) additional 1.8 K refrigeration unit existing additional Underground interconnection [U] existing [U] additional Surface interconnection [S] additional

Figure 43: Cryogenic architecture of distribution schemes.

11 Injectors and RF systems

The LHC upgrade implies a non-trivial performance upgrade of the injectors and of the different RF systems.

11.1 Scenarios in the PS Complex

The LHC injectors will provide the LHC with the nominal $(1.1 \times 10^{11}\,\mathrm{p/bunch})$ and later on with the ultimate $(1.7 \times 10^{11}\,\mathrm{p/bunch})$ bunch intensities within nominal emittances. The former beam is being routinely produced in the PS complex [1], while the latter was demonstrated but with somewhat larger transverse emittances. These achievements are closely linked to novel bunch splitting techniques [2] (one to two, one to three) by means of which microwave instabilities at high energy in the PS can be largely avoided. Bunch splitting, together with more classical procedures such as bunch merging and bunch compression by consecutive adiabatic harmonic changes, provide the PS complex with several interesting possibilities to increase the number of protons per bunch and to generate different bunch spacings.

The present performance of the LHC pre-injector is mainly limited by space charge at PSB (50 MeV) and PS (1.4 GeV) injection energies. This limitation may be overcome in the following ways (in ascending order of investment):

1. Concentration of the available intensity into a fraction of the PS circumference by a combination of these techniques. The RF gymnastics is carried out at high energy where space charge is not relevant.
2. Construction of a normal-conducting H-minus Linac (120 MeV, the front-end of the SPL) as an injector of the PSB. In this way, space charge effects are largely removed, and H-minus injection enables the PSB to generate LHC-type beams with independently (within limits) adjustable bunch intensity and emittance.
3. Construction of the SPL (2.2 GeV) [3] which would replace the PSB as PS injector, with a substantial improvement of the PS space charge limit and basically enabling "any" bunch spacing (with the appropriate variable-frequency RF system added to the PS).

Note that the SPL and its front-end linac would open up several applications for high-power beam users.

The improvements one could hope for with 25 ns bunch spacing are compiled in Table 21. If one accepts shorter bunch trains and thus longer LHC filling times, the bunch population can be substantially increased beyond the ultimate level, even staying with 50 MeV injection. The 120 MeV linac would enable one-batch filling of the PS, thus avoiding the PS injection front porch (detrimental to beam emittance) and substantially shortening the LHC filling time. Finally, with the SPL, 80 bunches with up to $4 \times 10^{11}\,\mathrm{p/bunch}$ are within reach, more than doubling the ultimate bunch intensity; moreover this scheme avoids two-batch injection into the PS, thus the "net" LHC filling time would be reduced to about 2.5 minutes per ring.

An alternative way to increase the LHC luminosity is colliding more bunches with a smaller spacing while keeping the same bunch population. To this end, ways to generate bunch spacings of 15, 12.5, and 10 ns were explored (although 12.5 ns is not compatible with the 200 MHz RF system of the SPS). These scenarios are compiled in Table 22. Bunch spacings of 15 ns and 10 ns require new fixed-frequency RF systems in the PS; to fully profit from the SPL, variable-frequency ($\sim$5% variation) systems must be envisaged. For each case, the detailed PS filling scheme and RF procedure is explained in Table 23. With the PSB as PS injector, a bunch population near or beyond the ultimate one can

be produced only by shortening the bunch train (typically ~1/2 of the PS filled), thus accepting longer LHC filling times. Here again, the SPL would combine all advantages: bunch population beyond ultimate, long bunch trains in the PS, flexibility in adjusting intensity and emittance by virtue of the H-minus injection, short LHC filling times. Significant development work would have to be invested in the rather involved RF gymnastics, and there is a risk of electron cloud effects [4] becoming harmful with the shorter bunch spacing in the PS.

Just to complete the picture, a bunch spacing of 5 ns appears feasible, but the unavoidable debunching-rebunching procedure in the PS limits the bunch population to about 1/4 of the nominal one, so there would not be any gain in luminosity.

References
[1] M. Benedikt et al., *Performance of the LHC pre-injectors*, presented at the 18th International Conference on High Energy Accelerators (HEACC2001), Tsukuba, Japan, 26–30 March 2001, CERN-PS-2001-011 (DR).
[2] R. Garoby, *Multiple bunch splitting in the PS, results and plans*, in Proc. 11th Chamonix Workshop, Chamonix, France, January 2001.
[3] The SPL Study Group (M. Vretenar, Editor), *Conceptual design of the SPL, a high power superconducting H-minus Linac at CERN*, CERN 2000-012, December 2000.
[4] R. Cappi et al., *Electron cloud effects in the CERN PS*, CERN/PS 2001-020 and Proc. IEEE Particle Accelerator Conference (PAC2001), Chicago, IL, USA, 18–22 June 2001, eds. P. Lucas and S. Webber (IEEE, Piscataway, NJ, 2001), pp. 682–684.

Scenario	#PSB pulses (rings) to fill PS	protons per bunch	bunches in PS (h=84)	protons per bunch limited by	cost M CHF	comments
Reference nominal PSB Inject. 50 MeV	2 (3+3)	$1.1 \ 10^{11}$	72	not at this level	0	available
Present "Ultimate" PSB Inject. 50 MeV	2 (3+3)	$1.7 \ 10^{11}$	72	space charge PSB: $\Delta Q{\sim}0.4$	0	demonstrated, but marginal in transverse emittances
Beyond "Ultimate" but shorter bunch trains (PSB 50 MeV)	2 (4+4)	up to $3.4 \ 10^{11}$	48	space charge PSB: $\Delta Q{\sim}0.4$	0	procedure {3} for 12.5 ns spacing without last bunch splitting.
120 MeV (H-) Linac for PSB: one-batch filling {1}	1 (4)	up to $1.9 \ 10^{11}$	72	space charge PSB: $\Delta Q{\sim}0.4$	70	shortens LHC filling time by $\sim$30%. Easier for PS (no inj. plateau 1.2 s)
SPL (2.2 GeV) replacing PSB (1.4 GeV)	-	up to $4 \ 10^{11}$	~ 80	space charge PS: $\Delta Q{\sim}0.25$	500	"any" spacing feasible but needs corresponding new variable ($\sim$5%) frequency RF systems

Table 21: Luminosity upgrade scenarios in the PS complex with a bunch spacing of 25 ns.

Scenario	#PSB pulses (rings) to PS	protons/bunch, (harmonic number h) in PS for bunch spacing			protons per bunch limited by	cost M CHF	comments
		15 ns {2}	12.5 ns {3}	10 ns {4}			
"ultimate", shorter bunch trains (PSB Injection 50 MeV)	2 (4+4)	$2.5 \, 10^{11}$ 64 (h=140)	$1.7 \, 10^{11}$ 96 (h=168)	$1.7 \, 10^{11}$ 96 (h=210)	space charge PSB: $\Delta Q{\sim}0.4$	5	New RF systems for {2} and {4}. Shorter bunch trains = longer LHC filling. No flexibility in intensity and emittance
120 MeV (H-) linac for PSB: PS one-batch filling {5}	1 (4)	$2.1 \, 10^{11}$ 64 (h=140)	$1.4 \, 10^{11}$ 96 (h=168)	$1.4 \, 10^{11}$ 96 (h=210)	space charge PSB: $\Delta Q{\sim}0.4$	70	LHC filling time about as in nominal scheme, in spite of shorter bunch trains
120 MeV (H-) linac for PSB: PS two-batch filling	2 (4+4)	$3.3 \, 10^{11}$ 64 (h=140)	$2.2 \, 10^{11}$ 96 (h=168)	$2.2 \, 10^{11}$ 96 (h=210)	space charge PS: $\Delta Q{\sim}0.25$	70	Longer LHC filling (short bunch trains). Flexibility in intensity and emittance
SPL (2.2 GeV) replacing PSB (1.4 GeV)	-	$2.4 \, 10^{11}$ 130 (h=140)	$2.0 \, 10^{11}$ 160 (h=168)	$1.6 \, 10^{11}$ 200 (h=210)	space charge PS: $\Delta Q{\sim}0.25$	500	PS ring fully filled with bunches. "Complete" flexibility in intensity and emittance

Table 22: Luminosity upgrade scenarios in the PS complex with bunch spacings of 15 ns, 12.5 ns, and 10 ns.

{1} The 120 MeV H- Linac is the normal-conducting pre-accelerator of the projected SPL. H- injection ("charge exchange") enables intensity and transverse emittances to be adjusted independently (if not limited by space charge) at PSB injection with much increased flexibility for LHC; this is not possible with the present H+ injection scheme.

For one-batch filling and bunch spacing 25 ns, the following scheme is contemplated: (i) the PSB delivers 12 bunches (4 rings, 3 bunches per ring, possibly after splitting 1 to 3, phasing slightly changed by h(PSB)=1 system) into the PS tuned at h=14; (ii) acceleration of 12 bunches on h=14 to 26 GeV/c, and the procedure follows the one of the nominal LHC beam, namely (iii) splitting 1 to 3 of the 12 bunches into 36 on h=42; (iv) splitting 1 to 2 of the 36 bunches to 72 bunches on h=84.

{2} 15 ns bunch spacing can be produced with the SPL as PS injector with a new variable-frequency RF system (63.5-66.7 MHz) in the PS. For the scenarios with the PSB, the following more complicated procedure is envisaged (R&D work needed): (i) inject 8 bunches (two PSB pulses, 4 rings each, tuned at h(PSB)=1) into the PS tuned at h(PS)=9; (ii) accelerate on h=9 to 26 GeV/c (to be defined); (iii) compress the 8 bunches into 8/17 of the PS by adiabatically changing from h=9 to 10,11,...,17; (iv) split the 8 bunches to 16, on h=34; (v) compress the 16 bunches into 16/35 of PS by adiabatically changing from h=34 to 35; (vi) apply two consecutive bunch splittings, yielding 32 bunches on h=70, and finally a train of 64 bunches on h=140. New (fixed-frequency) RF systems needed: 16.2+16.7 MHz (h=34, 35), 33.3 MHz (h=70), 66.7 MHz (h=140). Note that 15ns bunch spacing is compatible with SPS 200 MHz system.

{3} 12.5 ns bunch spacing can be produced with the SPL as PS injector using existing systems (with more RF voltage on the 80 MHz system for final bunch shortening). Proposed procedure with the PSB (R&D work needed): (i) inject 8 bunches (two PSB pulses, 4 rings each, tuned at h(PSB)=1) into the PS tuned at h(PS)=9; (ii) accelerate the 8 bunches to some intermediate energy (to be defined); (iii) compress the 8 bunches into 8/14 of the circumference by adiabatically changing from h=9 to 10,11,12,13,14; (iv) merge the 8 bunches 2 by 2 and split the result into 3, playing with voltages on h=7, 14, 21, yielding 12 bunches on h=21; (v) accelerate the 12 bunches on h=21 to 26 GeV/c; (vi) 3 consecutive double-splitting operations, changing the RF harmonics from 21 to 42, 84 and 168, resulting in a bunch train of 96 bunches filling 4/7 of the PS. Note that without the last bunch splitting step, there is a bunch train of 48 bunches, 25 ns spacing, in 84 PS buckets. 12.5 ns bunch spacing is not compatible with the SPS 200 MHz system.

{4} 10 ns bunch spacing can be produced with the SPL as PS injector with a new variable-frequency RF system (95.4-100 MHz) in the PS. With the PSB, there is also a way to produce this beam (R&D needed): (i) inject 8 bunches (two PSB pulses, 4 rings each, tuned at h=1) into the PS tuned at h=9; (ii) accelerate to 26 GeV/c; (iii) stepwise adiabatic harmonic change from h=9 to 10, 11, ..., 17; (iv) splitting 1 to 2 yielding 16 bunches on h=34; (v) adiabatic harmonic change to h=35 (16 bunches on h=35); (vi) splitting 1 to 3 resulting in 48 bunches on h=105; (vii) splitting 1 to 2 resulting in 96 bunches on h=210 (spaced 10 ns). New (fixed-frequency) RF systems in PS: 16.2 + 16.7 MHz (h=34, 35), 50 MHz (h=105), 100 MHz (h=210). 10 ns bunch spacing compatible with SPS 200 MHz system.

{5} For 15 ns, 12.5 ns, and 10 ns bunch spacings with one-batch filling from PSB the procedure is as follows: The PSB delivers 8 bunches (4 rings, 2 bunches per ring, their phases adjusted by h(PSB)=1 RF system before PSB extraction) into the PS tuned at h(PS)=9; then the procedure follows {2}, {3}, and {4}, for 15 ns, 12.5 ns, and 10 ns spacings, respectively.

Table 23: Detailed PS filling schemes and RF procedures corresponding to the different options in Tables 21 and 22.

11.2 Higher intensities in the SPS

The scenarios put forward above for the LHC beam in the PS pre-injector all suppose considerably higher single bunch and total intensities passing through the SPS than those foreseen for LHC.

In September 2002 the SPS achieved the nominal longitudinal parameters for the first time [1]. The parameters obtained at 450 GeV in the SPS were 4 batches of 72 bunches (spacing 25 ns), each bunch having 1.1×10^{11} protons and with an emittance $\varepsilon_L \leq 0.7$ eVs. ('nominal' is $0.5 < \varepsilon_L < 1$ eVs). The maximum time excursion between bunches due to beam loading effects were ± 0.2 ns. To reach this performance it has been necessary to carry out both a comprehensive impedance reduction programme in the SPS [2, 3], including the shielding of all inter-magnet pumping ports [4] mainly to control single bunch instabilities, and also to incorporate a significant number of changes to the RF systems [5]. These latter include RF feedback and feed-forward on each 200 MHz travelling wave cavity, a coupled bunch feedback system acting on low numbered modes and the use of the 800 MHz Landau damping system in bunch shortening mode to increase synchrotron frequency spread.

The main restriction at transfer to the LHC comes from the allowed losses in LHC at injection and possible quenching of the SC magnets. This translates with the inevitable energy and phase errors to a maximum allowable emittance in the SPS at 450 GeV. Phase errors include the beam loading effects mentioned above which also increase with intensity. The present situation with the nominal beam allows direct injection into the 400 MHz buckets of the LHC accelerating system. An additional 200 MHz capture system is foreseen in the LHC for the ultimate beam (1.7×10^{11} protons/bunch) – this will allow bunches with ε_L up to 1.2 eVs at 450 GeV to be transferred with acceptable losses.

Measurements [3], carried out in 1999 and 2001, show that for a single bunch with emittance $\varepsilon_L = 0.15$ eVs and length $\tau_{\mathrm{FWHM}} = 1.6$ ns at $E = 26$ GeV, the single bunch instability threshold has increased by at least 2.5 times following the impedance reduction campaign to 10^{11} protons/bunch. The microwave instability threshold scales as $\varepsilon_L^2/(\tau E)$ and so allowing an emittance increase to 1.2 eVs at 450 GeV and with comparable bunch lengths, the threshold intensity will be 3.7×10^{11}. The emittance can be increased from about 0.4 eVs at injection to the 450 GeV level in a programmed way to keep a constant threshold. Nonetheless the high total intensity would require large powers in the cavities and the RF couplers and amplifier system itself may require upgrading. For coupled bunch instabilities an estimate of the maximum intensity allowed with 1.2 eVs can be obtained from results with the nominal bunches already accelerated and knowledge of the increase in energy and synchrotron frequency spread produced by the 800 MHz system which is necessary for stability. The expected improvement using the 800 MHz system and allowing the emittance to increase to 1.2 eVs is about a factor two. This is therefore a stronger restriction than with the single bunch instability.

Therefore it seems reasonable from longitudinal considerations to expect up to a factor two increase in intensity over nominal, i.e. 30% more than 'ultimate' if the 200 MHz system is installed in the LHC. To go further, either the impedance must be reduced or possibly a wide-band feedback system could be used. For the former it is necessary first to identify the impedance and then find some way to reduce it.

In the transverse plane the resistive wall instability presents probably the most severe restriction. The damper is already designed to cover all modes when the bunch spacing is 25 ns [6]; smaller bunch spacing would require an upgrade for larger bandwidth. Use of octupoles and chromaticity can also help, but is restricted by the need to keep small transverse emittances. The electron cloud effect may also present significant problems at

higher bunch intensities, though there is evidence that 'beam scrubbing' is effective to nominal intensities.

In conclusion it is clear that, while an improvement in intensity of a factor two over nominal can be hoped for, the higher intensity regimes in the SPS must be explored by a significant machine study programme to give definite answers to the maximum intensity possible for the LHC beams in the SPS.

References

[1] Ph. Baudrenghien, T. Bohl, T. Linnecar, E. Shaposhnikova, and J. Tuckmantel, *Nominal Longitudinal Parameters for LHC Beam at 450 GeV in the SPS*, CERN SL-Note-2002 MD - to be published.

[2] P. Collier, Ed., *The SPS as Injector for the LHC – Conceptual design*, CERN/SL-97-07 DI (1997).

[3] T. Bohl, T. Linnecar, and E. Shaposhnikova, *Impedance Reduction in the CERN SPS as seen from Longitudinal Beam Measurements*, 8th EPAC 2002, Paris.

[4] P. Collier, M. Ainoux, R. Guinand, J-M. Jimenez, A. Rizzo, A. Spinks, and K. Weiss, *Reducing the SPS Machine Impedance*, 8th EPAC 2002, Paris.

[5] Ph. Baudrenghien, T. Bohl, T. Linnecar, E. Shaposhnikova, and J. Tuckmantel, *Approaching Nominal Longitudinal Parameters with a Single LHC Batch in the SPS*, CERN SL-Note-2002-029 MD (2002).

[6] W. Höfle, *Progress with the Damper*, Chamonix XI, CERN SL-2001-003 DI (2001).

11.3 The RF system for bunch length reduction in LHC Phase 1

11.3.1 Beam Parameters

In LHC Phase 1, the β^* will be lowered by a factor 2 to 0.25 m. In order to take full advantage of this change, it is interesting to decrease the r.m.s. bunch length τ_{rms} accordingly. In general we want $\tau_{\mathrm{rms}} \ll \beta^*$. With the new β^* and a crossing angle of $424\,\mu$m, a decrease in bunch length by a factor 2 from 7.7 cm to 3.8 cm will give an increase in luminosity of about 30%.

LHC Phase 1 also consists of a two-staged increase in beam current. The first is by going from the nominal bunch intensity, 1.1×10^{11}, to the ultimate bunch intensity, 1.7×10^{11}. The second is by an increase in the number of bunches, with a possible change of bunch spacing from 25 ns to 15 ns. These two upgrades increase the average beam current, I_{av}, first from 0.56 A to 0.85 A, and then to 1.41 A.

11.3.2 Consequences for existing RF systems

The associated increase in the RF component of the beam current I_{RF} has significant consequences on the power requirements of all RF systems in the machine. Both the capture RF system (200 MHz) and the acceleration RF system (400 MHz) will need their power plants increased in size in roughly the same ratios. One area of concern is the power couplers which will certainly need to be improved in the second stage. Couplers are delicate items and this will involve research and development effort. An alternative is to lower the voltage that each cavity provides and install more cavities to compensate for this lack of voltage. This will not only be expensive but will increase the impedance in the machine at a time when the intensity is increasing: beam stability will become an issue. We will come back to R&D in the coupler field later.

11.3.3 RF system for bunch length reduction

To obtain the bunch length reduction it is most efficient to use a high harmonic RF system. However since this system cannot be used for acceleration and will only be used during the high-energy store we have to transfer the bunches from the accelerating RF buckets to the higher harmonic buckets. At 7 TeV, beam gymnastics with possible beam losses, such as bunch rotation and capture, are preferably avoided, even if possible, and so it is assumed here that an adiabatic transfer will be used. This is most easily done when the accelerated bunch length is shorter than the higher harmonic system wavelength. These considerations lead to the choice of 1.2 GHz for the higher harmonic RF. A further question arises as to whether the bunch shortening can be achieved by a passive cavity system. The cavity, probably super-conducting, would be tuned slightly away from the beam frequency such that the beam-induced voltage has the correct phase and amplitude to shorten the bunch. An active system, although more expensive due to the high powers involved, offers far more security. Complete control of the RF parameters is then maintained under all beam-loading conditions. The risks inherent in using a passive system are not evaluated here and only the parameters for an active system will be considered.

11.3.4 Main RF parameters

In Table 24 the parameters for the bucket and bunch are given at 7 TeV for different RF frequencies. In order to fit into the bucket at 1.2 GHz the maximum longitudinal beam emittance ε_{L} that can be allowed is 1.5 eVs. This gives a full bunch length, 4 times τ_{rms}, of 0.8 ns. This emittance is lower than the nominal 2.5 eVs foreseen and implies a reduction in beam stability margin for both coupled and single bunch instabilities [1].

For this reason it may be necessary to transfer to the higher harmonic system at a lower energy. The threshold shunt impedance for longitudinal multi-bunch instabilities scales as $R_{\text{th}} \propto \varepsilon_{\text{L}}^2 h^2/E\tau$, where h is the harmonic number, ε_{L} the longitudinal emittance, and E the beam energy, and so a suitable energy would be around 1.75 TeV. Once the transfer to the higher harmonic system is made, h increased by three times, the beam becomes much more stable. From Table 24 we see that an RF voltage of 43 MV at 1.2 GHz, in addition to the 16 MV at 400 MHz, will give the reduction in bunch length required even with a longitudinal emittance of 1.75 eVs. The r.m.s. relative energy spread σ_{E} is increased to 1.52×10^{-4}.

frequency f_{rf} MHz	voltage V_{rf} MV	Bucket			Bunch		
		half height dE/E 10^{-4}	full length τ_{full} ns	area A eVs	energy spread σ_{E} 10^{-4}	length τ_{rms} ns	emittance ε_{L} eVs
400	16	3.43	2.5	7.62	**1.1**	**0.27**	**2.5**
					0.84	0.2	1.5
400	45	5.75	2.5	12.8	1.41	0.21	2.5
1200	43	3.25	0.83	2.40	1.45	0.15	1.75
1200/400	43/16	3.66	0.83	2.86	1.75	0.18	2.5
					1.52	**0.14**	**1.75**

Table 24: LHC bucket and bunch parameters at 7 TeV for various RF systems and longitudinal beam emittances. The first and last row of bunch parameters, in bold, refer to nominal LHC and to LHC Phase 1 conditions, respectively.

11.3.5 RF implementation

The cavities could be single cell, to make the application of strong RF feedback easier (no extra pass-band modes), and super conducting, to permit lower R/Q. Both these options reduce beam-loading effects.

With $I_{\text{av}} = 1.4$ A and a bunching factor of about 0.72 at 7 TeV, the RF beam current I_{rf} is 2.1 A. During acceleration, zero voltage with full beam current compensation is required, while 43 MV is needed at 7 TeV. This implies a variable coupler to optimise the power requirements and in particular to reduce power requirements in coast, where maximum reliability is essential. For full control, the total RF power per beam $V_{\text{rf}} I_{\text{rf}}/8$ (see [2]) is $P_{\text{tot}} \sim 11$ MW. RF power couplers can work reliably in CW at about 500 kW. This would mean that there are 22 cavities per beam, each supplying 2 MV. These 22 SC cavities would occupy typically 50 m in the straight section. A preliminary estimation of the total cost is sketched in Table 25.

1.2 GHz power amplifiers	23 MCHF
HT Power	8 MCHF
Cavities, cryostats	17 MCHF
Infrastructure, Controls, Cabling	8 MCHF
Total	56 MCHF

Table 25: Preliminary estimation of the cost of the 1.2 GHz bunch shortening system based on 2 rings with 22 cavities per ring at 500 kW.

11.3.6 Discussion

It would certainly be interesting to work at a higher voltage with less cavities, to make use of higher power klystrons or their equivalent, and occupy less space in the tunnel. This would imply higher power couplers. Coupler design is an area where a vigorous R&D programme would be of great interest. The large number of cavities also implies very strong damping of the higher order cavity modes.

References

[1] E. Shaposhnikova, *Longitudinal beam parameters during acceleration in the LHC*, LHC Project Note 242 (2000).

[2] D. Boussard, *RF Power Requirements for a High Intensity Proton Collider*, CERN SL-RFS/91-16, SL-DI/91-20 (1991) and Proc. IEEE Particle Accelerator Conference, San Francisco, CA, USA, 6–9 May 1991 (IEEE Conference Record 91CH3038-7, 1991), pp. 2447-2449.

11.4 RF parameters for LHC super-bunches

We discuss possible longitudinal RF parameters for a 300 m long super-bunch in the LHC with 1 A DC current. Assuming that the super-bunch is obtained by merging some 3000 LHC bunches with ultimate intensity, a longitudinal emittance larger than or equal to 15 keVs can be anticipated. This corresponds to an energy spread of $\pm 10^{-3}$ and requires a peak voltage of 3.4 MV for a sine-wave barrier bucket at 10 MHz or 680 kV for a harmonic RF system at 500 kHz. As shown in Table 26, proportionally higher voltages are required at higher RF frequencies. In case of barrier bucket, the super-bunch would have a smooth parabolic edge extending over about 20 ns. The necessary 500 kHz RF system could be made of 15 low Q/low impedance cavities, each one 1 m long with a diameter of 1.5 m and providing 45 kV. These could be septum cavities, in view of the limited beam separation.

RF frequency (single sine-wave)	100 MHz	40 MHz	10 MHz
peak voltage	34 MV	13.6 MV	3.4 MV
RF frequency (harmonics)	500 kHz ($h = 44$)	22 MHz ($h = 1780$)	165 MHz ($h = 13350$)
number of bunches	1	40	300
peak voltage	680 kV	27 MV	202 MV

Table 26: Parameters of barrier bucket (top) or harmonic RF systems (bottom) at different frequencies for an LHC super-bunch.

Beam stability may be better with a low frequency harmonic RF system than with a barrier bucket, but the latter is more flexible for the number of super-bunches. A momentum deviation of 10^{-3} would give more than 100% beta-beating, assuming a 5 km β_{max}, with possible problems of background and beam-beam. Therefore a local chromatic correction scheme may be envisaged. The super-bunch longitudinal emittance of 15 keVs is obtained assuming a nominal LHC bunch emittance of 2.5 eVs and a 20% safety margin for uncontrolled blow-up: we may try to save on this.

For fixed beam intensity and crossing angle, longer super-bunches would yield a luminosity inversely proportional to the bunch length. Possible beam losses during the delicate process of merging 3000 bunches into a single super-bunch may be a concern for machine protection, however losses would occur only in case of instabilities. In case of barrier bucket, one would probably need to bypass the normal RF system.

12 Beam Dumping system

A beam dumping system operating with highest reliability is a vital element of the LHC. The energy contained in the circulating beam of a machine like the LHC is such that stopping or dumping it internally, like done in the SPS, is impossible. Already one of the about 2800 circulating bunches, when hitting a metallic surface like copper or iron, would melt it [1]. Therefore, the only viable concept is to fast-extract the beam loss-free from each ring of the collider and to transport it to an external dump, positioned sufficiently far away to allow for appropriate beam dilution in order not to overheat the absorber material. A loss-free extraction requires a particle-free gap in the circulating beam, during which the field of the extraction kicker can rise to its nominal value.
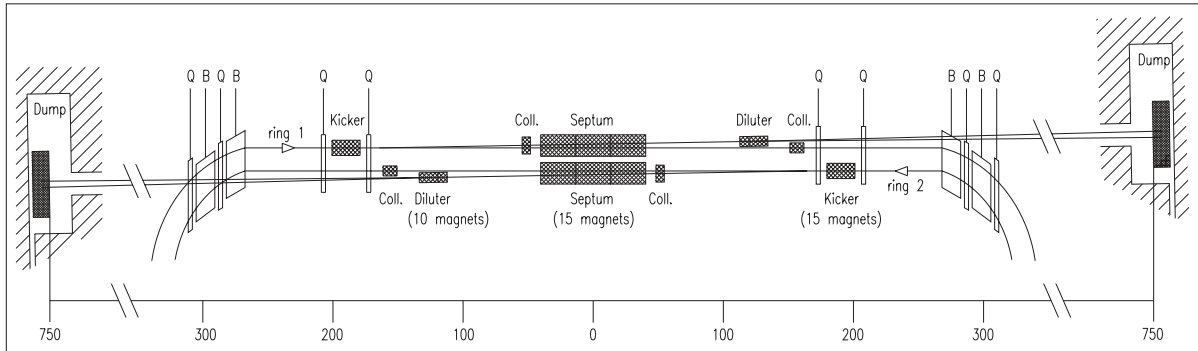
12.1 The present system

Figure 44: Schematic layout of the LHC beam dumping system in long straight section 6.

A layout of the system under construction is shown in Fig. 44. It will be installed in straight section 6 and comprises for each ring, following the beam direction, 15 modules of extraction kicker magnets (3 μs rise time, overall length 25 m), 15 modules of steel septum magnets (overall length 72 m), 10 modules of two types of dilution kicker magnets (overall length 22 m), and finally the beam dump (overall dimensions $4 \times 3.5 \times 12.4 \,\mathrm{m}^3$, weight about 1000 tons), situated in a cavern at 630 m from the dilution kickers and 750 m from the centre of the septum magnets [2, 3, 4, 5]. The two types of dilution kickers are orthogonally deflecting and let the extracted beam describe a circle-like pattern of 35 cm diameter on the front face of the dump. The chosen distance between the dump and the dilution kickers is a trade-off between the cost of the kicker magnets and the cost of the transfer tunnels. Other methods of diluting the beam were found to be less efficient [6]. For instance, blowing up the beam with quadrupoles would require longer transfer tunnels. Also, the transverse dimensions of the dump would have to be larger when taking into account the spread of trajectories of the extracted beams.

The material of the central absorbing parts of the beam dump is carbon with a density of 1.7 and 1.1 g/cm³. This material is chosen for its low atomic weight and density and its excellent mechanical properties at very high temperatures. It is also easy to handle and cheap. Other light materials have been considered, like liquid lithium or water, but it was estimated much more difficult and expensive to arrive at a practical and safe design.

The system under construction can cope safely with multi-bunch beams of average currents of 0.85 A (about 2800 bunches of 1.7×10^{11} protons per bunch) at 7 TeV. It can also cope with beams of 7.5 TeV, but at somewhat lower currents such that the energy

stored in the beam is kept at the same level of 540 MJ. The maximum temperature in the carbon parts of the dump is about 1250 °C when hit by the diluted 86 μs long beam burst, which results in mechanical stresses safely below the elastic limit [7, 8, 9], taking into account thermal shock phenomena.

The beam dumping system acts at the request of the machine protection system, which collects the status and messages from all critical machine subsystems. It is essential that the active elements of the beam dumping system (kickers and septa) function with utmost reliability. Although great effort is undertaken in this respect (*e.g.*, by building-in appropriate margins, redundancy, energy autonomy, failure tolerant signal transmission, and by monitoring of all vital parameters such that a safe dumping action can still be launched before the machine is in danger), failures cannot be totally excluded [10].

One such failure, with potentially destructive consequences, would be the firing of the extraction kickers before or after the arrival of the beam gap. This could happen, *e.g.*, by a sudden accidental firing of one of the high voltage/high current switches of the pulse generators, with subsequent automatic triggering of all others, or by the loss of synchronisation with the beam gap. In such case the beam is swept over the machine aperture and part of it would hit the steel septum and melt it. To avoid this, protective collimators, made of suitable low density materials, such as carbon, are placed upstream of the septum and also in front of the first quadrupole downstream of the septum [11]. These collimators are very critical elements since they see the undiluted beam as circulating in the machine. It is very difficult to be specific on the hypothetical but not entirely unconceivable event of a complete failing of a required dump action.

12.2   Upgrades

An increase of the beam current beyond 0.85 A and beam energies higher than 7 TeV require to upgrade the beam dumping system. While higher currents at 7 TeV only affect the beam dump and beam dilution, higher beam energies require both upgrades of the dump and beam dilution and of the extraction elements. In any case the questions of safety and protection against failures become more critical.

12.2.1 *Increase of current of multi-bunch beams at 7 TeV*

Increasing the beam current from the nominal 0.56 to 0.85 A by raising the bunch intensity to 1.7×10^{11} p/bunch is still compatible with the present system. Further increases, *e.g.*, to 2.0×10^{11} p/bunch (corresponding to 1 A) or slightly higher, could still be tolerated accepting somewhat reduced safety margins or implementing moderate upgrades.

In the next phase, where the number of bunches is increased (by shortening the bunch distance from 25 to 15, 12.5, or 10 ns), the currents go up to about 2.5 A, assuming bunch intensities of 2.0×10^{11} p/bunch. They would reach 3 A if the injectors could deliver bunches of 2.5×10^{11} p/bunch. Such increases call for substantial upgrades of the beam dumping system. Possible measures to be considered are to improve the capacity of the beam dump by using carbon qualities of still lower density as foreseen at present, to increase the strength of the dilution kickers (so as to enlarge the diameter of the dilution pattern) or their frequency (to produce a kind of spiral) or to install quadrupoles to increase the beam divergence. Next, it can be envisaged to move the dump further away from the extraction point, which would require extra civil engineering work. More dilution could mean that the transverse dimensions of the dump are increased with the eventual consequence that the dump cavern is to be enlarged.

Altogether, there is no fundamental limitation. The challenge would rather be to find the best compromise. Within the constraint of the existing tunnels and caverns, solutions could be found for beam currents up to at least 2 A.

As for what concerns the septum and quadrupole protecting collimators, the possibilities for upgrades are restricted. One could think of using lower density carbon, of changing their shape (wedge), or of segmenting them to dilute the electromagnetic shower. However, beyond a beam current of 2 A the risk of damage would be considerably increased. Shortening the rise time of the extraction kicker would help in this respect, but this would not be an easy route to go and it would be expensive. Experience with the present system will show how often failures leading to unsynchronised extractions will occur and how their frequency could be further reduced.

12.2.2 The 300 m long super-bunch at 7 TeV

In this case the whole beam of 1 A average current (5.5×10^{14} p, 635 MJ) is concentrated in about 1% of the machine circumference. The extraction system is compatible with this, but dumping requires substantial upgrades. As the beam is only 1 μs long, the method used for diluting the 86 μs long multi-bunch beams is no longer suited. To be efficient, the dilution kickers would have to operate at a much higher frequency which, for providing the same bending strength, would be extremely difficult, if not impossible. The way out here would be to de-focalise the beam with quadrupoles to a size compatible with the dump material. For an upgraded dump (see previous section), a 4σ beam size of at least 120 mm ($\beta = 1.8 \times 10^6$ m) would be needed. With an integrated quadrupole strength of about 2000 T/m · m, which is realistic using superconducting magnets, and a distance to the dump of 2 km, this would be feasible. An inconvenience of this solution is, as already mentioned, that also the spread in extraction trajectories (due to changes of the closed orbit, to the pulse shape of the extraction kicker and to failure modes) is magnified and that the transverse dimensions of the beam dump and the aperture of the transfer channel would become much larger. For the variant where the beam is divided up into 10 shorter (0.1 μs) bunches distributed around the circumference, the argument given above applies as well and the same method for dumping must be used. It should be kept in mind that the system chosen has to remain compatible with the bunch pattern in the machine before the super-bunch or its variant is formed.

The problem of protecting the septa, when hit in case of an unsynchronised extraction, cannot be solved. However, the probability that this happens is lower than in the case of multi-bunch beams (in proportion to the beam occupation) and the risk is reduced accordingly.

In conclusion, dumping the super-bunch or its variant is feasible, but it requires important investments (in the order of 50 MCHF), mainly into civil engineering.

12.2.3 Increasing the beam energy to 14 TeV

As already mentioned an increase of beam energy requires both, an upgrade of the extraction elements as well as of the dilution devices and the main absorber. Going as far as doubling the energy might lead to substantial rebuilding. Simply doubling the number of kicker and septum modules would probably be incompatible with the available space. Therefore higher operating fields must be considered. This is possible for the extraction kickers at the price of increasing their rise time. This in turn implies that also the beam gap must be lengthened correspondingly and that the protection of the septa becomes more critical in case of an unsynchronised extraction. As for the steel septum magnets,

higher fields are possible by increasing the septum thickness. For both, rebuilding the kickers and the septa, one might profit from the fact that, depending on the injection energy, an LHC operating at 14 TeV has a smaller aperture.
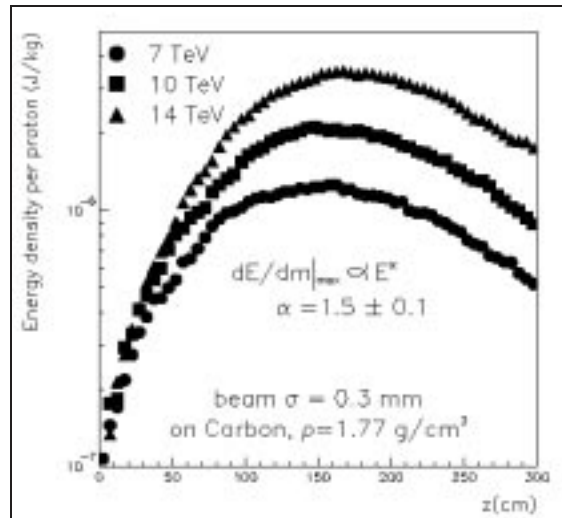

Figure 45: Longitudinal distribution of energy deposition densities (courtesy Paola Sala).

The energy deposition densities and hence the temperatures in the dump rise more than in proportion to the beam energy. An energy increase from 7 to 14 TeV would cause a temperature increase by a factor of 2.8 (see Fig. 45). It should also be taken into account that beams of higher energy have smaller emittances, which further increase the temperatures. With this, and assuming beam intensities in the same range as above, more dilution and larger dimensions of the dump would be required. Depending on the characteristics of the beam, multi-bunch or super-bunch, much stronger dilution kickers or quadrupoles and longer transfer tunnels (several km) with probably enlarged dump caverns would be needed. Although in principle possible, this requires important investments. Those would probably be in the order of 100 MCHF depending, of course, on the assumed beam currents. Within the constraint of the present tunnels and caverns, the current of multi-bunch beams would have to stay below 1 A.

The problems of safety and survival of failure modes are still more difficult to solve and might become a limiting factor.

12.3 Summary

The performance of the LHC beam dumping system under construction and the upgrades needed for higher beam intensities and energies can be summarised as follows:
 - The system under construction is designed to cope safely with 7 TeV multi-bunch beams with an average current of 0.85 A (bunch intensity 1.7×10^{11} p/bunch). Slightly higher beam currents, say up to about 1 A (corresponding to bunch intensities up to 2.5×10^{11} p/bunch), could still be handled accepting somewhat reduced safety margins or with very modest upgrades.
 - Beam currents significantly higher than 1 A require upgrades. Within the existing transfer tunnels and caverns and with realistic upgrades of the dilution kickers and the dumps, beam currents of at least 2 A are possible. The cost will be in the range of a few MCHF.

94

- For currents even higher, it will become necessary to move the dumps further away from the extraction points. There is no fundamental limitation to this, but the involved cost could become important (for instance, the cost of civil engineering alone, when moving the dump caverns by 500 m, would be of the order of 15 MCHF).
- For the $1 \mu s$ long super-bunch of 1 A average current a method for diluting the beam, different from the present one, must be used (quadrupoles instead of dipolar dilution kickers) with the dumps moved further away by more than 1 km. The cost would be of the order of 50 MCHF.
- A beam energy of 14 TeV requires to rebuild the extractions with kicker and septum magnet systems twice as strong as at present. Within the existing tunnels and caverns and with upgrades of the beam dilution system and the dump, solutions for dumping 14 TeV beams of about 1 A could be found. For higher currents sufficient dilution can only be provided with the dumps moved further away. Assuming the same maximum currents as for 7 TeV, the investment would be in the 100 MCHF range, including the cost for the extractions.

For all considered upgrades the questions of safety and survival of failure modes are increasingly difficult. Careful analysis is needed, since it might be in this domain that limitations arise.

References

[1] G.R. Stevenson, CERN/TIS-RP/IR/93-10.
[2] CERN/AC/95-05 (LHC).
[3] J. Bonthond et al., LHC Note 286.
[4] M. Mayer, U. Jansson, and G. Schröder, LHC Note 362.
[5] SL-Spec 98-31 MS.
[6] A. Ferrari, G.R. Stevenson, and E. Weisse, CERN/SL/92-15.
[7] J.M. Zazula and S. Péraire, LHC Project Report 96-80.
[8] J.M. Zazula and S. Péraire, LHC Project Report 96-87.
[9] L. Bruno, S. Péraire, M. Ross, and P. Sala, LHC Project Note 217.
[10] J.H. Dieperink et al., LHC Project Report 113.
[11] N.V. Mokhov, A.I. Drozhdin, I.L. Rakhno, M. Gyr, and E. Weisse, LHC Project Report 478.

A Appendix
A.1 Crab Cavities

A larger crossing angle allows reducing the effect of the parasitic collisions and early separation of the two beams, which could be fed into different final triplets, each of which with smaller aperture and higher gradient than in the present LHC.

A large crossing angle would lead to an unacceptable loss in geometric luminosity. In order to avoid this loss, either the beams are bent between the collision point and the last quadrupole (as in RHIC), or crab cavities [1] are employed.

The distance between the last quadrupole and the collision point is about 20 m. Assuming an outer quadrupole radius of 25 cm, if we want to pass the two beams through two separate final quadrupoles, a full crossing angle as large as 25 mrad would be required.

The transverse deflecting voltage is related to the crossing angle θ_c and the cavity frequency by

$$V_\perp = \frac{cE \tan(\theta_c/2)}{e\omega_{\mathrm{rf}}\sqrt{\beta_x^* \beta_{\mathrm{crab}}}} \quad (67)$$

where β_{crab} denotes the beta function at the crab cavity.

Table A.1 compares the specifications of the KEKB crab cavities with those required for the LHC upgrade. The rf wavelength must be large compared with the bunch length, in order to stay in the linear range of deflection. A few meters length of super-conducting 1.3-GHz dipole-mode cavities should provide the necessary deflection. The relative phase of the crab cavities on either side of the collision point should be kept stable to within

$$\Delta\phi \leq \frac{\Delta x \, 2\pi}{\lambda_{\mathrm{rf}}\theta_c} \quad (68)$$

where Δx is the tolerance on the horizontal centroid displacement at the IP. For our estimate of $\Delta\phi$ in Table A.1 we have assumed that $\Delta x \approx 1 \ \mu$m.

variable	symbol	KEKB HER	LHC
beam energy	E	8.0 GeV	7 TeV
RF frequency	f_{rf}	508.9 MHz	1.3 GHz
half crossing angle	$\theta_c/2$	11 mrad	12.5 mrad
IP beta function	β_x^*	0.33 m	0.25 m
cavity beta function	β_x	100 m	2000 m
required kick voltage	$V_\perp$	1.44 MV	144 MV
phase tolerance	$\Delta\phi$		2 mrad

Table 27: Parameters for the crab cavities of KEKB [1] and example values for the LHC Upgrade.

References
[1] R. Palmer, *Energy Scaling, Crab Crossing, and the Pair Problem*, DPF Summer Study Snowmass '88, "High Energy Physics in the 1990s," SLAC-Pub-4707 (1988).

A.2 High-Field Wiggler

A wiggler based on NbSn might conceivably reduce the damping time and the average beam emittance at 7 TeV. The damping time from the wiggler alone is

$$\tau_{x,w} \approx \frac{2\rho_w^2}{C_p J_x E^3} \frac{l_{\text{wiggler}}}{C} \tag{69}$$

where ρ_w is the peak bending radius inside the wiggler, $C_p = (c/3) r_p / ((m_p c^2)^3) \approx 0.18$ TeV^{-3}s^{-1}, E the beam energy, l_{wiggler} the total wiggler length, and C the ring circumference. For a 16-T peak field, the above expression evaluates to 18 h l_{wiggler}/C. Then for 16 T the effect of the wiggler is likely insignificant compared with a damping time of about 52 h from the 8.4 T arc magnets.